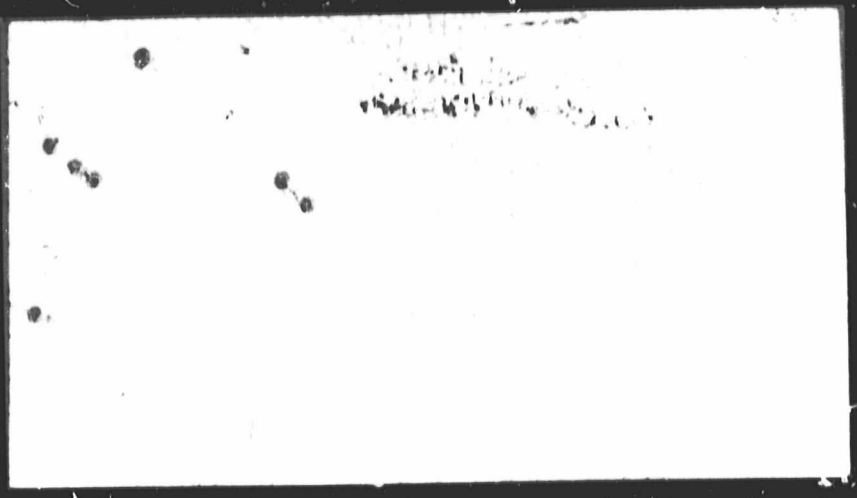

Microwave and Electronics

Electrical and Computer Engineering

University of Massachusetts at Amherst

A 94 GHz IMAGING ARRAY USING SLOT LINE RADIATORS

by

Thomas L. Korzeniowski

LAMMDA Technical Report
GRANT NAG-1-279
NASA LANGLEY RESEARCH CENTER
September 1985

A 94 GHZ IMAGING ARRAY USING SLOT LINE RADIATORS

A Dissertation Presented

by

THOMAS LEO KORZENIOWSKI

Submitted to the Graduate School of the
University of Massachusetts in partial fulfillment
of the requirements for the degree of

DOCTOR OF PHILOSOPHY

September 1985

Department of Electrical and Computer Engineering

A 94 GHz IMAGING ARRAY ANTENNA USING
SLOT-LINE RADIATORS

A Dissertation Presented

by

THOMAS L. KORZENIOWSKI

Approved as to style and content:

K. Sigfrid Yngvesson, Chairman of Committee

Paul F. Goldsmith, Member

Daniel H. Schaubert, Member

Karl D. Stephan, Member

Keith R. Carver, Professor and Head
Electrical and Computer Engineering

TABLE OF CONTENTS

ABSTRACT

A 94 GHz Imaging Array Antenna Using Slotted Line Radiators

(September 1985)

Thomas L. Korzeniowski, B.S., Massachusetts Institute of Technology

M.S. and Ph.D., University of Massachusetts

Directed by: K. Sigfrid Yngvesson

A planar endfire slotted-line antenna structure has been experimentally investigated. It was found that the H-plane beamwidths are basically dependent upon the substrate properties, whereas the E-plane beamwidths are more strongly a function of the slot's shape and size. It is shown that these antennas produce symmetrical E- and H-plane beamwidths while following Zucker's standard traveling-wave antenna beamwidth curves over some range of antenna normalized length. An empirically derived design formula for effective substrate thickness is shown to predict this range for linearly tapered slotted-line antennas.

These antennas were subsequently arrayed and mutual impedance data measured with a vector network analyzer and infered from their measured single element and arrayed radiation patterns. It was found that the antennas could be spaced up to 1.5 wavelengths before mutual impedance could be measured using the vector network analyzer and up to 2.5 wavelengths before any change in the radiation patterns were found.

Arrays of these LTSA antennas were constructed for operation at 94 GHz with inter-element spacings of 1.5 and 2.5 wavelengths and evaluated

with a Cassegrain reflector antenna. The experimental imaging properties of these arrays were presented and imaging theory was discussed. It was shown that a minimum spacing of elements is necessary for exact reconstruction of a sampled image in a diffraction limited system. Because these LTSA elements employ the traveling-wave mechanism of radiation, they can be spaced two times closer than a conical feed horn of comparable beamwidth. An LTSA array with 2.0 wavelength inter-element spacing would be capable of exact image reconstruction when used in a complex E-field sampling system.

LIST OF TABLES

LIST OF FIGURES

CHAPTER I

INTRODUCTION

The aim of this dissertation was to investigate the feasibility of integrable focal plane array imaging systems for millimeter waves and to demonstrate a prototype of such a system at 94 GHz. Of principal concern for the proper operation of an imaging array system is the radiation properties of tne feed elements. There exists a variety of different kinds of feed elements which can be used for this purpose. Examples are scalar feed horns, which have been shown to efficiently match to a reflector antenna [1], bow tie antennas, which have been used with a lens system [2], and notch antennas which have been used in a phased array radar system [3]. Although each type of feed element has advantages in a particular application, they have drawbacks for usage in the design of the present prototype system. Scalar feed horns and notch antennas are difficult to fabricate and the radiation pattern of the bow-tie antenna does not match to a parabolic reflector without some intermediate lens system. Hence, an investigation into the radiation properties of the class of endfire slotted-line radiation elements, which consist of slots of varying cross-section cut into the ground plane of a dielectric substrate, was undertaken. In particular, work was focused on the Vivaldi antenna (exponentially tapered slotted line structure) and the LTSA (Linearly Tapered Slotted-line Antenna) topologies (Figure 1.1). Due to the planar nature of this class of

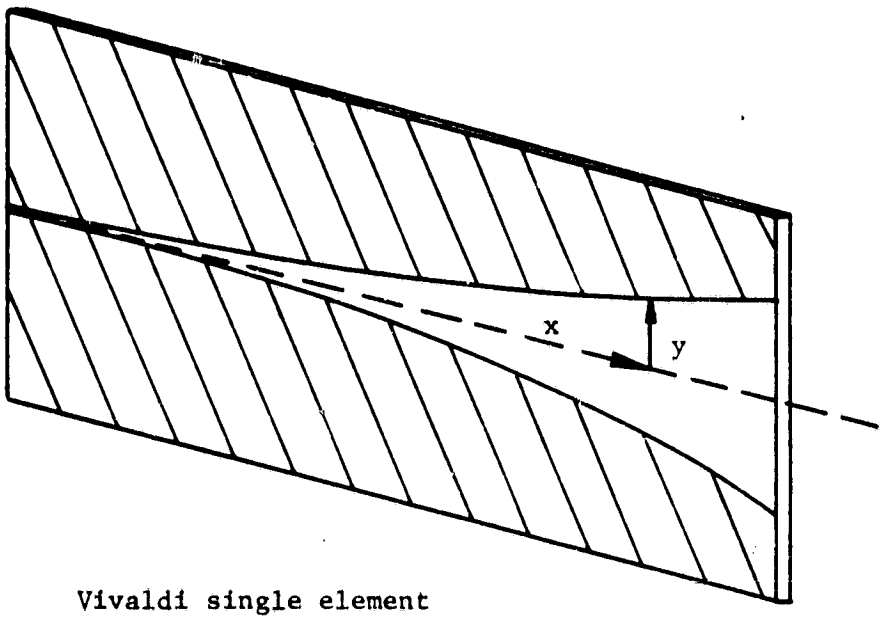

Vivaldi single element

Figure 1.1a

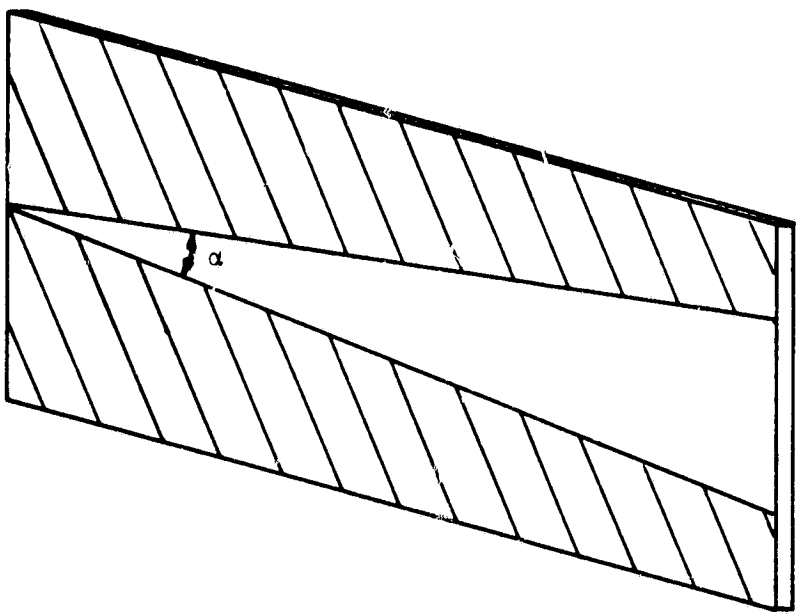

LTSA single element

Figure 1.1b

antennas, fabrication of single and multiple elements is greatly simplified over the previously mentioned candidates.

A cursory investigation into the properties of the slot line radiator was performed by Reuss [4]. He compared the radiations patterns and input VSWR for a circular arc taper with that of two exponentially tapered slot antennas on alumina substrates. He concluded that the exponentially tapered versions promised the greater bandwidth for matching with more symmetric E- and H-plane radiation patterns. Prasad and Mahapatra [5] constructed slot line radiators with linear tapered slots also on alumina substrates. However, their antennas were only one wavelength long and it would be expected that other phenomena such as resonances seen in the Notch antenna [6] may be occuring in an antenna of this length. Other early work on slot line radiators was done by Gibson [7]. His antennas consisted of exponentially tapered slots on alumina substrates, which he called Vivaldi antennas. An experimental investigation of these elements with lengths greater than a wavelength was therefore begun with the goal of elucidating the effects of conductor shape, substrate thickness and substrate dielectric constant on the radiation properties and coupling impedance of the antennas.

Another aim of the dissertation was to develop an array of antenna elements suitable for use in the focal plane of a reflector antenna. Such a system could be used for imaging and other multibeam applications. Optimum illumination of a reflector antenna requires a feed antenna with a radiation intensity which at the edge is 10-12 dB below the maximum at its center [1]. A uniform illumination function

would produce the maximum gain, but the abrupt edge taper is of course not realizable and would result in high sidelobes. The optimum illumination of a reflector antenna is a compromise between the aperture taper losses incurred, when the dish is not uniformly illuminated, and the spill over loss of the feed element. To approach uniform illumination of the dish, a feed element must have a broad radiation pattern, while to keep the efficiency of the system high, one wants to illuminate only the subreflector. An illumination which minimizes these losses and also still insures low sidelobe levels would have an amplitude taper at the edge of the dish which would be 10 dB below the maximum illumination at the center of the dish. Since the parabolic reflector has a circular symmetry, a feed with similar E- and H-plane radiation patterns is desirable. A study of the Vivaldi antenna [7] was first undertaken because it met this requirement. The antenna described by Gibson was fabricated from a metalized alumina substrate and used an exponentially tapered slot in the metalization. These devices were capable of producing radiation patterns which had constant half power beamwidths over greater than decade bandwidths, but with 10 dB beamwidths of greater than 60 degrees. Thus, Gibson's antenna will match efficiently to an imaging system with f/d=0.9, but not for the f/d=1.9 reflector antenna which was available. An array of LTSA elements was successfully developed which would match optimally to the f/d=1.9 dish. Data were obtained on the radiation and coupling of the elements in such an array. Two 94 GHz imaging systems utilizing 7-element arrays and a four element monopulse array were constructed.

Measurements showed that the individual beam patterns had low sidelobes, and reasonably high efficiency. A major new advantage of the LTSA array is that the spacing of the elements can be at least a factor of two closer than for comparable waveguide feed arrays, providing improved coverage of the focal plane.

This dissertation has been divided into 6 Chapters as follows: Chapter I is the introduction to the dissertation, while Chapter II describes the experimental methods and their limitations. Chapter III consists of a brief overview of the properties of traveling-wave antennas and reviews the experimentally measured data of endfire tapered slotted line antennas. A generalized model was developed from the data to predict the traveling-wave behavior of the LTSA antennas based on the effective thickness of the substrate. Subsequently, LTSA arrays were tested and modified until the specifications were met, as described in Chapter IV. Chapter V then describes the results obtained with the prototype imaging system and offers some theoretical interpretations of the data. Chapter VI, finally, offers my conclusions and recommendations for further work.

C H A P T E R II

MEASUREMENT TECHNIQUES

2.1 Radiation Pattern Measurements

Radiation pattern measurements of the antennas were performed on the semi-automatic antenna range depicted in Figure 2.1. In this system, the test frequency, anywhere between 2 and 94 GHz, is modulated at a one kilohertz rate and transmitted from a rectangular feed horn to the antenna testing area inside an anechoic chamber. Up to four separate antennas may be measured at any one time and all can be characterized simultaneously by duplicating the receiver section for each antenna that will be tested. The antenna under test is then connected to a diode which is used to detect the one kilohertz modulation envelope. In the case of a slotted line antenna, a diode is connected across the narrowest section of the slot. The impedance of the diode can be varied by changing the DC bias applied to it and a good match to the slot assured. As an alternative to placing a diode across the slot, a transition from the slotted line to a coaxial cable can be made and a matched coaxial detector diode used to detect the signal. The AM signal is then sent to a tuned narrow band amplifier and rectifier (in this case a standing wave meter) the output of which is a DC voltage that is proportional to the power received at the antenna under test. This voltage is then sampled and digitized by a digital multi-meter and relayed via an IEEE-488 interface to an HP-85

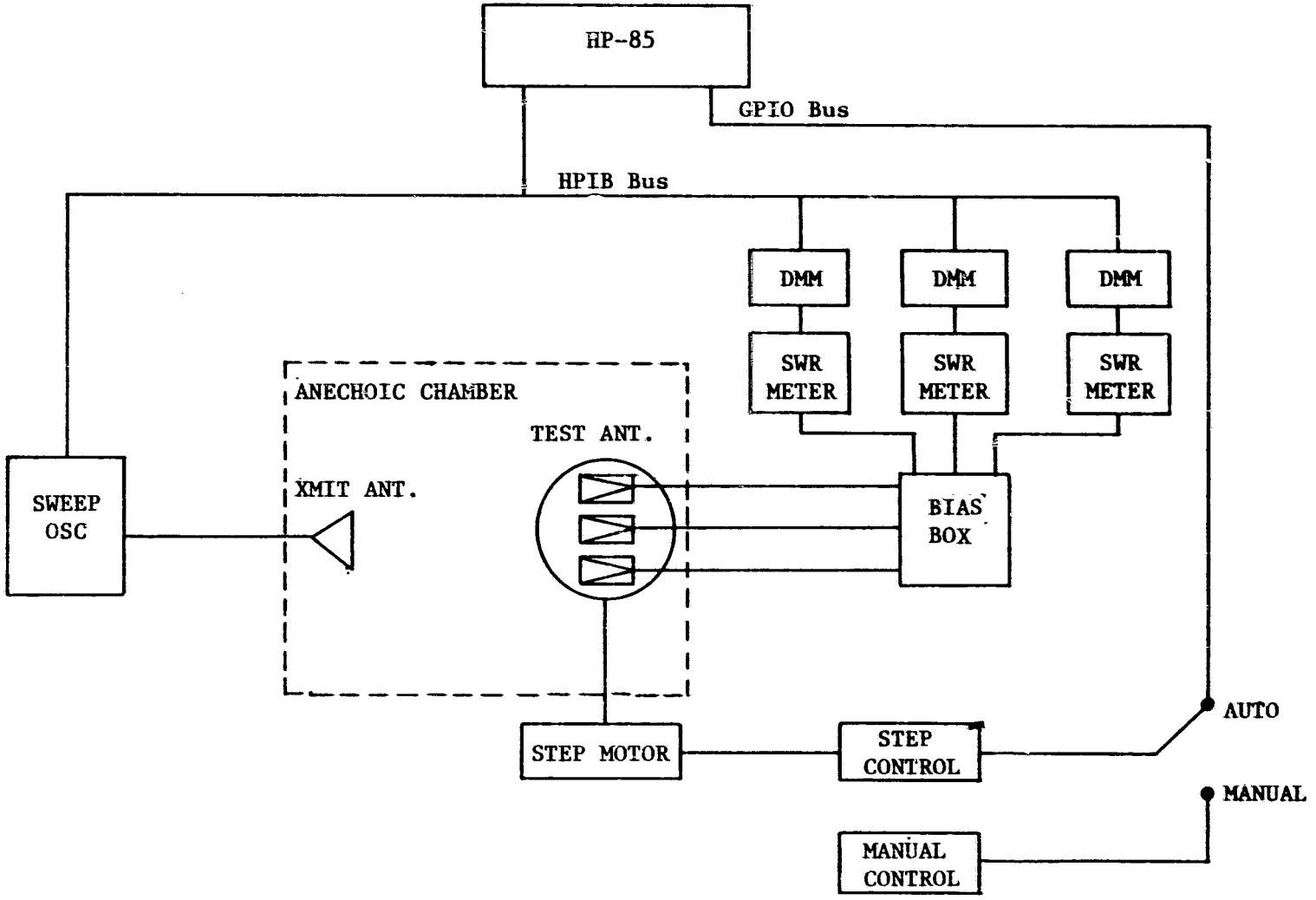

Antenna Range
Figure 2.1

microcomputer where the digitized data is stored. The microcomputer also exercises control over a stepping motor to which the antenna under test is attached through a GPIO interface. After making a power measurement, the computer steps the motor and antenna pointing by 1.8 degrees and repeats the measurement process. This continues for 200 angular step positions until the full 360 degree radiation pattern is recorded. Either E- or H-plane patterns can be made in this system by simply rotating both the transmitting feed horn and antenna under test by 90 degrees.

The linearity and dynamic range of the system were checked using an attenuator to vary the transmitted power and observing the detected output. The useful dynamic range of the system was found to be about 25 dB, and is limited only by the linearity and dynamic range of the SWR meter's output voltage. The system's overall dynamic range could easily be increased to about 40 dB, which is approximately the square-law range for a detector diode, by using an auto-ranging VSWR meter. In any case, the system proved quite adequate to measure the radiation patterns of these antennas for the purpose of extracting the obvious parameters of 3 dB and 10 dB beamwidths.

Although this anechoic chamber was found to be quite sufficient for making far field radiation pattern measurement on the slot-line antenna elements, it is far too short to be used with a Cassegrain reflector antenna. To be in the far field of an antenna, one should maintain a minimum distance of $2D^2/\lambda$ between the transmitter and receiver antennas. For the case of a 30.4 centimeter diameter reflector dish designed to

operate at 94 GHz, this value becomes 41 meters, about 10 times the length of the anechoic chamber itself. Also, because the receiver antenna was a Cassegrain dish with a 100 wavelength wide aperture, one expects to measure half power beamwidths on the order of one degree, which is much finer than the stepping motor gradations. Hence, a second range with a transmitter/receiver distance of approximately 50 meters. This range besides being able to also make measurements on up to four antennas simultaneously and being computer controlled, had the added feature of controlling both the elevation and azimuth planes to an accuracy of 0.05 degrees and 0.0625 degrees respectively.

2.2 Directivity and Efficiency Data

Besides the previously mentioned antenna properties, the antenna directivity and beam efficiency can also be calculated from the radiation data. Both directivity and efficiency are found to be useful figures-of-merit to indicate how effectively an antenna radiates into a certain angular region of space.

We can approximate the radiation from an x-polarized feed element as:

$$E(r) \alpha \frac{e^{ikr}}{4\pi r} [\hat{\theta}\, U_E - \hat{\phi}\, U_H] \qquad (2.1)$$

where

$$U_E = U_1 \cos\phi \; ; \; U_H = U_2 \sin\phi \qquad (2.2)$$

Here, U_1 and U_2 are the measured field patterns in the E-plane and H-plane respectively and r is the distance between the transmitter and the

feed element. These equations for the field patterns assume that the actual radiation patterns will be well behaved and do not have large sidelobes off the E- or H- measurement planes so that a smooth $\sin\phi/\cos\phi$ interpolation can be used for the radiation pattern between the E- and H-plane. Also, it is assumed that the maximum radiation intensity is along the z-axis with θ being measured from the z-axis.

Because directivity is defined as the maximum radiated intensity divided by the average radiated intensity, it can be calculated using the formula:

$$D = \frac{4\pi[U_E^2+U_H^2]_{\theta=0}}{\int_0^{\pi}\int_{\pi}^{\pi}[U_E^2 + U_H^2]\sin\theta\, d\theta d\phi} \qquad (2.3)$$

For our case this reduces to:

$$D = \frac{8\, U_1^2(\theta=0)}{\int_{-\pi}^{\pi}[U_1^2 + U_2^2]\sin\theta d\theta} \qquad (2.4)$$

where $U_1=U_2$ at $\theta=0$, which is taken as the direction of maximum response. Beam efficiency is defined as the radiated power within some prescribed angular region divided by the total radiated power. To calculate the 10 dB beam efficiency, the quantity of importance for optimum performance of this imaging system, one can use the formula:

$$\eta_B = \frac{\int_0^{\pi}\int_{\theta_{-10dB}}[U_E^2+U_H^2]\sin\theta d\theta d\phi}{\int_0^{\pi}\int_{-\pi}^{\pi}[U_E^2+U_H^2]\sin\theta d\theta d\phi} \qquad (2.5)$$

Since the radiation pattern data are taken in digital form, the integrals in the above equations can be done numerically on the HP-85.

2.3 Impedance Measurements

Another parameter characterized during the course of this dissertation was the input impedance of the slotted-line antenna elements. Because the slotted-line is a balanced transmission line, one cannot simply connect these antenna elements directly to a network analyzer and measure the input impedance. Fortunately, there do exist other methods which allow one to obtain this quantity. The most straight-forward method consists of constructing a balun from the slotted line to a coaxial cable which can then be directly coupled to the vector network analyzer. The problem with this method lies in the fact that the input impedance is masked by the transition. In order to obtain the input impedance, one must also know the properties of the transition exactly.

There exists another less complex method to uncover the input impedance of these antenna elements. Due to the symmetry of the elements, one is allowed to cut the antenna in half and form its image by placing the half antenna over a ground plane (Figure 2.2). By attaching a coaxial connector through the ground plane at the input of the antenna, one can directly measure the input impedance of this new antenna system. This measured impedance can be related to the input impedance of the original by multiplying the measured data by a factor of 2, since the new antenna is half of the original. Measurements of impedance in this work were done using this method.

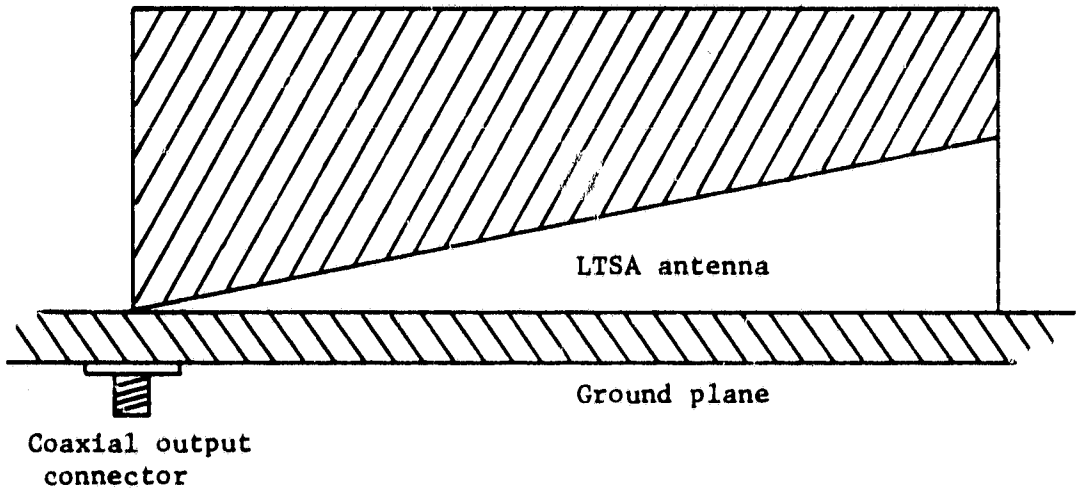

Input impedance measurement of LTSA

Figure 2.2

Besides being able to apply the ground plane method to input impedance measurements, it was also used to make antenna coupling measurements of slot line antennas in one and two-dimensional arrays. By placing an antenna half and its next nearest whole neighbor on a ground plane in the same configuration as described above, one can calculate mutual coupling from the difference in the input impedance of the antenna half when the neighbor's input is shorted and alternately opened. Another condition which indicates antenna coupling when placed in an array is a change in an element's radiation pattern. As will be shown in later chapters, this does indeed indicate coupling between elements, but gives no exact value for this quantity.

C H A P T E R III

LTSA/VIVALDI SINGLE ELEMENTS

3.1 Overview

An antenna which could be fabricated in a planar geometry and therefore would be light, easily manufactured, and simpler to integrate with other components than presently available waveguide feeds, would be an advantage to the proposed imaging system. Until Gibson introduced the "Vivaldi aerial," no such planar antenna element existed which produced a symmetric beam with appreciable gain. His antenna consisted of a metalized alumina substrate with an exponential taper etched into the metalization with the taper in the slot, in this case by the formula:

$$y = \pm A \exp(px) \tag{3.1}$$

where y is the halfwidth separation and x is the length parameter of the antenna (see Figure 1.1a). An antenna based upon this equation can be frequency independent because for any given wavelength only a small section of the taper will radiate efficiently. The phase difference between a wave coupled to the structure and that of a free space wave remains constant over frequency. Thus the antenna's effective length scales inversely to frequency, producing frequency independent radiation properties. Although this was desirable for his application, it does not satisfy the requirements for the prototype imaging system. To elucidate the performance parameter dependence of slot line antennas

upon the antenna's physical attributes, another similar topology was investigated, i.e. the the LTSA antenna. These antennas can be defined through the full angle subtended by the two edges of the slot (Figure 1.1b). A large volume of experimental data were compiled for these Vivaldi and LTSA endfire antennas, the bulk of these data is presented in the Appendix. Some results are also discussed in a paper, accepted for publication in the IEEE Transactions on Antennas and Propagation [8], and a previously published paper in the 8th International Conference of Infrared and Millimeter Waves [9]. In this chapter, we will concentrate on presenting selected data for LTSA single elements, from which it was possible to derive empirical design rules for such antennas. The design rules enable one to predict the performance of LTSA elements in terms of the well-known theory of traveling-wave antennas, and the standard data for such antennas given by Zucker [10] and reviewed in section 3.2. The design rules specify the range of values which should be used for LTSA opening angle, substrate thickness, and substrate dielectric constant, in order to achieve this performance. It is also shown how the design guidelines were used to obtain radiation patterns which met the specifications for the specific imaging system which is described later in this dissertation.

3.2 Review of Traveling-wave Antenna Standard Data

Radiating elements of the kind described by Gibson [7] fall into the broader category of antennas known as traveling-wave antennas (TWA),

because their active length is much greater than a wavelength. Two distinct classes of traveling-wave antennas exist, defined by their relative phase velocity, $P = c/v_{ph}$. Antennas with $v_{ph}>c$, called leaky wave antennas, tend to have beam maxima which occur in other than the end-fire direction. Surface wave antennas, for which $v_{ph}<c$, can produce radiation in the end-fire direction. The directivity of a surface wave antenna is a function of its relative propagation constant, P, and reaches a maximum depending upon the length, L, of the antenna. Hansen and Woodyard [11] have shown that for antennas with uniform amplitude distribution as a function of length the maximum gain for an antenna of length L is achieved when

$$P = 1 + \frac{1}{2L} \tag{3.2}$$

which is equivalent to saying that there should be a phase increase of 180 degrees along the structure. However, most surface wave antennas do not have constant field amplitude across their active length. The amplitude will be a function of the position on the antenna with the maximum actually occuring near the input of the antenna. Thus the actual phase difference for maximum gain will also be a function of the length. Ehrenspeck and Poehler [12] have shown that the optimum phase difference for non-uniform antennas is about 60° for short antennas, 120° for antennas between 4λ and 8λ long and approaches 180° for antennas 20λ and longer.

The effects of varying P on directivity for an axisymmetric traveling wave antenna has been reviewed by Milligan [13] whose curves are reproduced here in Figure 3.1. One sees that there exists a

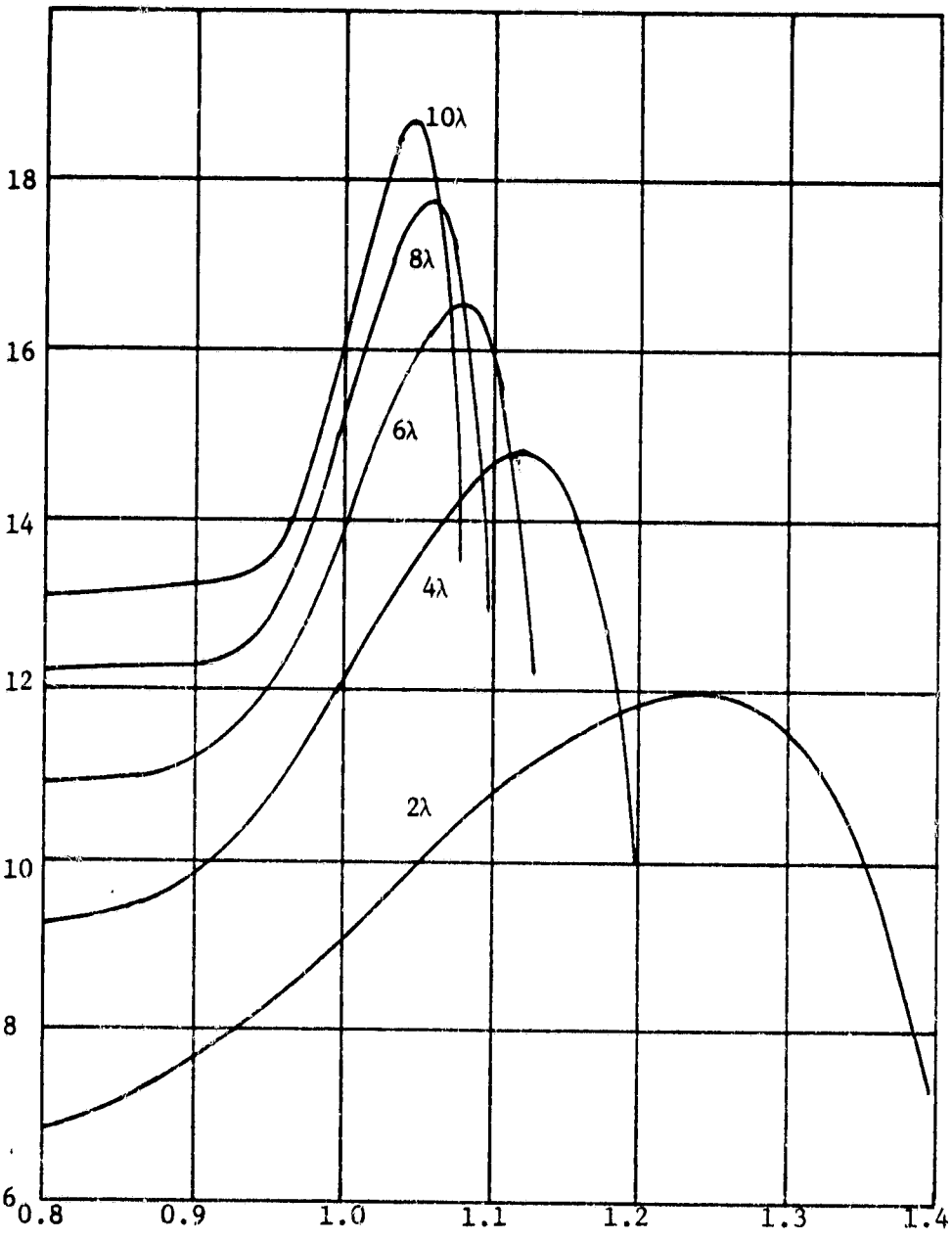

Directivity of axisymmetrical uniform distribution traveling wave

Figure 3.1

different P for optimum directivity with different normalized lengths, L/λ_o, of the antennas. Maximum directivity occurs for some specific slowing of the phase velocity and directivity decreases if the phase velocity is varied in either direction.

The gain of an element which satisfies the Hansen-Woodyard condition is approximately

$$G = \frac{7L}{\lambda_o} \tag{3.3}$$

If the antenna design is based upon the Ehrenspeck and Poehler optimum phase velocity and taper dimension, then the gain will be

$$G = \frac{10L}{\lambda_o} \tag{3.4}$$

for antennas between $3\lambda_o$ and $8\lambda_o$ in length. Zucker [10] has plotted curves of optimum gain and beamwidth of traveling-wave antennas which are reproduced in Figure 3.2. Maximum gains reported in the literature are indicated as the solid gain line. Notice also how this curve follows Equation 3.4 for values of normalized length up to about 20, after which it begins to follow the curve of Equation 3.3.

The half power beamwidth for the optimum design is approximately

$$BW = 55(\lambda_o/L)^{1/2} \quad \text{(degrees)} \tag{3.5}$$

In this case the high gain half power beamwidth plotted by Zucker lies just below the values calculated from this formula.

Another case of interest is when P = 1, i.e. when the antennas are true endfire in nature. For this case the gain becomes:

$$G = \frac{4L}{\lambda_o} \tag{3.6}$$

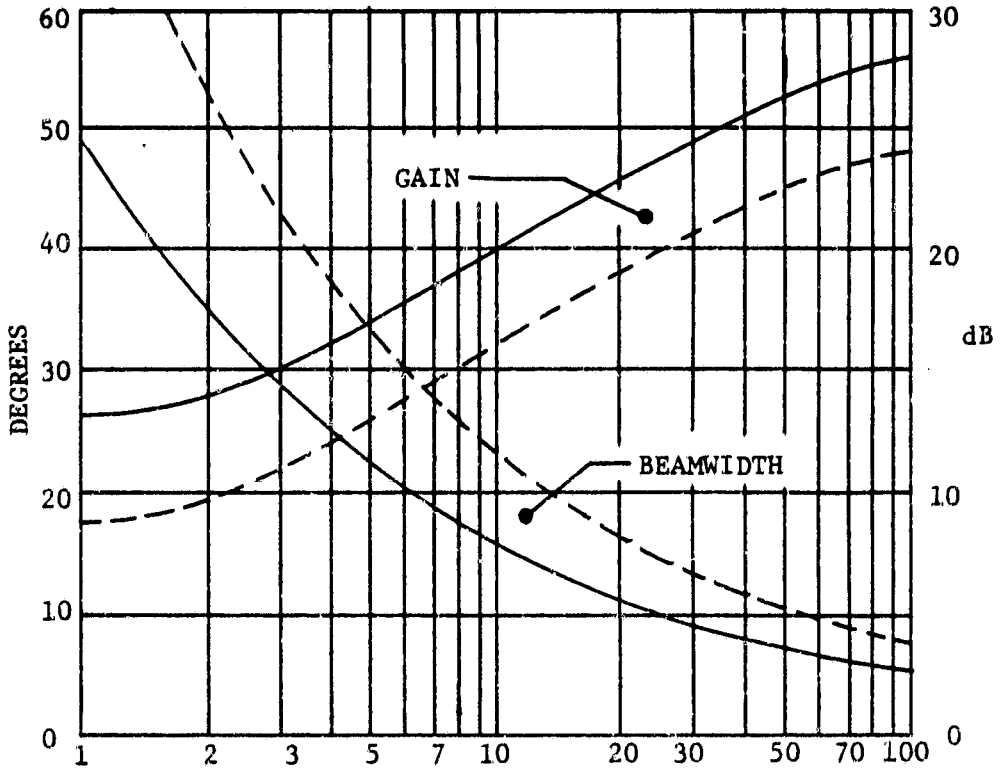

Cain and beamwidth of surface wave antenna

Figure 3.2

The beamwidth for a structure with this gain is shown plotted in Figure 3.3. Because the gain of these elements is much lower than that of the surface wave case, the beamwidths are correspondingly increased.

Some important traveling-wave antenna characteristics have been reviewed in this section. It is clear that some amount of phase velocity slowing is necessary to achieve maximum gain of the element. This value will be closely tied to the antenna's normalized length. In the following section, data will be presented for tapered slot antennas. These data will also be compared to the Zucker's standard TWA curves presented here. Although exact agreement with the optimum curves is not expected, tapered slot antennas should remain reasonably close to the theory if they employ the traveling wave mechanism of radiation.

3.3 Linearly Tapered Slot-Line Antennas: Experimental Data and Design Guidelines

The empirical design study of LTSA single elements was primarily restricted to an LTSA opening angle of 11.2 degrees. As shown in the appendix, some effects on the beamwidth were found when the opening angle was increased, primarily in the E-plane. It was, however, found easiest to match the TWA data by using the opening angle of 11.2 degrees, and the full study of the effects of this parameter was left for future work. The parameters which were studied in detail were thus the dielectric constant of the substrate (ε_r) and the thickness of the substrate (t). The design guidelines were derived for the case of

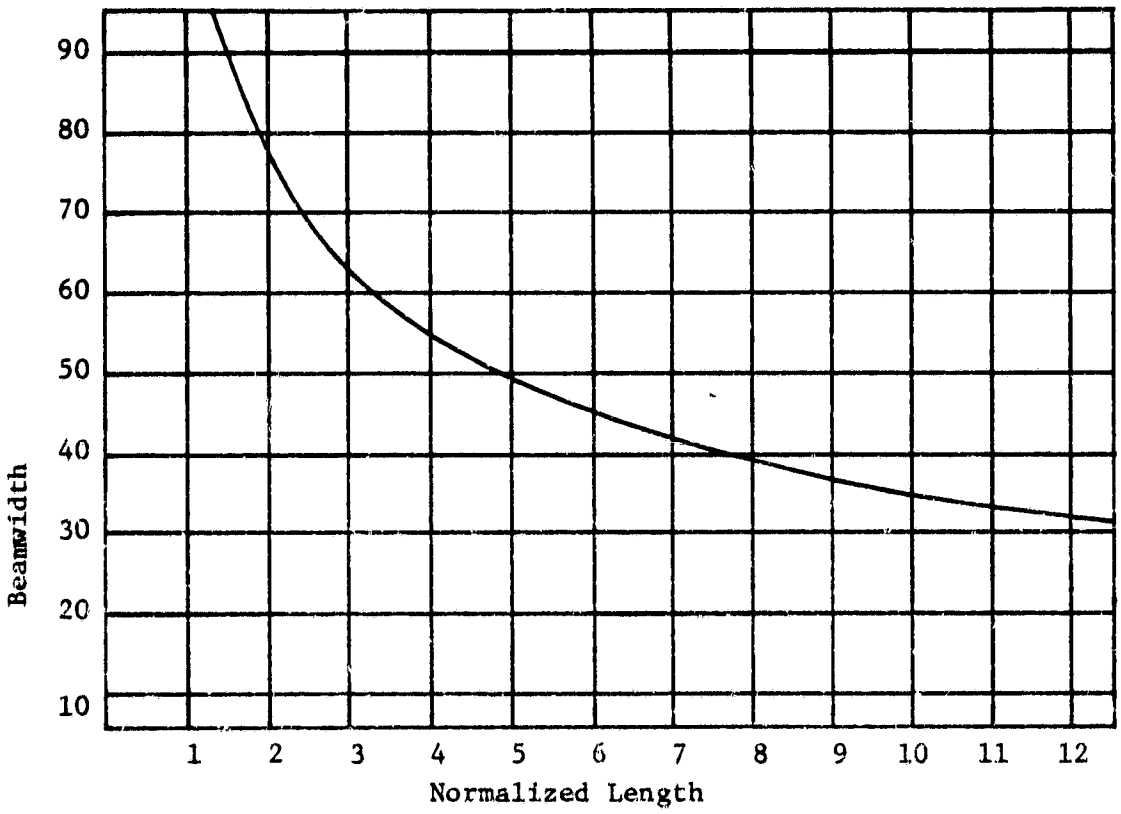

Beamwidth of traveling wave end-fire antenna

Figure 3.3

changing the physical length (L) of the antenna, while keeping the substrate thickness and the frequency constant, since this proceedure was deemed to be most useful in practice. Below, we thus present data obtained in this manner for different dielectric substrates, including the "air" case.

One "air" LTSA antenna with full taper angle of 11.2 degrees was constructed and measured as a function of length at 8, 10, and 12.4 GHz. Shown in Figure 3.4 a graph of beamwidth as a function of the antenna's normalized length. The E- and H-plane beamwidths are symmetrical and roughly track each other for all three frequencies. They do not, however, follow the optimum TWA antenna curves. As was discussed in the previous section, traveling wave antennas with $v_{ph} \rightarrow c$ do not satisfy the optimum gain conditions and as can be seen from Figure 3.1, the gain decreases as the wave velocity approaches c. Milligan's P=1 half power beamwidth curve has also been included in Figure 3.4 for comparison purposes. We see that these "air" LTSA's have beamwidths which lie between the optimum curves and $v_{ph} = c$ curve, indicating that there still exists some small amount of phase velocity slowing even though there is no dielectric substrate present.

A second series of measurements taken as a function of length were performed on a similar LTSA antenna with full taper angle of 11.2 degrees on a 0.15 mm thick OAK-605 laminated substrate at 8, 10, and 12.4 GHz. The half power beamwidths of this antenna are shown plotted versus normalized length in Figure 3.5. In this case the H-plane beamwidth curves are following the low sidelobe TWA curves while in the

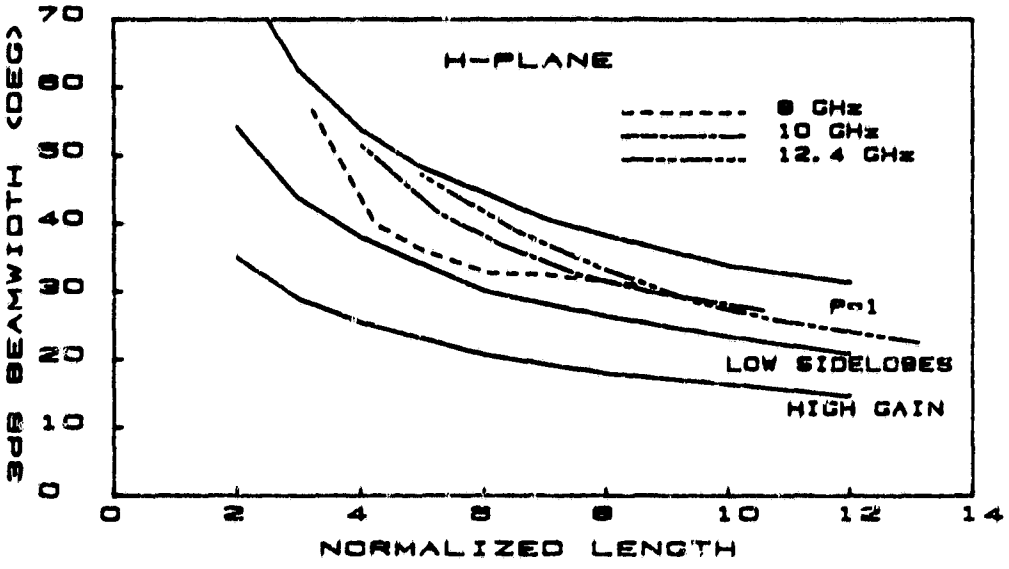

3dB beamwidth of "air" LTSA antenna (H-plane)

Figure 3.4a

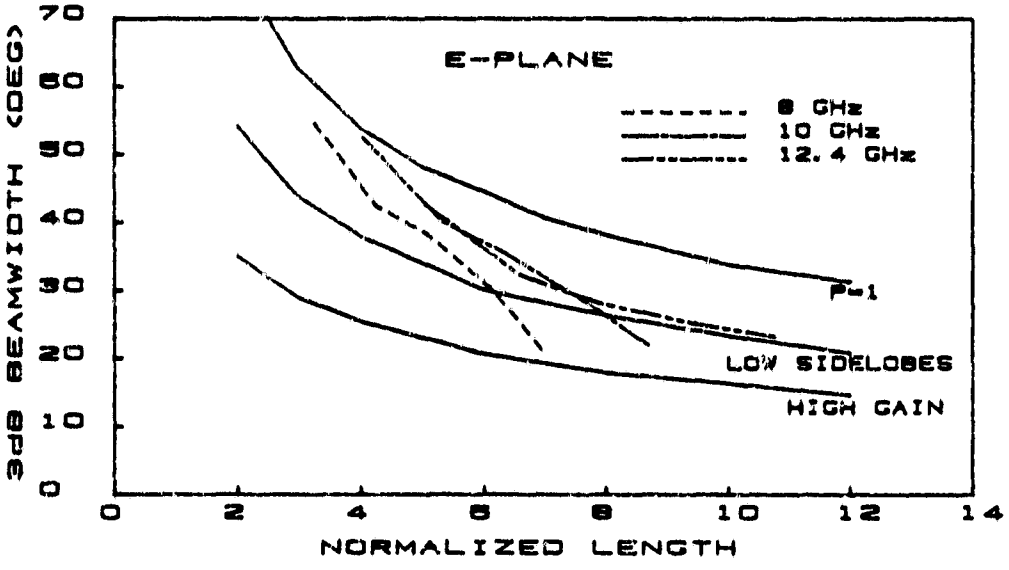

3dB beamwidth of "air" LTSA antenna (H-plane)

Figure 3.4b

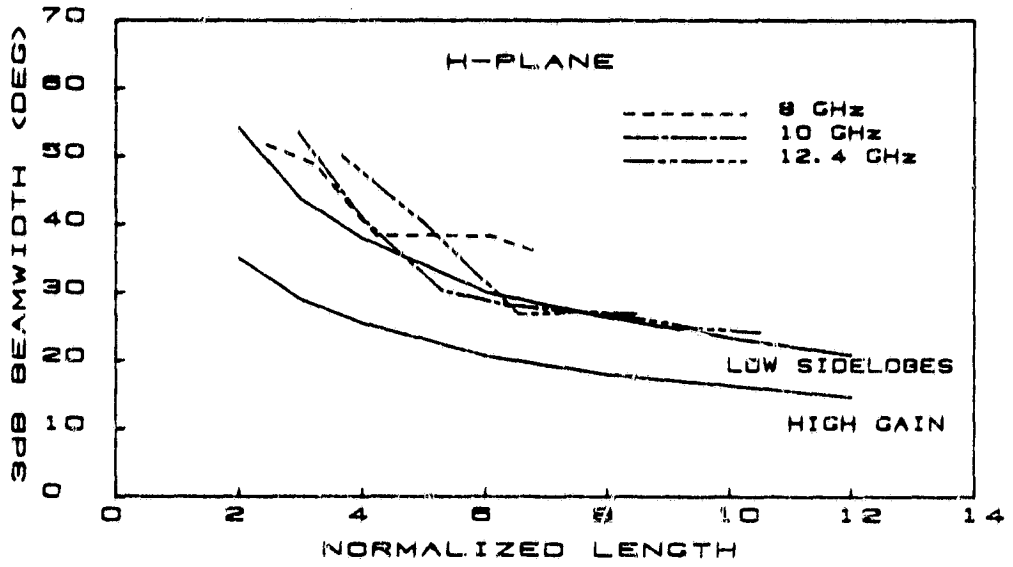

3dB beamwidth of LTSA on 0.15 mm thick OAK-605 substrate

Figure 3.5a

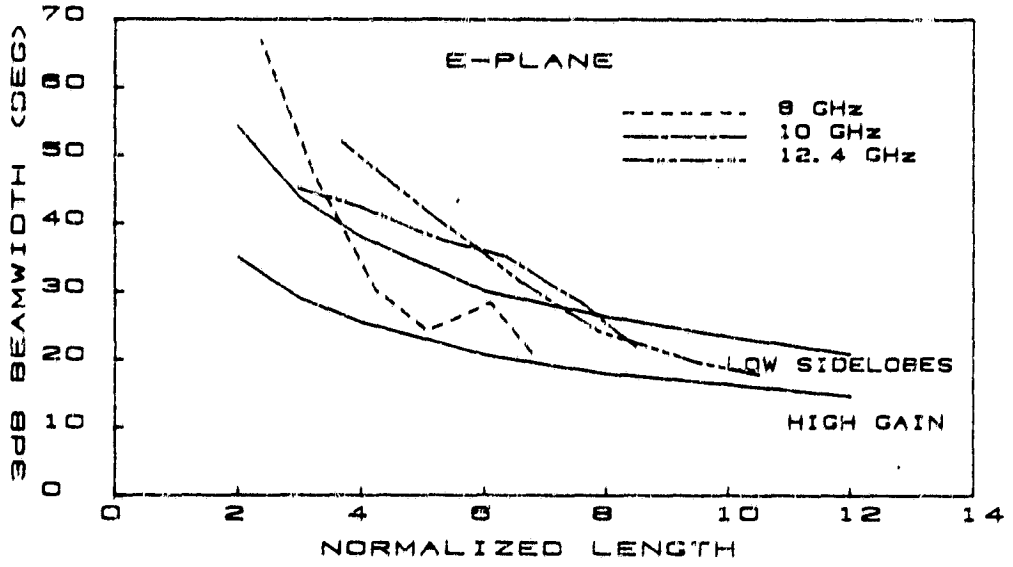

3dB beamwidth of LTSA on 0.15 mm thick OAK-605 substrate

Figure 3.5b

E-plane the beamwidths begin in the same place and end up between the two TWA curves for long lengths. This indicates that we are approaching the optimum directivity for these antennas with a rather thin dielectric substrate.

Another set of measurements were made at 94 GHz on three LTSA antennas with 11.2 degree full taper angle for various substrate thicknesses as a function of length. The substrate material was Kapton (ε_r = 3.5) of thicknesses 0.025 mm, 0.051 mm, and 0.076 mm respectively (see Figure 3.6). This series shows a radical progression from the low sidelobe curve, to high gain, to asymmetrical E- and H-plane beamwidths.

An identical 11.2 degree taper angle LTSA antenna was fabricated on a 0.127 mm thick Duroid (ε_r = 2.33) substrate and beamwidth measured as a function of length, see Figure 3.7. As with the 0.051 mm Kapton substrate (Figure 3.6b), the beamwidths tend to follow the high gain curve. X-band models on thick low dielectric constant substrates (ε_r = 2.33) have not duplicated the symmetrical high gain beams seen in these higher dielectric constant (ε = 3.5) materials. For instance, Figure 3.8 is a graph of half power beamwidth of an 11.2 degree taper angle LTSA on a 25.4 cm long, 1.54 mm thick OAK-605 laminated substrate. They do have symmetrical beams which lie between the standard data curves for short normalized lengths. However, as the normalized length of the antenna increases, the H-plane beam width broadens. Similar behavior for low dielectrics was (ε = 2.22) also seen in data taken at Chalmers University [8].

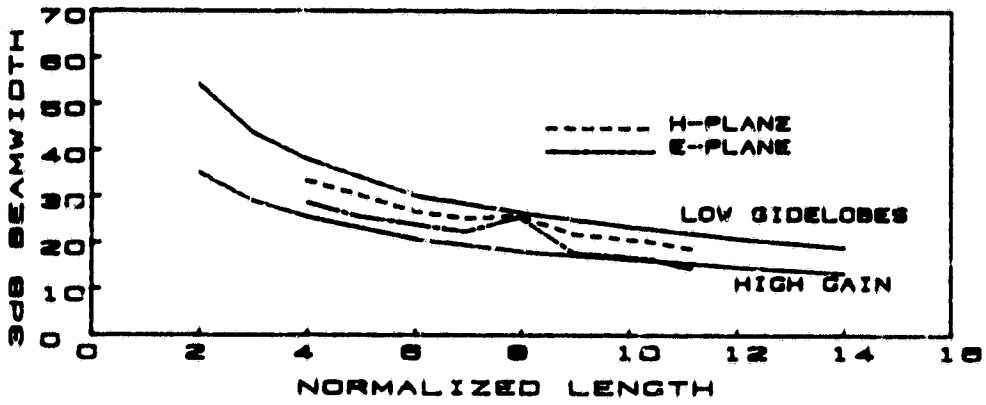

3dB beamwidth of LTSA on 0.025 mm thick Kapton substrate

Figure 3.6a

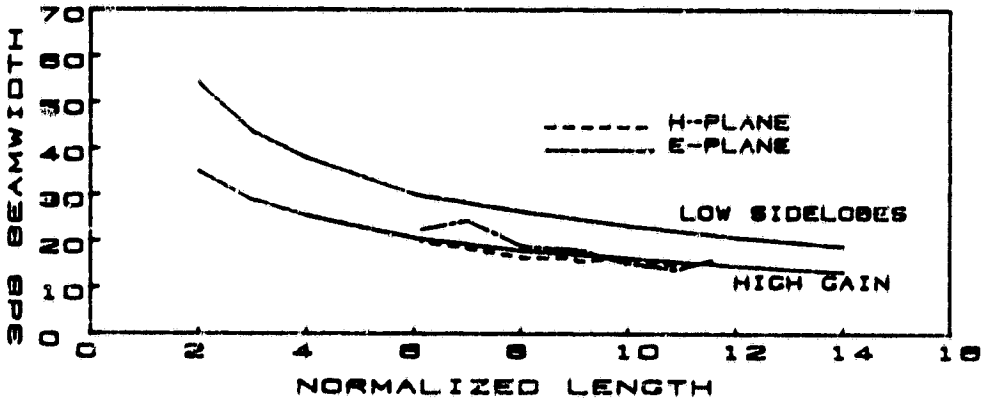

3dB beamwidth of LTSA on 0.051 mm thick Kapton substrate

Figure 3.6b

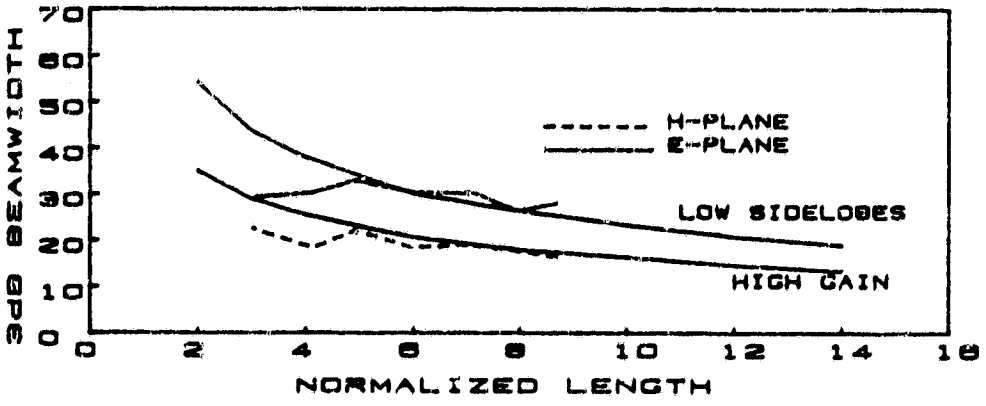

3dB beamwidth of LTSA on 0.076 mm thick Kapton substrate

Figure 3.6c

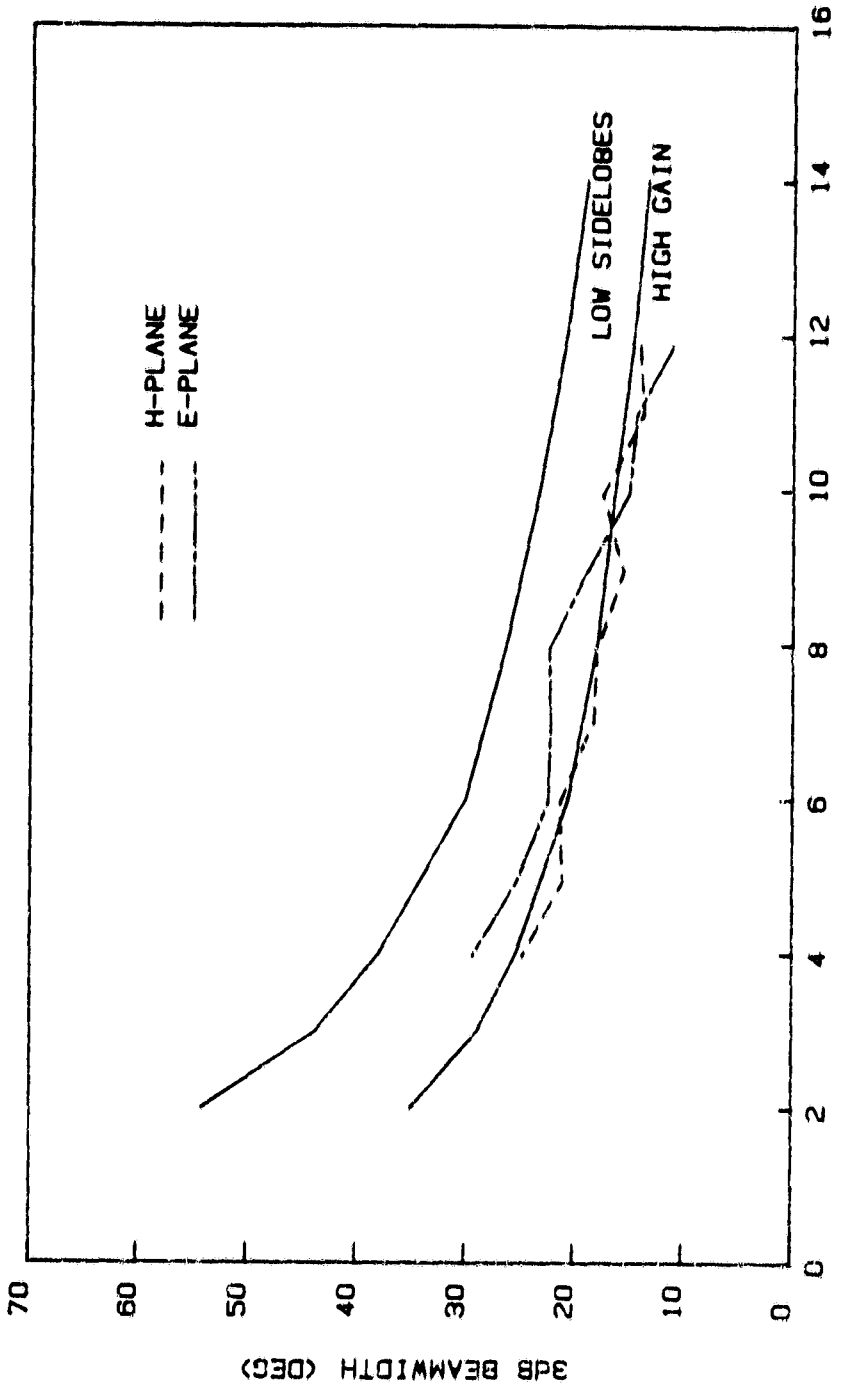

3dB beamwidth of LTSA on 0.127 mm thick Duroid substrate

Figure 3.7

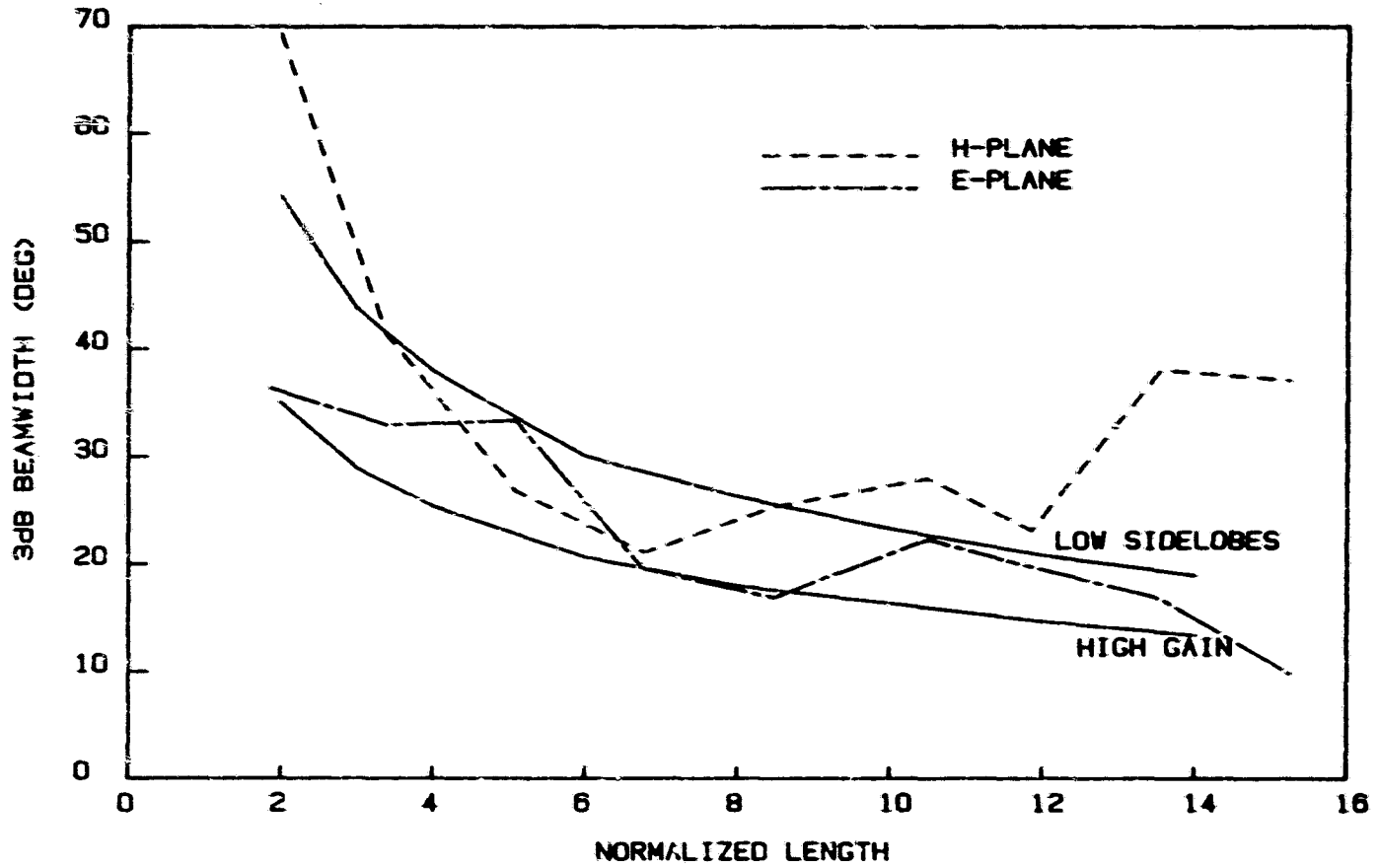

3dB beamwidth of LTSA on 1.54 mm thick OAK-605 substrate

Figure 3.8

In order to summarize the effects of the dielectric substrate thickness and permittivity, Table 3.1 has been generated for several LTSA antennas based upon the effective thickness of the substrates using the empirical formula (found by trial-and-error):

$$t_{eff} = t(\varepsilon_r - 1)/\lambda_o \qquad (3.7)$$

One can conclude that t_{eff} offers a rough, empirical guide to predicting the qualitative behavior of LTSA antennas, which has been discussed in the previous paragraphs. In particular, an important conclusion is that symmetric E- and H-plane patterns and close to optimum TWA data can be obtained for a wide range of normalized lengths, if t_{eff} is in the interval .02 to .05. For t_{eff} below this range, beamwidths are wider, while for larger t_{eff}'s, the behavior is less predictable (see figures in the appendix).

To indicate the usefulness of this formula, consider the case of the 1.57 mm thick OAK-605 substrates. Using the formula, it is predicted that an 11.2 degree LTSA on this material will have symmetric beams within the standard curves for a wavelength of 5.22 cm. Looking at Figures A.7c and A.11 which are for LTSA antennas on 1.57 mm thick OAK-605 substrates and 25.4 cm in length, reveals that this is indeed the case. The 0.76 mm thick Rexolite LTSA of Figure A.7b can be seen to be following the rules as is the Vivaldi antenna of Figure A.2b.

For the case of high dielectric constant substrates (Epsilam-10) of 0.25 mm thickness, the formula indicates that the operating wavelength for symmetrical TWA beams is 5.7 cm. From Figures A.12, this data was taken by changing frequency, we can see that the agreement is close,

MATERIAL	DIELECTRIC CONSTANT	FREQUENCY	SUBSTRATE THICKNESS	t_{eff}
OAK-605	2.33	10	0.152	0.0067
KAPTON	3.5	94	0.025	0.019
KAPTON	3.5	94	0.051	0.040
REXOLITE	2.54	10	0.79	0.041
STYROFOAM	1.05	10	25.4	0.042
DUROID	2.33	94	0.127	0.053
KAPTON	3.5	94	0.076	0.060
OAK-605	2.33	10	1.57	0.070
EPSILAM-10	10.2	10	.254	0.078

Effective thickness

Table 3.1

however, for data taken by changing the length, Figure A.13, the data no longer follows prediction. Not only does the high dielectric constant material disobey the t_{eff} predictions, but the thick styrofoam substrate also did not follow expectation.

At this point, it is useful to briefly review the system constraints placed upon the LTSA radiators. For this imaging system with a f#=1.9 Cassegrain dish, an antenna feed element with 10 dB beamwidth of 30 degrees is required for optimum illumination (Figure 3.9). Also, high element beam efficiency is desirable. A ten wavelength long LTSA element with taper angle of 11.2 degrees on a 0.127 mm thick OAK-605 (ε_r = 2.33) substrate, was found to fulfill these requirements at 10 GHz, see Figure 3.10a. Because Duroid is not available in thicknesses less than 0.127 mm, Kapton, a material with dielectric constant ε_r = 3.5 was chosen to be used at 94 GHz with a thickness of 0.025 mm. Figure 3.10b shows that the antennas made with the two different dielectric constant materials have 10 dB beamwidths which behave similarly as a function of normalized length, with the 94 GHz E- and H-plane beamwidths being only slightly different from those of the X-band antennas. Thus, the beamwidth specification could be met for the millimeter wave imaging system by using 0.025 mm thick Kapton

The directivity of the 0.127 mm thick Duroid LTSA antennas was also calculated from the measured radiation patterns and is shown plotted in Figure 3.11 for 8, 10, and 12.4 GHz. Also included in this figure are the standard TWA curves for directivity. In this case, and most other cases for the LTSA antennas, directivity is about 2 dB below the

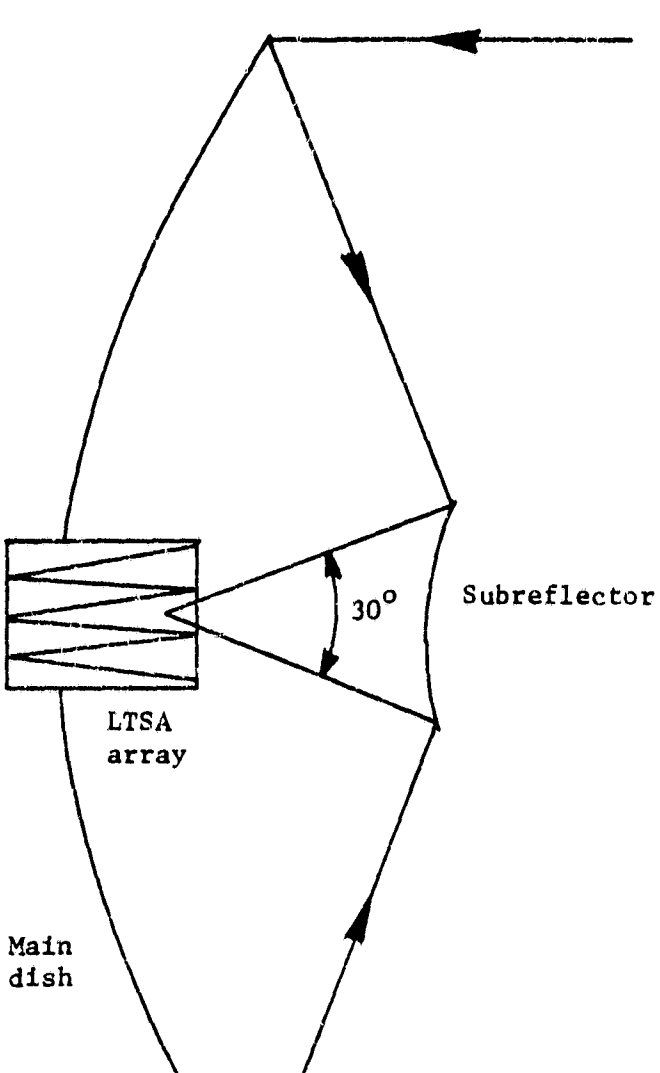

Illumination of Cassegrain subreflector

Figure 3.9

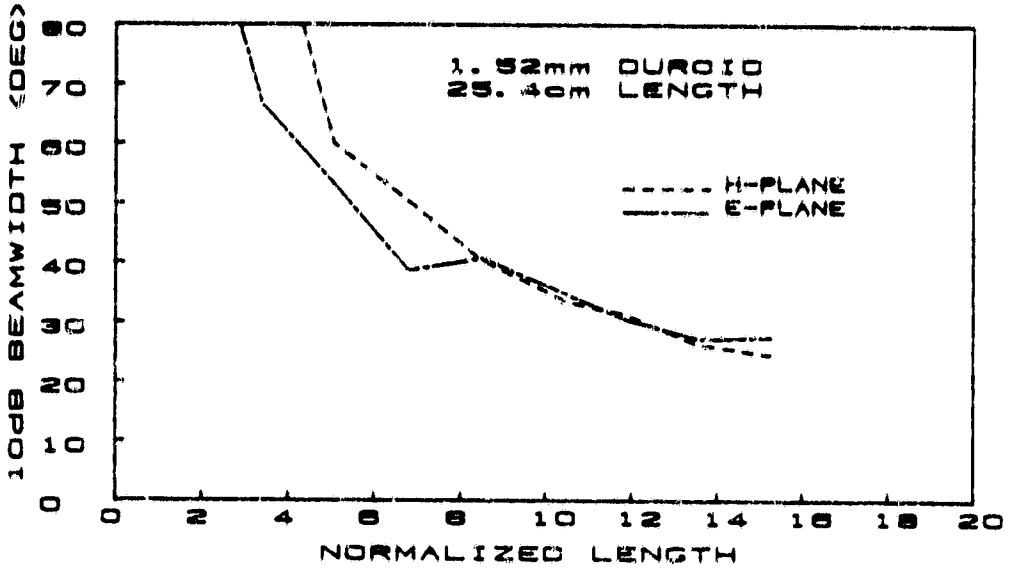

10dB beamwidths of LTSA on 0.127 mm thick OAK-605 substrate

Figure 3.10a

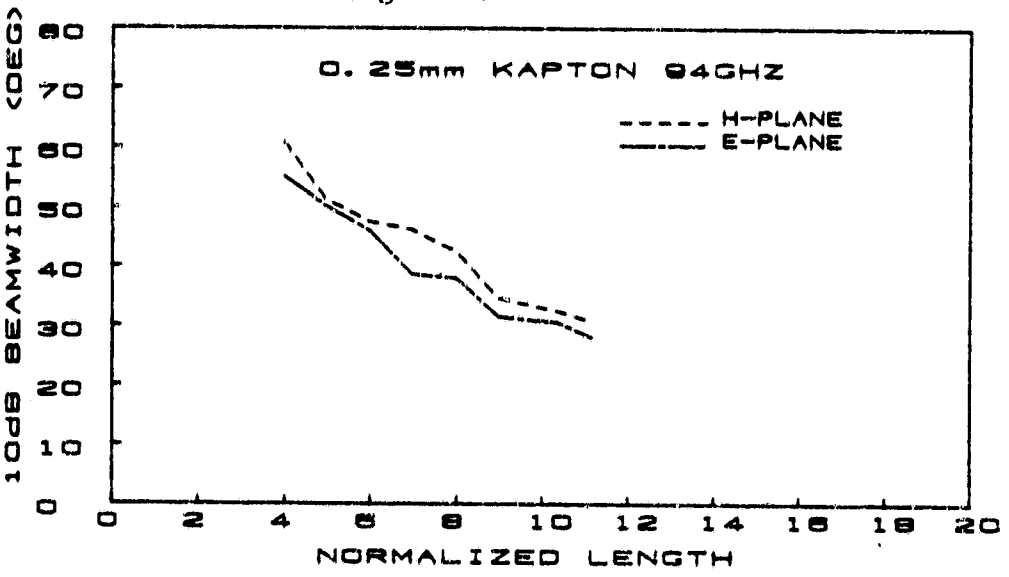

10dB beamwidths of LTSA on 0.025 mm thick Kapton substrate

Figure 3.10b

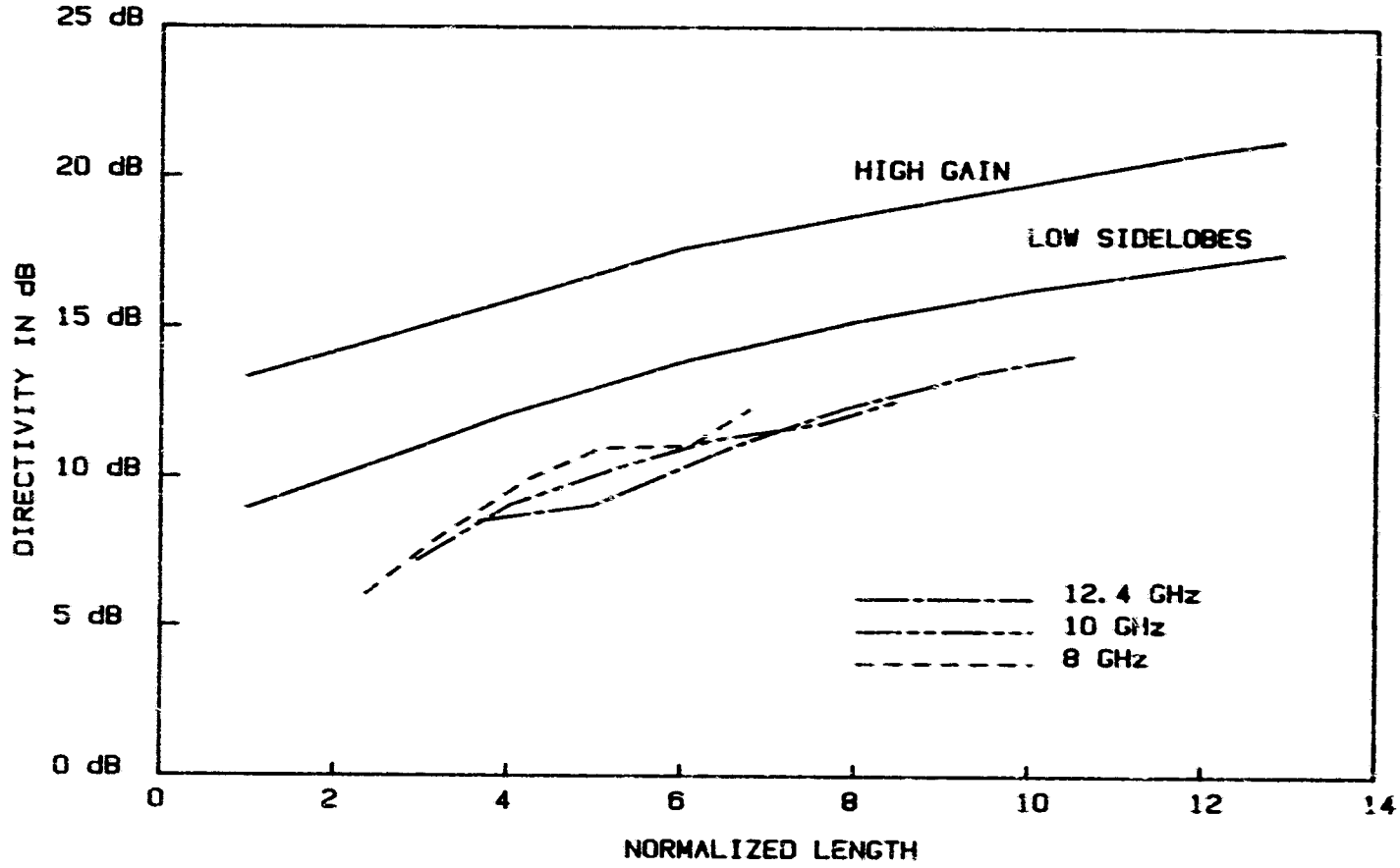

Directivity of LTSA on 0.127 mm thick OAK-605 substrate

Figure 3.11

expected value for a low sidelobe design. This is not completely surprising, because these LTSA antennas do not normally exhibit optimum half power beamwidths. Figure 3.12 is a graph of the directivity of the candidate 94 GHz LTSA feed elements. In this case, the directivity is still about 2 dB worse than expected, with the LTSA on a 0.025 mm thick Kapton substrate showing the greatest promise. This was the case despite the fact that the 0.052 mm thick Kapton LTSA and the 0.127 mm thick Duroid and LTSA at 94 GHz had half power beamwidths which followed the optimum gain curves. These antennas, although having narrow beamwidths, also tend to have higher sidelobes and thus lower gains. The 10 dB beam efficiencies were also calculated for these antennas and shown in Figure 3.13. In this plot one can see that the 0.025 mm thick Kapton LTSA has by far the greatest efficiency for a $10\lambda_o$ length antenna at 94 GHz, about 25%, and also met the previously explained beamwidth requirement and was therefore the element chosen for use in the prototype imaging system.

3.4 Input Impedance

The input impedance of LTSA antennas can be measured through a ground plane and using the method of images as discussed above. Two structures that were measured for input impedance are shown in Figure 3.14. The shaded areas of the figure represents conducting fins without a substrate. It can be seen from the figure that the second antenna consists of only one radiating side. One is tempted to say that the

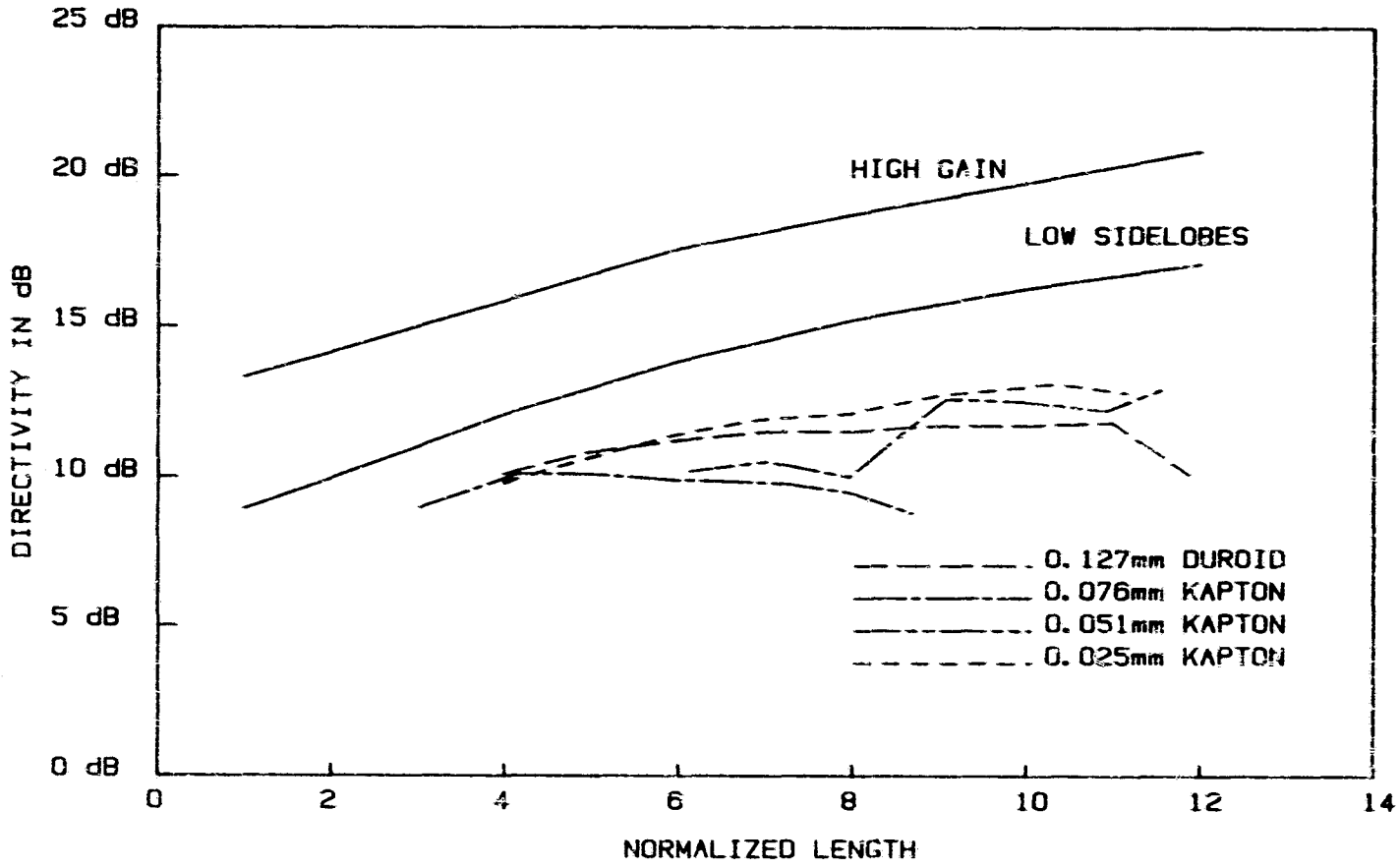

Directivity of LTSA antenna on various substrates

Figure 3.12

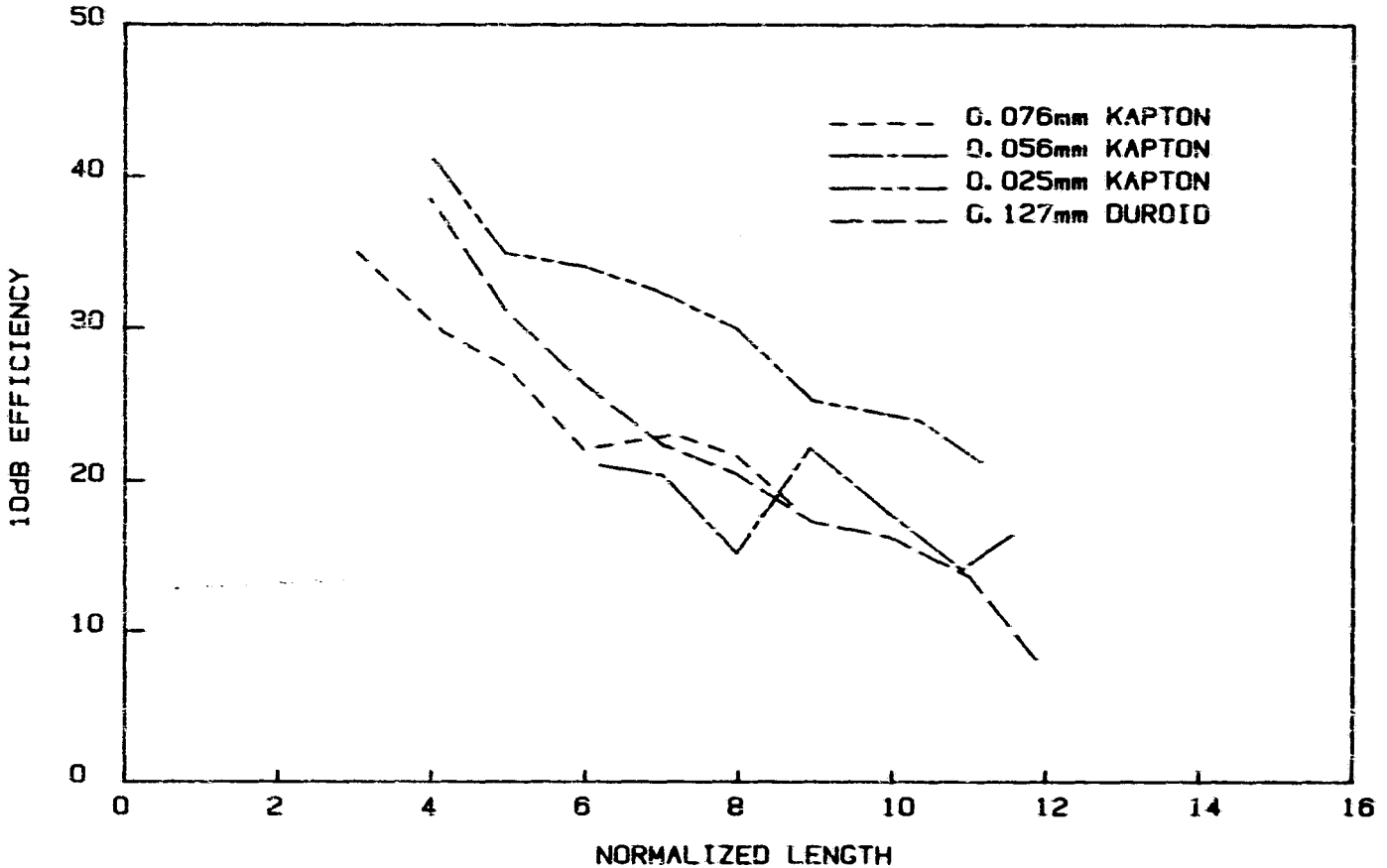

10dB efficiency of LTSA on various substrates

Figure 3.13

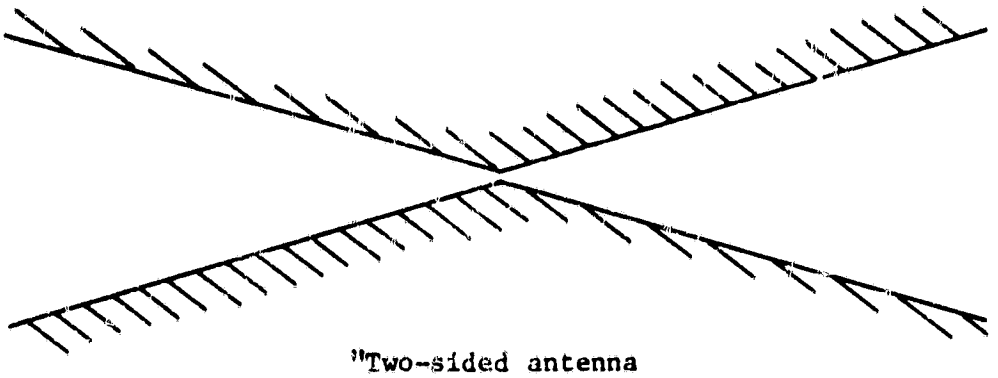

"Two-sided antenna

Figure 3.14a

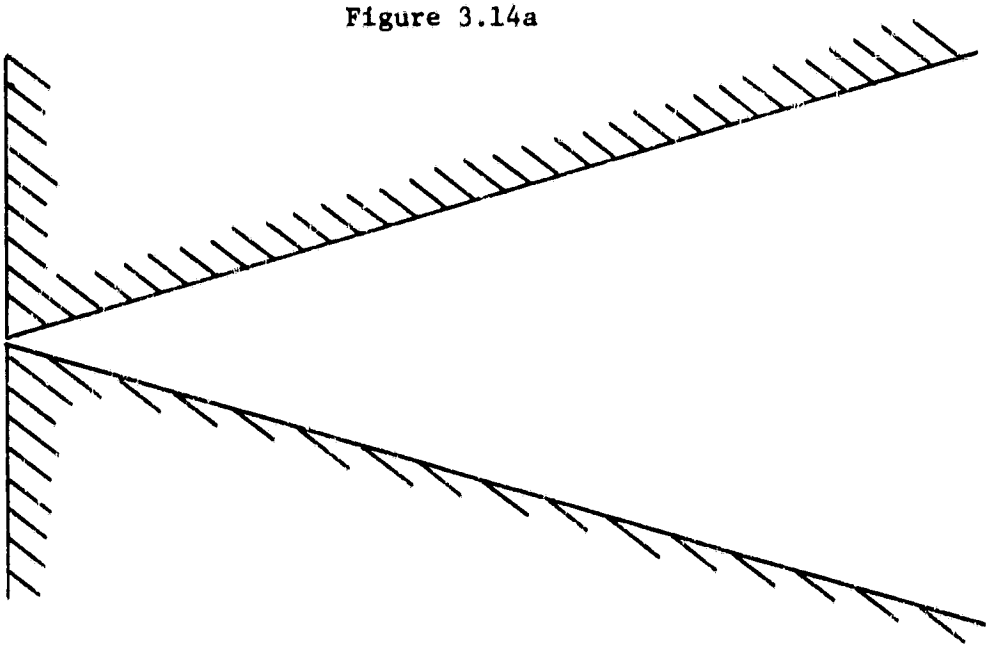

Single sided antenna

Figure 3.14b

impedance of the first is only half that of the second, since on the surface it appears that the first is constructed from a parallel combination of the second. This is not strictly true because the back half of the first will also radiate and have some characteristic input impedance of its own. This would be in parallel with the impedance of the radiating side, altering the measured input impedance. Thus, one expects that the input impedance of the second antenna should be somewhere between one and two times the impedance of the first.

A method of calculating the input impedance of structures with geometries similar to the LTSA was first introduced by Carrel [14] and a similar method developed by Rutledge [15]. Carrel showed that infinite metallic structures of this kind will support the propagation of TEM spherical waves. Further, he showed that, with the boundary conditions which must be satisfied, the solutions to the wave equation reduced to a solution of Laplace's equation and are conjugate harmonic functions for which conformal mapping techniques apply. Although the fields that would be calculated from this model are static, they can be used to derive the input impedance of an antenna.

Conformal mapping allows a set of transformations to be performed on the LTSA geometry that reduce it into a known problem; in this case, a parallel combination of parallel plate waveguides. The impedance of a parallel plate waveguide is well known to be simply $Z = \eta_o \, d/b$, where d is the distance between the two plates and b is the width of the plates. In the transform domain, the structure becomes a parallel combination of two parallel plate waveguides. Performing the inverse transformation, it

can be shown that the input impedance of this antenna is $Z = \eta_o K/K'$, where K and K' are the complete elliptic integrals of the first kind, and the modulus is

$$k = (1 - k'^2)^{1/2} = \frac{\tan(\alpha 1/2)}{\tan(\alpha 2/2)} \qquad (3.8)$$

The angles $\alpha 1$ and $\alpha 2$ are shown in Figure 3.15.

Input impedance measurements were made of the two antenna systems and of two LTSA antennas on 0.152 mm thick OAK-605 substrates with different taper angles through the aid of a ground plane. The data were taken over a frequency range of 2 to 12 GHz for different styrofoam substrate antennas. The general trend of the impedance locus as a function of frequency was to spiral into some impedance value as the frequency increased, Figure 3.16. Impedance data were collected this way for two types of LTSA antennas. Case 1, shown in Figure 3.17, is for a "two-sided" antenna with equal and opposite tapers on a styrofoam ($\varepsilon_r = 1.02$) substrate. The theoretical curve for this case calculated using the conformal mapping method is also included. The agreement between the calculated and measured values is very good. In case 2, impedance measurements were performed on an antenna with a single sided taper. Shown in Figure 3.18 is the results of these experiments. The measurements of impedance for taper angles of 25, 30, 45 and 60 degrees were achieved with a styrofoam ($\varepsilon_r = 1.02$) substrate and agree well with the theoretical curve. The other two data points represent the measured input impedance of 11.2 and 16.4 degree full taper angle LTSA antennas on 0.127 mm substrates. As can be seen, these have slightly higher

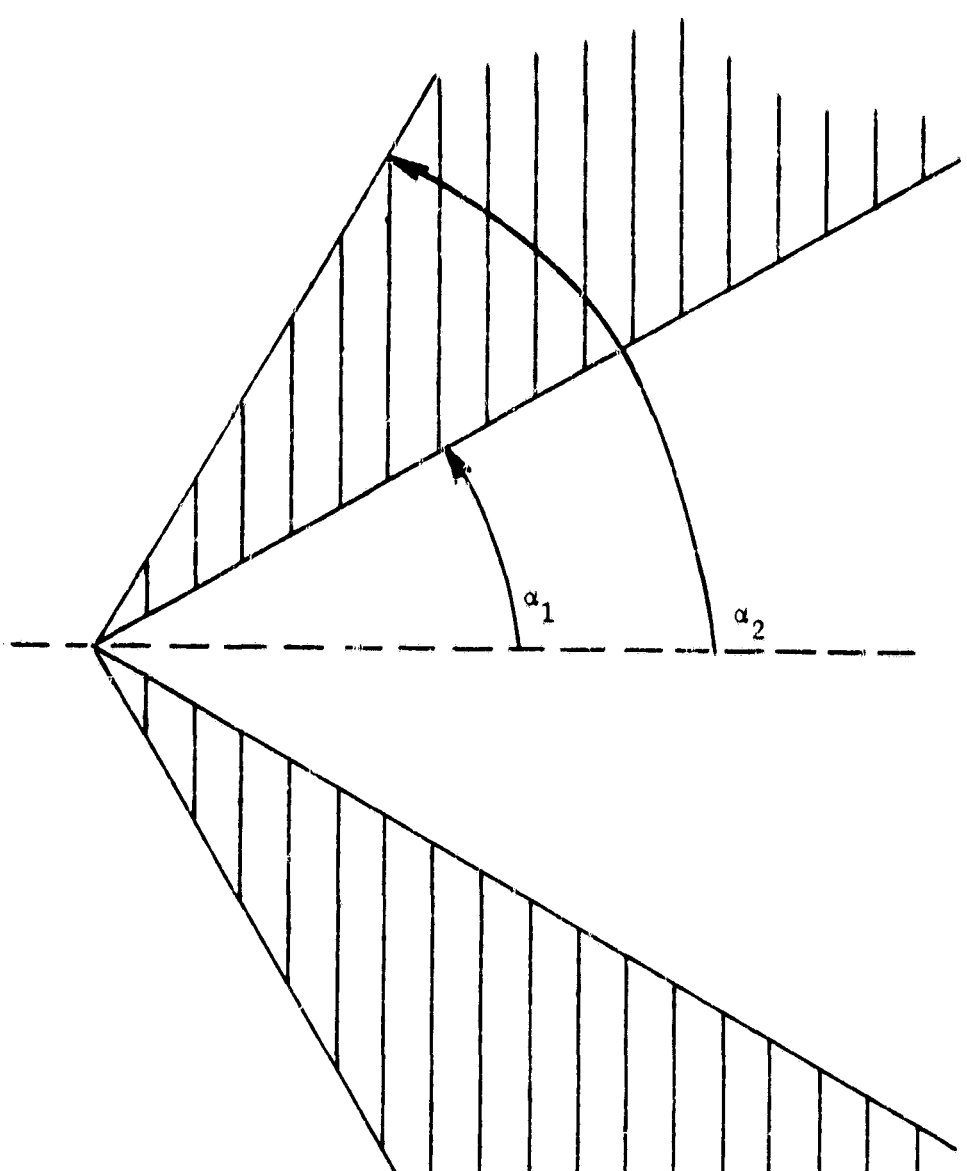

Geometry for computing input impedance
using conformal mapping

Figure 3.15

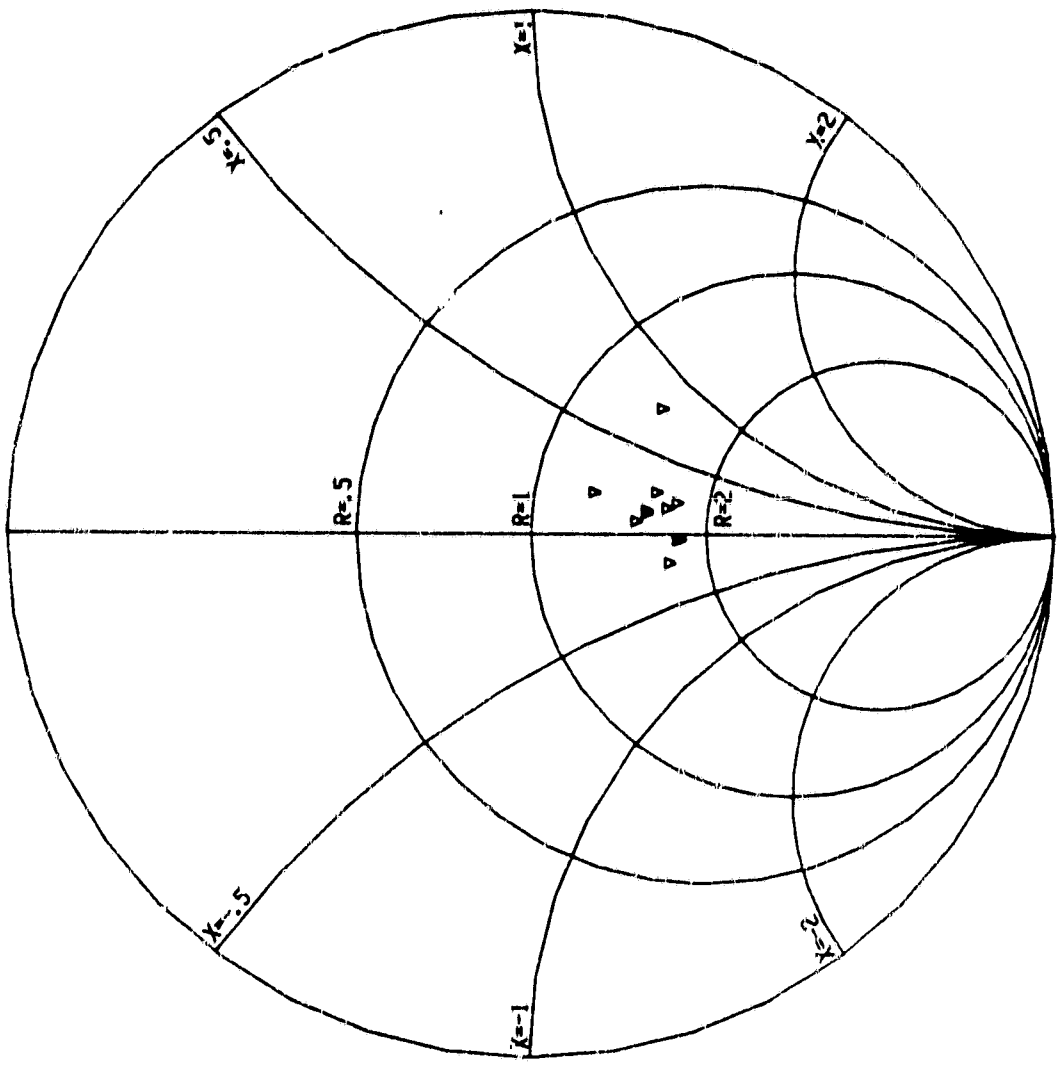

Input impedance locus behavior

Figure 3.16

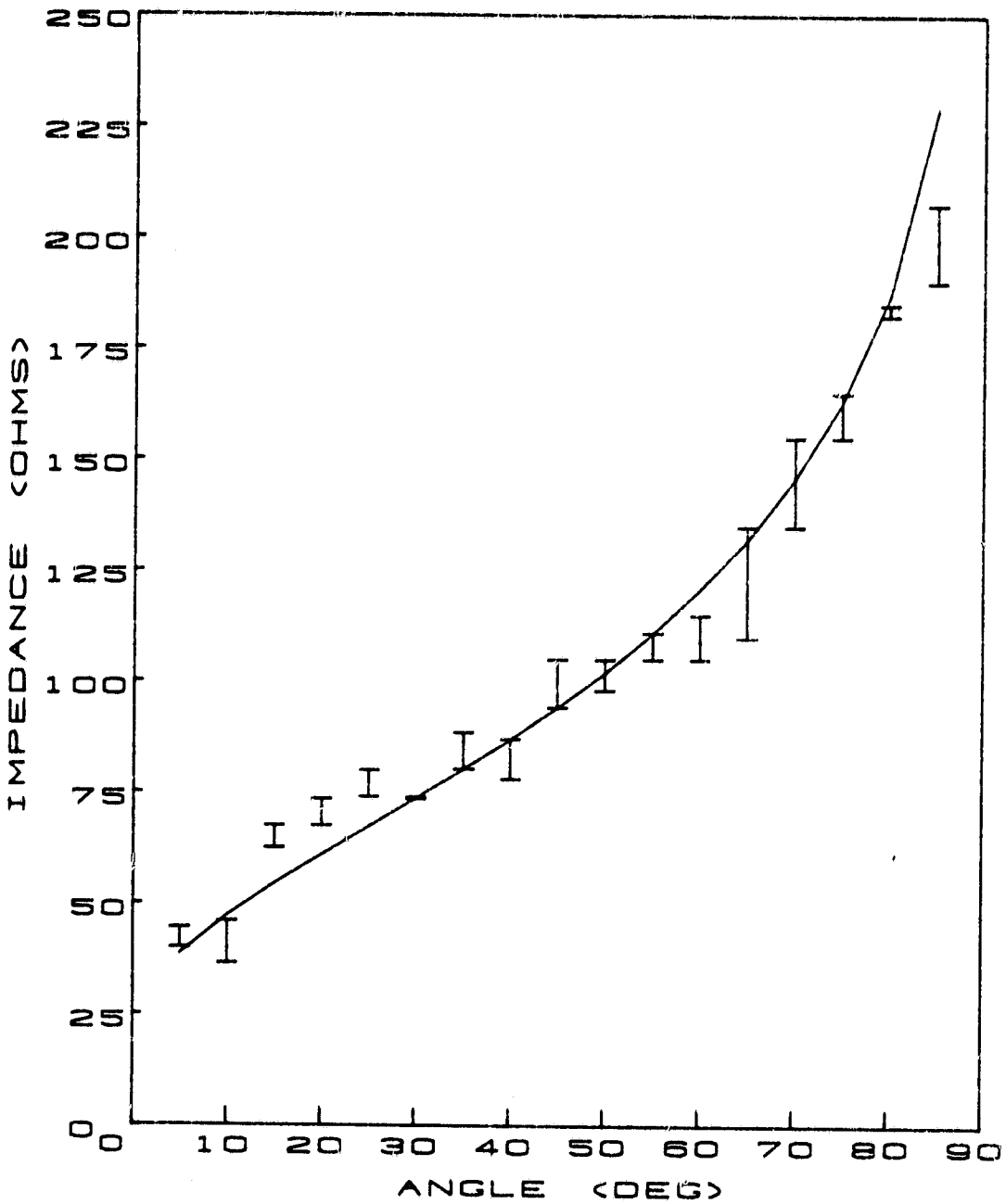

Input impedance of "two sided" antenna

Figure 3.17

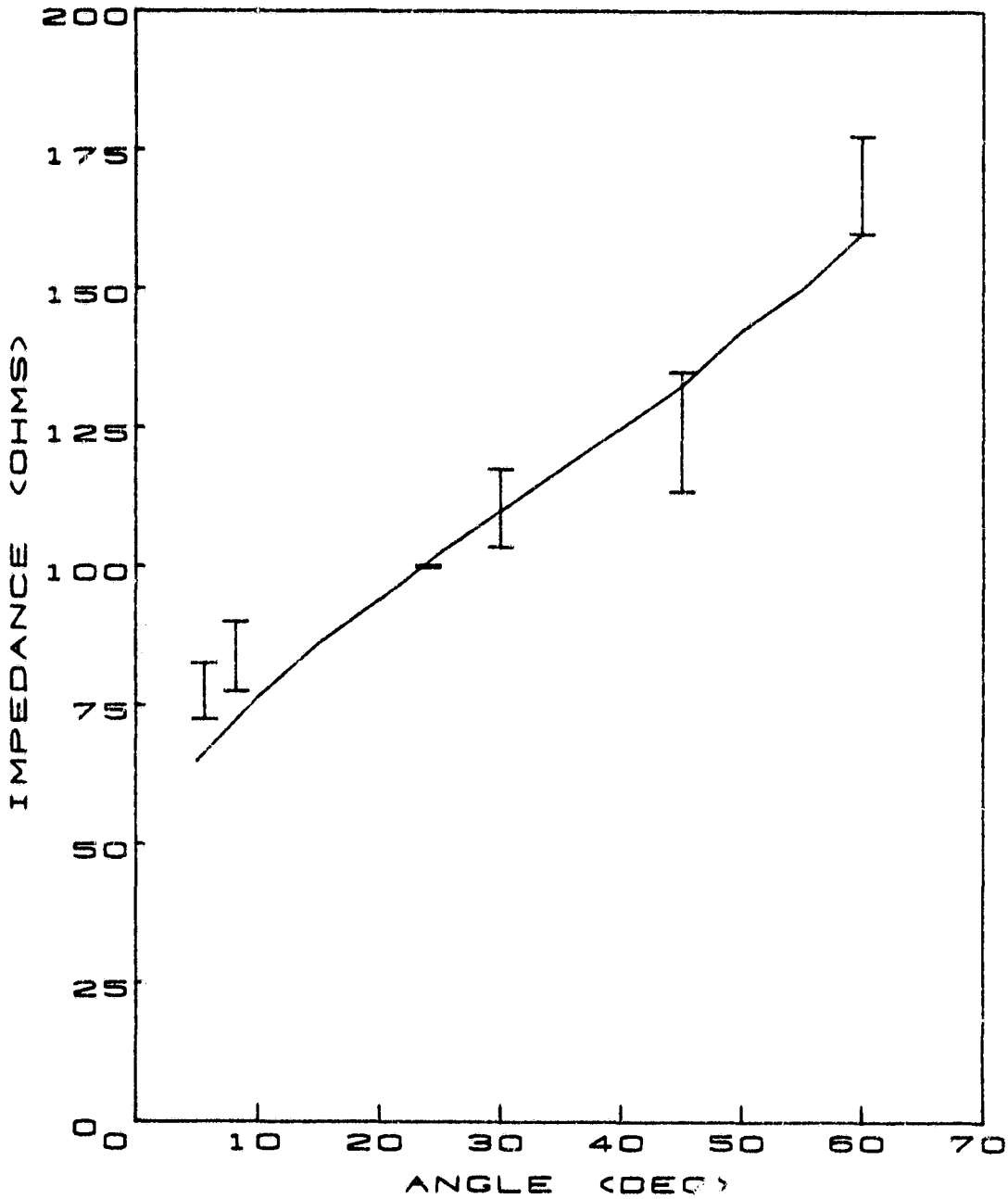

Input impedance of single sided antennas

Figure 3.18

input impedances than expected by the theory which assumes an "air" antenna.

3.5 Conclusion

In this chapter, LTSA elements were studied and a feed antenna design was developed for use as a focal plane receiver element in a f#=1.9 parabolic reflector antenna. Their efficiency and directivity was also studied. It was found that these antennas do not have optimum directivity but do approach to within 2dB of the standard curves.

An "air" LTSA antenna was constructed and measured as a function of length for 3 separate frequencies (8, 10, and 12.4 GHz). It was found that radiation patterns were fairly symmetrical in the E- and H-planes and the half power beamwidths for these 3 different frequencies do follow each other when plotted versus normalized length. They do not, however, follow the standard $v_{ph} = c$ curves indicating that the structure has some dispersion of its own.

Design guidelines were derived which can be summarized as follows: in most cases, LTSA antennas give beamwidths that are in the range expected for TWAs. Further, the dielectric thickness can be used to control primarily the H-plane beamwidth and bring about a roughly symmetrical beam in the E- and H-planes. The effective dielectric thickness (t_{eff}), defined in Eqn. 3.7, should be in the range 0.02 to 0.05 for this to occur. For the smaller values of t_{eff}, beamwidths close to the low sidelobe case are obtained, while increasing t_{eff} yield

beamwidths closer to the high-gain curve. The best agreement with TWA standard data is probably obtained for the 11.2 degree opening angle, for which the majority of the data in this dissertation were taken. If this opening angle is used, TWA standard data, plus the condition on t_{eff} constitute a set of useful guides, which are a major result of the study of single tapered slot-line antenna elements in this dissertation. The implied model of a traveling wave with retarded phase velocity and a uniform, axisymmetrical field distribution, is of course not useful for representing the actual fields in an LTSA antenna. This field distribution is beyond the scope of this dissertation.

C H A P T E R IV

EXPERIMENTAL RESULTS ON ARRAYS OF LTSA ELEMENTS

4.1 Array Radiation Patterns

The environment that an antenna is subjected to can influence its radiation characteristics. This is true of an antenna placed into an array of identical elements. The mutual coupling of the array elements will be contingent on their spacing, normalized to wavelengths. As antenna elements are brought closer together, their fields will increasingly overlap and tighter coupling occur. When this happens, the radiation patterns of the elements will also be altered. One way to investigate empirically these effects is to array a known element and study the radiation patterns of the elements while in that array, using different element spacings and configurations.

Arrays of LTSA elements can be arranged with different packing densities which keep constant the first nearest neighbor distance. Two possible systems of closest packing are shown in Figure 4.1. In the square configuration shown in Figure 4.1a an internal element has 4 nearest neighbors, while the hexagonal array in Figure 4.1b has 6 nearest neighbors. Using the LTSA's center position as a centroid, one sees that the second configuration offers more efficient coverage of elements for a given inter-element spacing, if one uses a circular aperture.

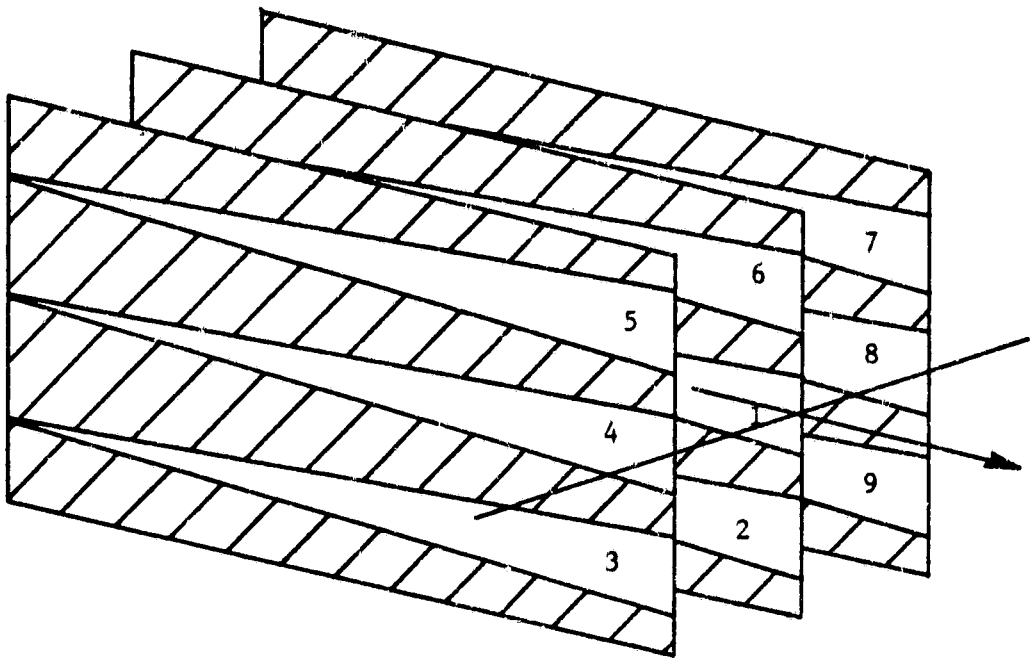

LTSA array with square symmetry

Figure 4.1a

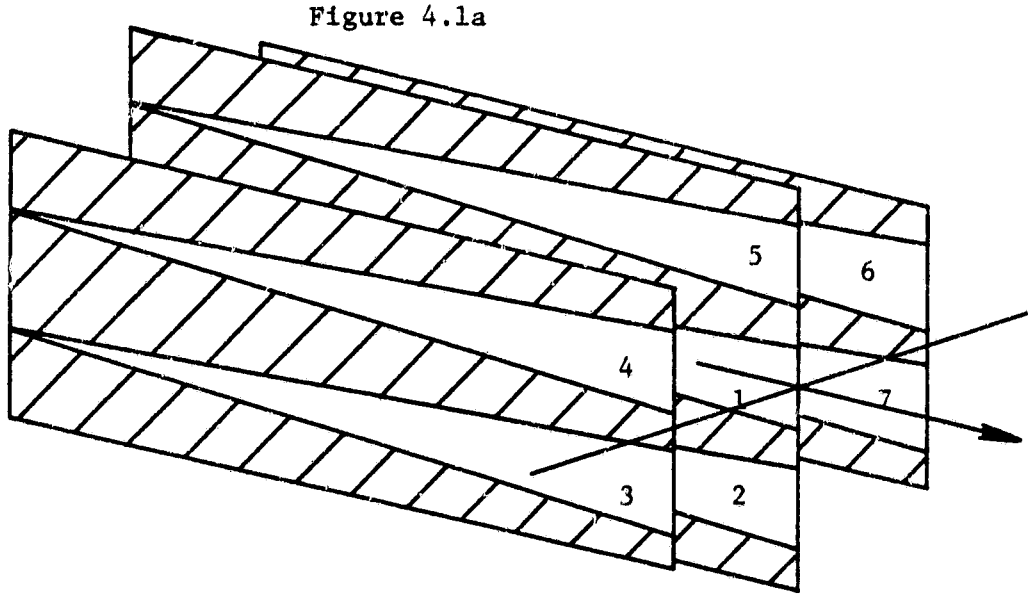

LTSA array with hexagonal symmetry

Figure 4.1b

To investigate the extent of the effects the neighbors have on an LTSA antenna radiation pattern, linear and two-dimensional arrays of these antennas were constructed. Single elements were characterized and subsequently placed into linear 3 element arrays on a single substrate. Radiation patterns were taken over frequency for a single antenna on a 0.15 mm thick Duroid substrate of 11.2 degree full taper angle and 22.9 cm length, as well the same antenna arrayed in the E-plane with a 7.62 cm spacing (as discussed in Chapter III, this single element antenna met the specifications for the prototype imaging system). Figure 4.2 contains representative radiation patterns of the single and arrayed elements at 10 GHz. The 3 and 10dB beamwidths of these antennas taken versus frequency are plotted in Figures 4.3 and 4.4 respectively, and indicate that the arrayed elements are affected only slightly, showing some widening of the 10 dB beamwidth in the H-plane at all lengths, and a widening of the 3 dB E-plane beamwidth for electrically short antennas.

Three of these 3 element substrates were subsequently arrayed in the H-plane with a 7.62 cm spacing and measured over frequency. The 3dB and 10dB beamwidths for the center middle and lower, and left center elements of the array, elements number 1, 2, and 4 in Figure 4.1a, are shown plotted in Figures 4.5 and 4.6, respectively, compared with the single LTSA element beamwidths. As seen previously, the H-plane beamwidths have been broadened by the arraying process while the E-plane beamwidth has suffered only minor changes. The E- and H-plane radiation

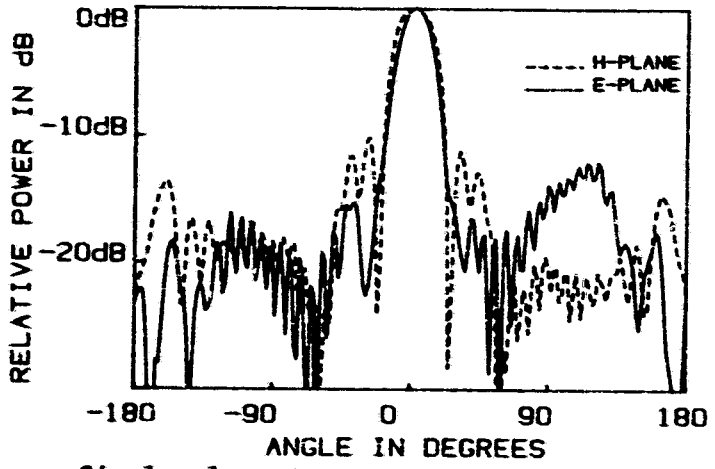

Single element pattern

Figure 4.2a

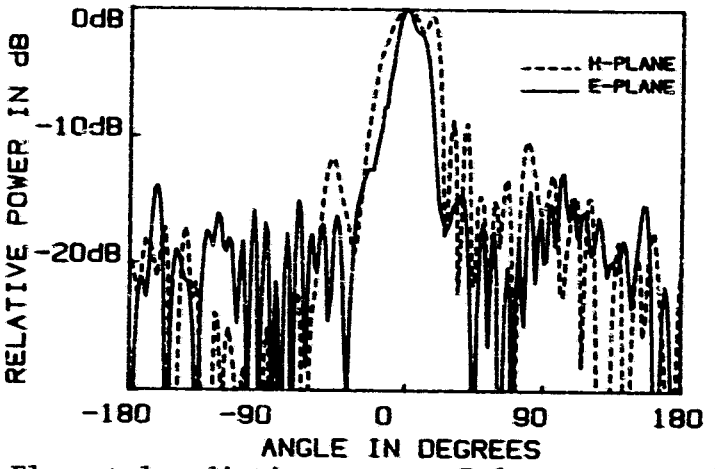

Element 1 radiation pattern 7.6 cm spacing ("LEFT" element)

Figure 4.2b

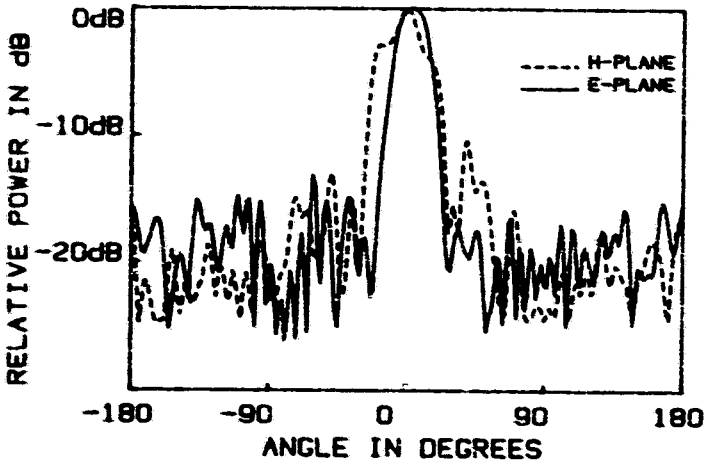

Element 2 radiation pattern 7.6 cm spacing ("CENTER" element)

Figure 4.2c

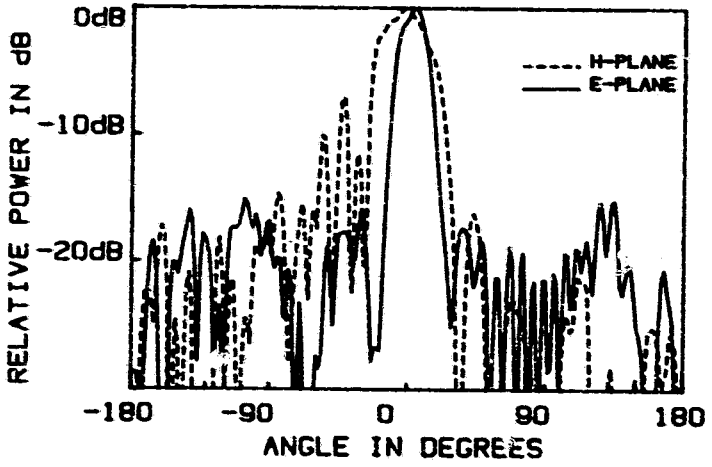

Element 3 radiation pattern 7.6 cm spacing ("RIGHT" element)

Figure 4.2d

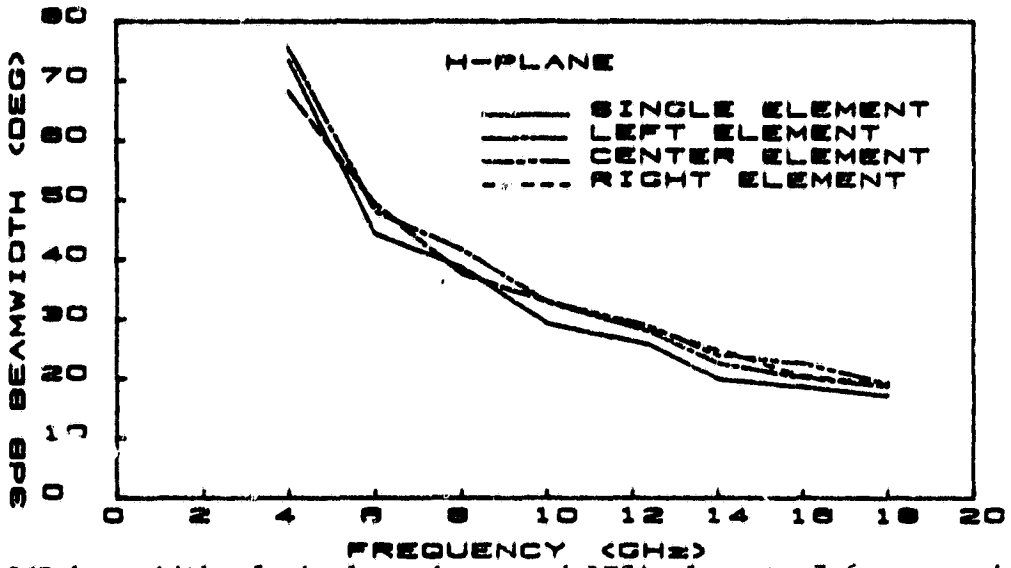

3dB beamwidth of single and arrayed LTSA elements 7.6 cm spacing

Figure 4.3a

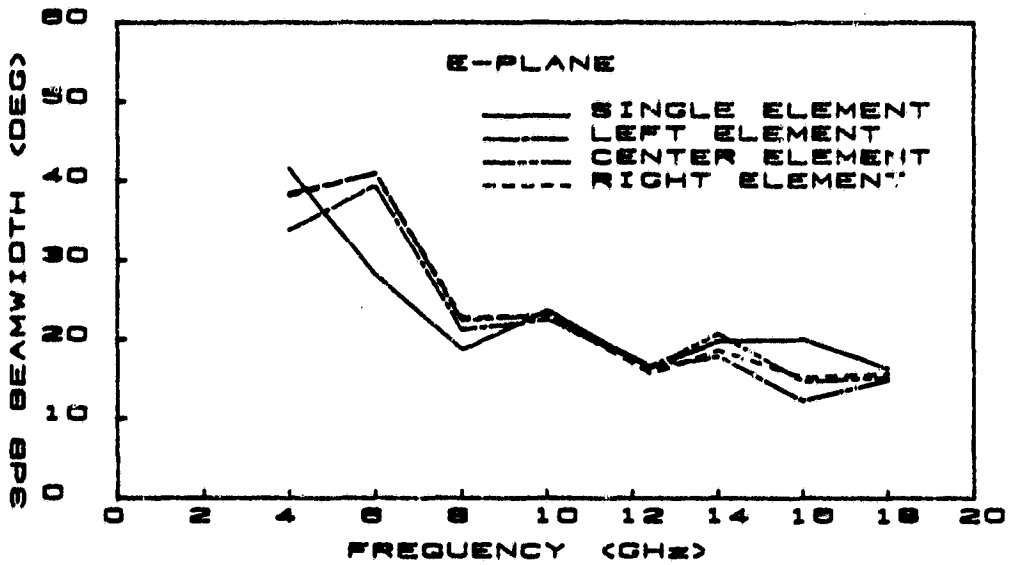

3dB beamwidth of single and arrayed elements 7.6 cm spacing

Figure 4.3b

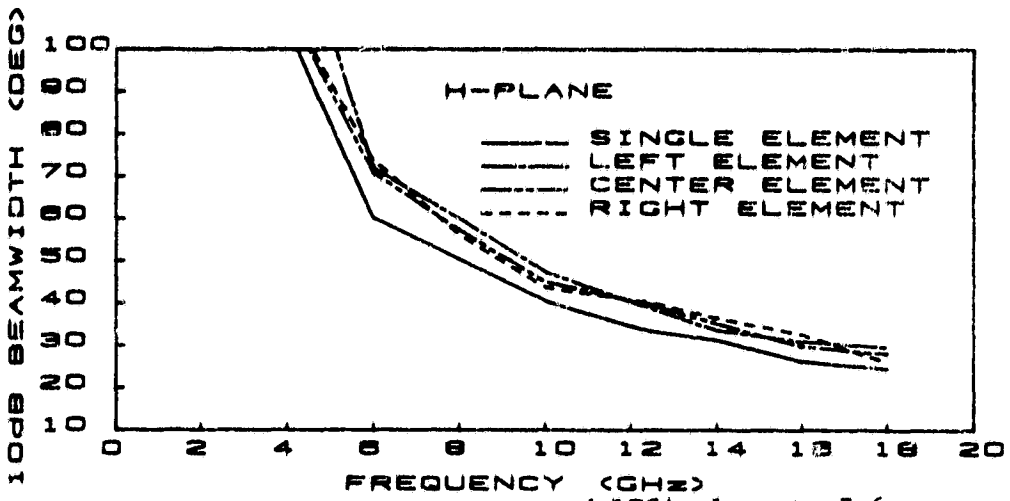

10dB beamwidth of single and arrayed LTSA elements 7.6 cm spacing

Figure 4.4a

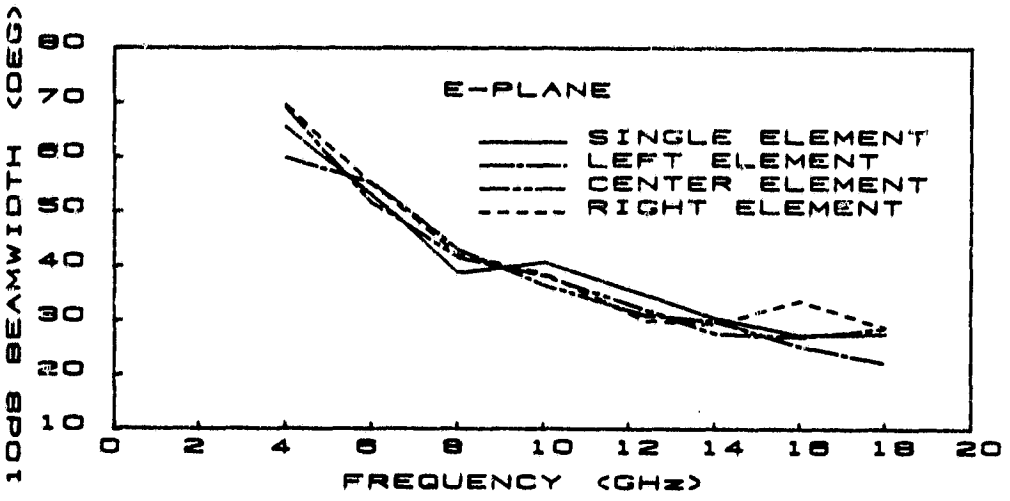

10dB beamwidth of single and arrayed LTSA elements 7.6 cm spacing

Figure 4.4b

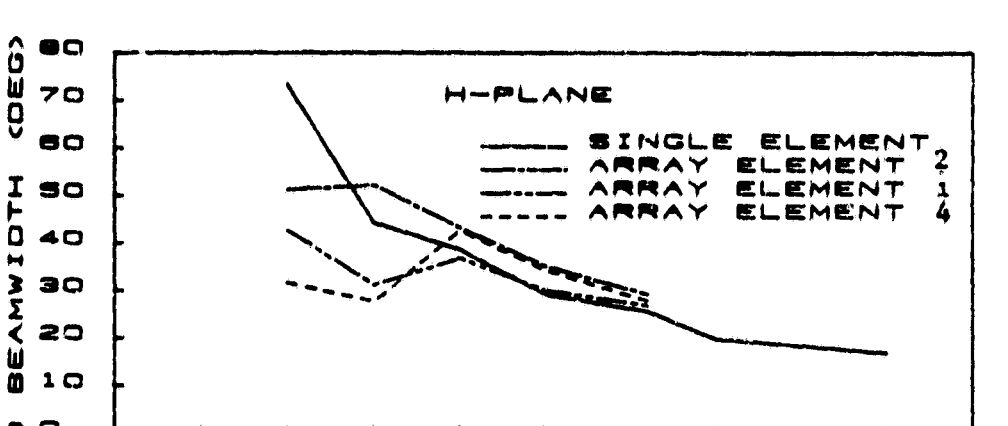

3dB beamwidth of single and arrayed LTSA elements 7.62 cm spacing

Figure 4.5a

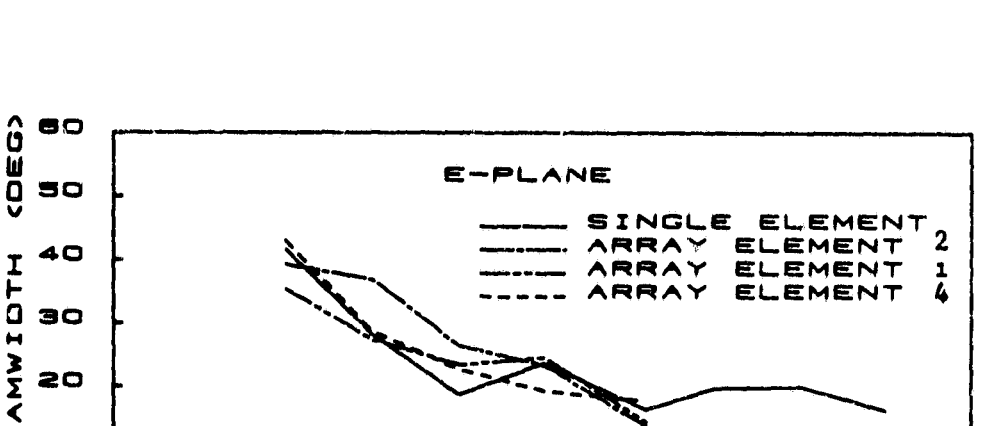

3dB beamwidth of single and arrayed LTSA elements 7.62 cm spacing

Figure 4.5b

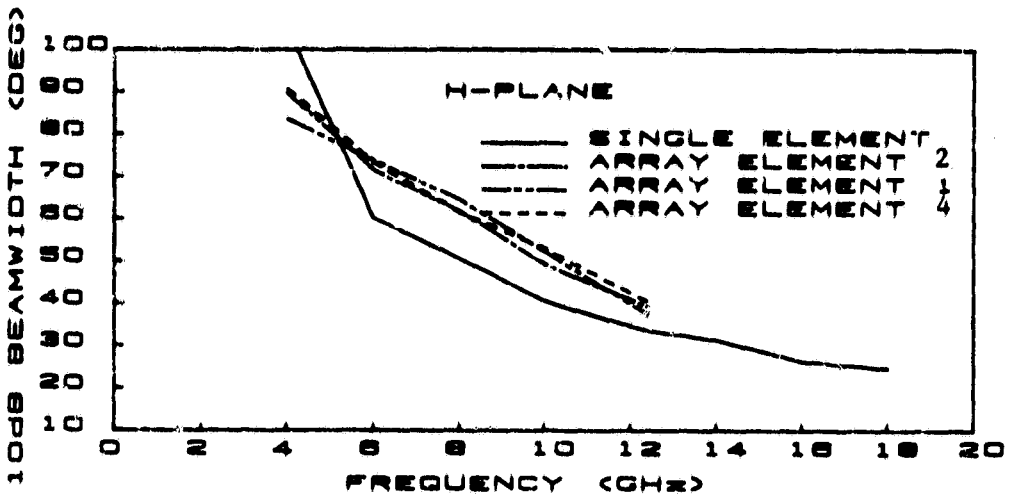

10dB beamwidth of single and arrayed LTSA elements 5.06 cm spacing

Figure 4.6a

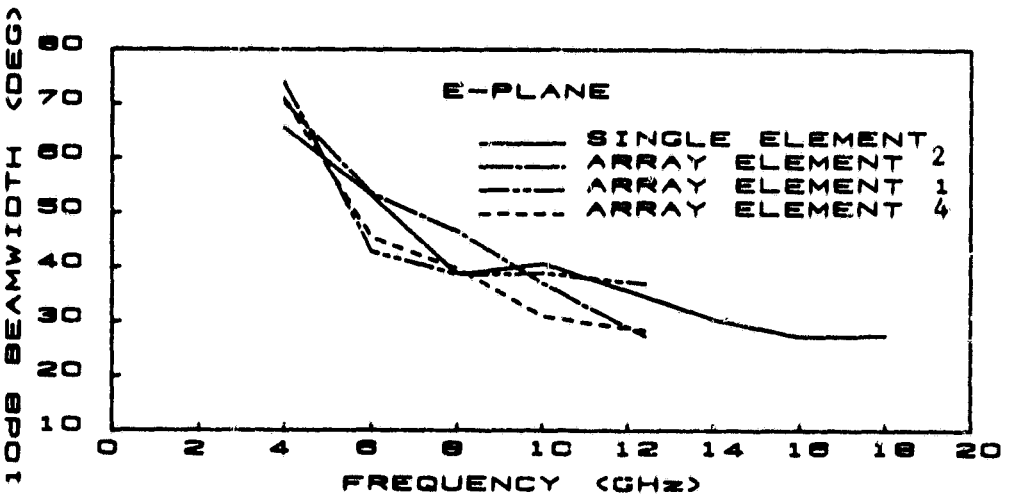

10dB beamwidth of single and arrayed LTSA elements 5.06 cm spacing

Figure 4.6b

patterns for the single and arrayed elements of length $10\lambda_o$ are shown in Figure 4.7.

Another 2-dimensional array of LTSA elements was formed from these 3 element substrates, this time with a 5.08 cm H-plane spacing, and E-plane spacing of 7.62 cm as before. Figures 4.8 and 4.9 show the drastic effect on beamwidth this closer spacing has for the measured frequency range. Although the E-plane half power beamwidth appears to be fairly unaffected, the H-plane beam shows a broadening trend similar to that seen in the thick low dielectric constant substrate cases. In both the E- and H-planes the 10dB beamwidths have broadened noticeably for the 10 wavelength antenna. At longer lengths than $10\lambda_o$, broadening by as much as a factor of two is seen in the H-plane, but no effect in the E-plane. Thus, coupling between the array elements is severe at this distance with the 30 degree beam efficiency degrading appreciably.

Arrays of LTSA elements were fabricated to operate at 94 GHz on 0.025 mm Kapton substrates. Using the X-band models as a guide, arrays were designed with 7.9 mm and 5 mm spacings from 11.2 degree LTSA elements. The 7.9 mm spaced antennas were originally made 3.43 cm long and trimmed in length until they attained approximately 30 degree 10 dB beamwidth in both planes. Both square symmetry and hexagonal symmetry arrays were constructed and tested at 94 GHz. In the case of the arrays with 5mm spacing, the maximum length for an 11.2 degree antenna, i.e. when the antennas began to touch each other, was 2.54 cm. Thus, larger than optimum beamwidths and therefore, lower beam efficiencies will have

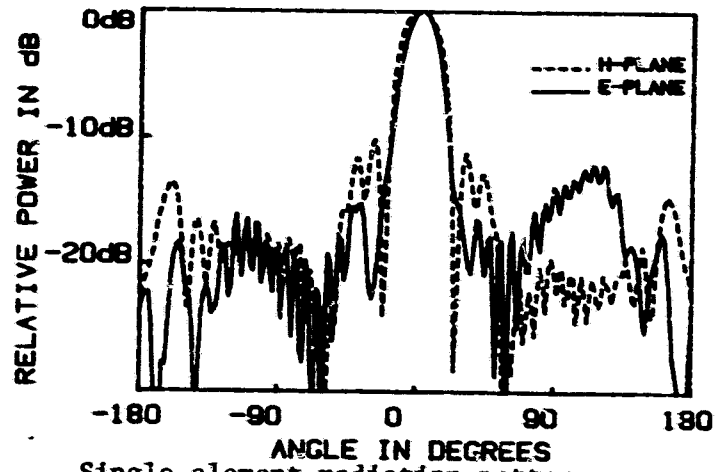

Single element radiation patterns

Figure 4.7a

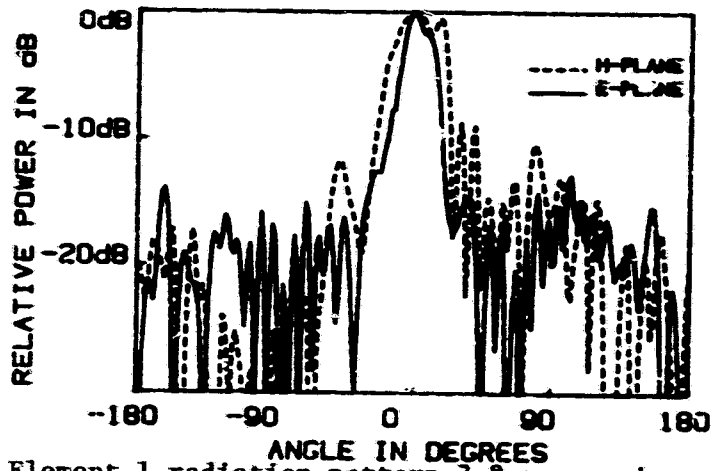

Element 1 radiation pattern 7.6 cm spacing

Figure 4.7b

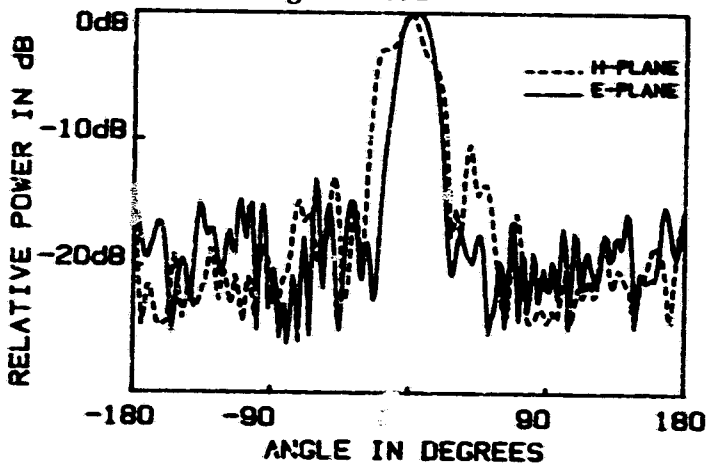

Element 2 radiation pattern 7.6 cm spacing

Figure 4.7c

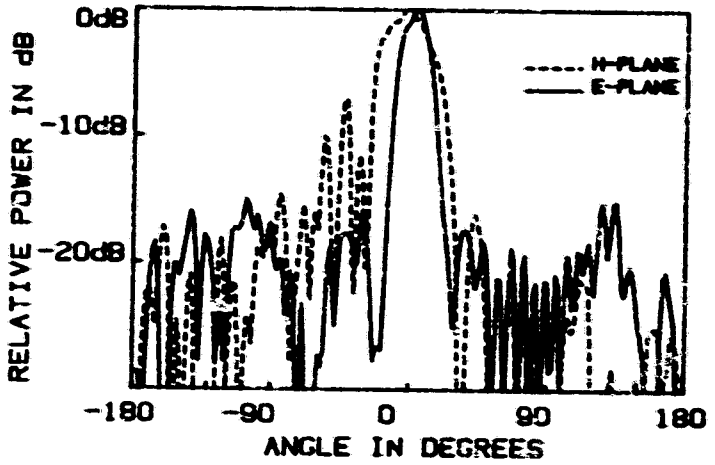

Element 4 radiation pattern 7.6 cm spacing

Figure 4.7d

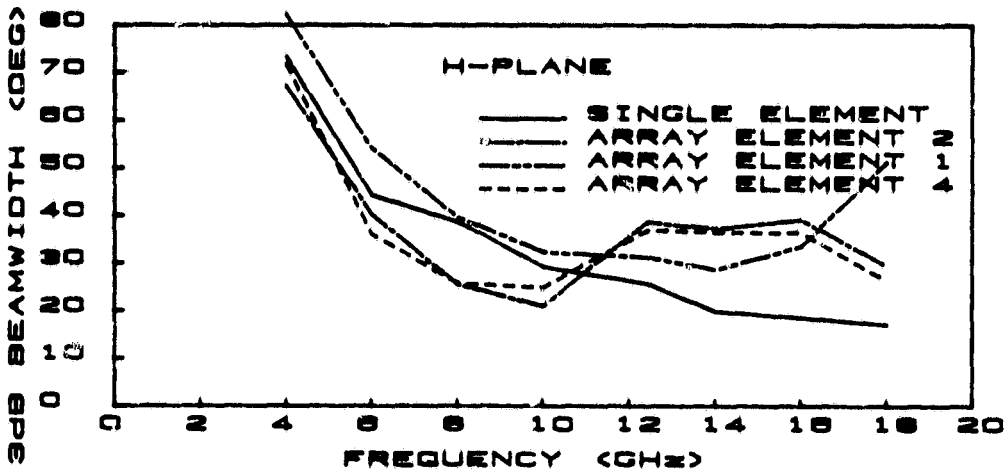

3dB beamwidth of single and arrayed LTSA elements 5.08 cm spacing

Figure 4.8a

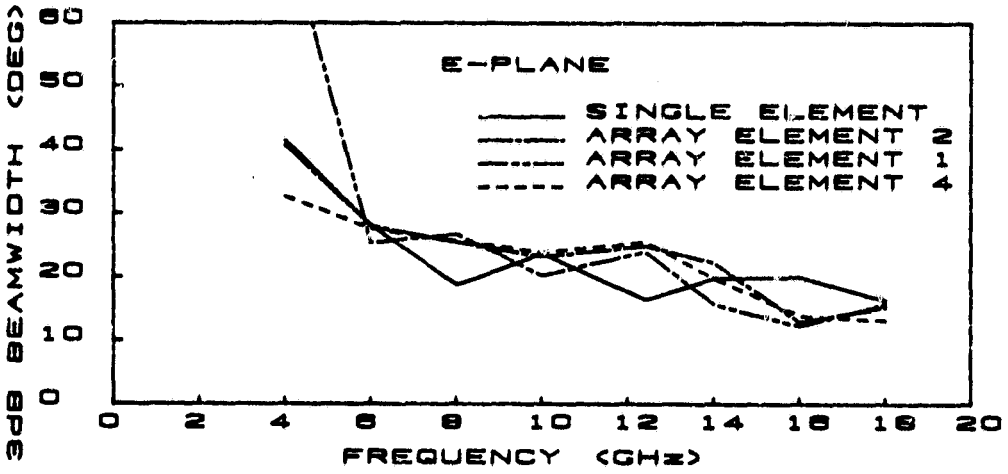

3dB beamwidth of single and arrayed LTSA elements 5.08 cm spacing

Figure 4.8b

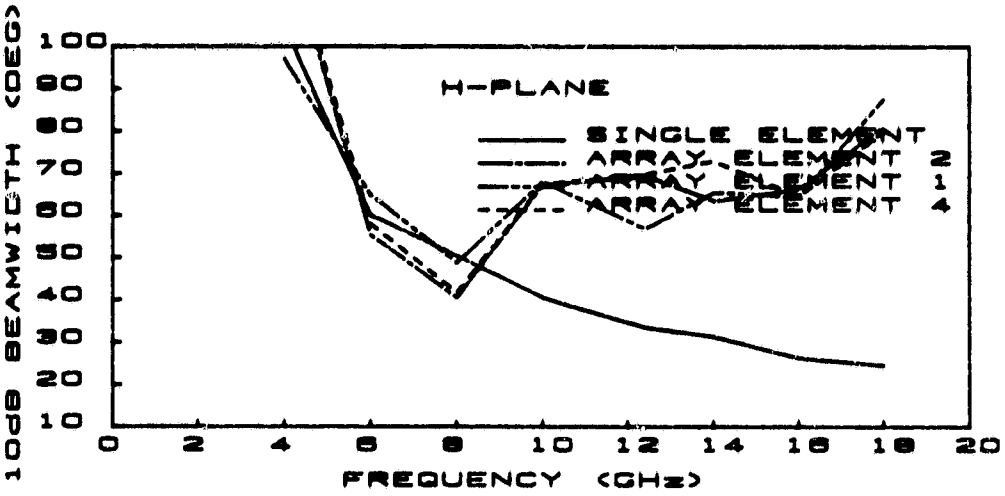

10dB beamwidth of single and arrayed LTSA elements 5.08 cm spacing

Figure 4.9a

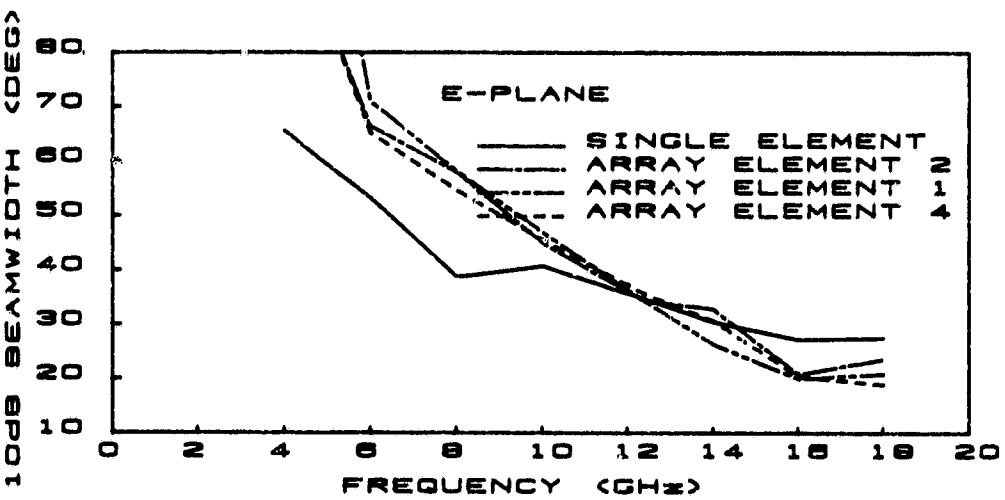

10dB beamwidth of single and arrayed LTSA elements 5.08 cm spacing

Figure 4.9b

to be tolerated if these 5mm spaced arrays are used in this f# = 1.9 Cassegrain imaging systems.

Shown in Figure 4.10 are the radiation patterns at 94 GHz for elements 1, 2, and 3, in a hexagonal symmetry array, see Figure 4.1b, with 7.9 mm spacing. Also shown is the pattern of an identical single LTSA element. The main beam has not been noticeably affected by the arraying process. Note, however, that the two first sidelobes in the H-plane, visible in the single element pattern, have decreased substantially in the array--a beneficial feature. A second array using the square symmetry design of Figure 4.1a was also constructed with these elements and the first nearest neighbor distance was kept at 7.9 mm. Shown in Figure 4.11 are the radiation patterns for the middle, bottom center, and left side center elements of this array (element numbers 1, 2, and 4 in Figure 4.1a). Only the element displaced in the H-plane has been noticeably affected. One explanation for this revolves around the fact that this element has only one H-plane neighbor whereas the other 2 elements are sandwiched between two other substrates. Hence the center elements can be expected to excite both its neighbors in an identical way, helping to keep the radiation patterns symmetrical. Table 4.1 contains the 3 and 10 dB beamwidths for these elements in both array configurations. One can see that for all cases the half power beamwidths have narrowed slightly when arrayed, and elements 1 and 2 have narrower 10 dB beamwidths, while element 3 has a broader 10 dB beamwidth in the H-plane.

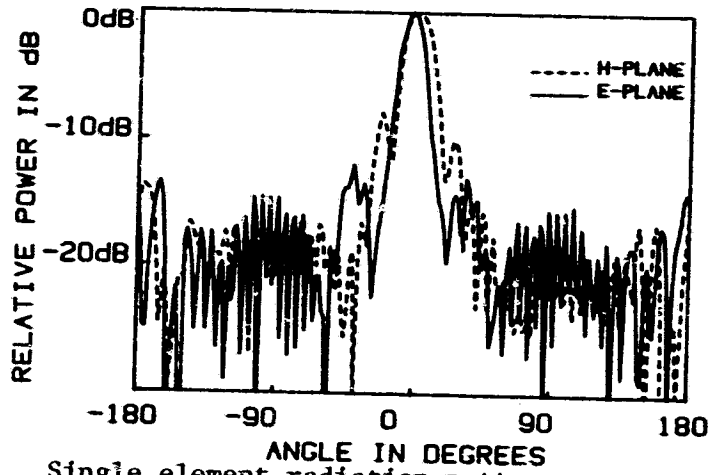

Single element radiation patterns

Figure 4.10a

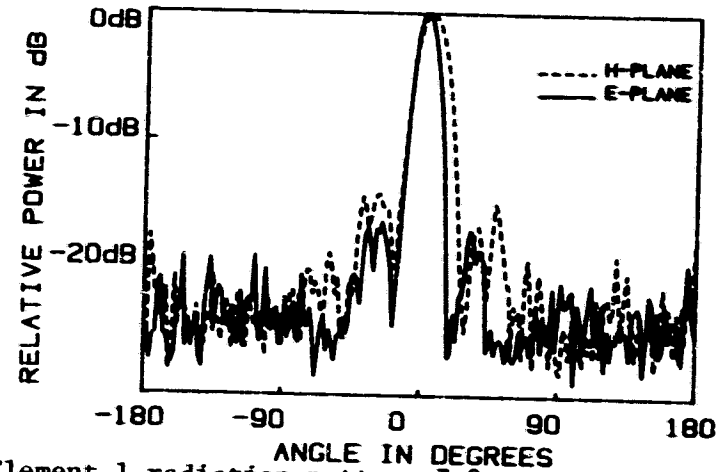

Element 1 radiation pattern 7.9 mm spacing

Figure 4.10b

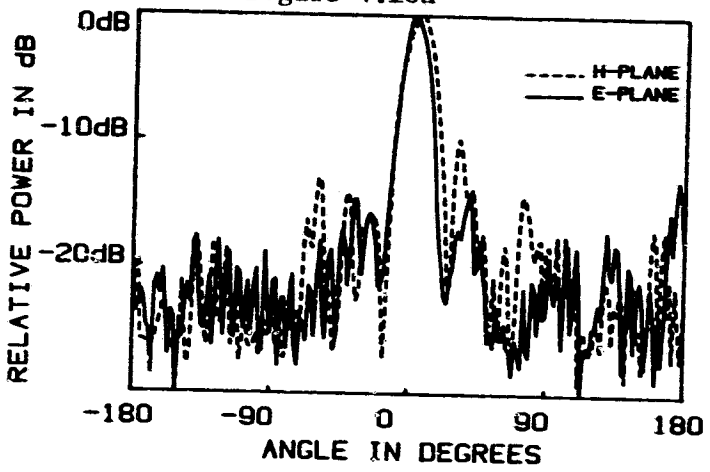

Element 2 radiation pattern 7.9 mm spacing

Figure 4.10c

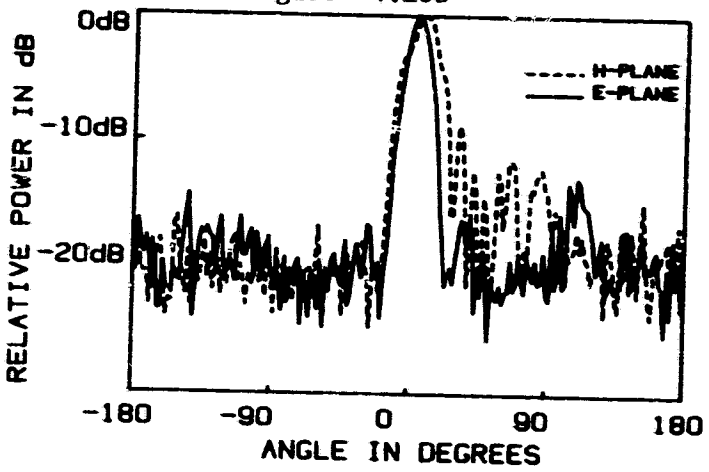

Element 3 radiation pattern 7.9 mm spacing

Figure 4.10d

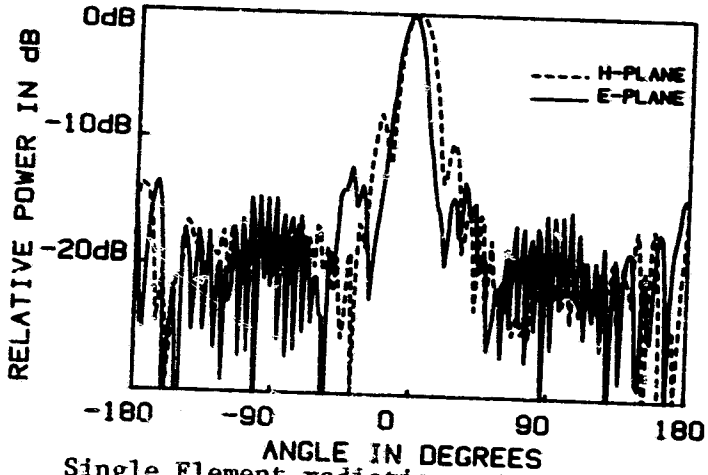

Single Element radiation pattern

Figure 4.11a

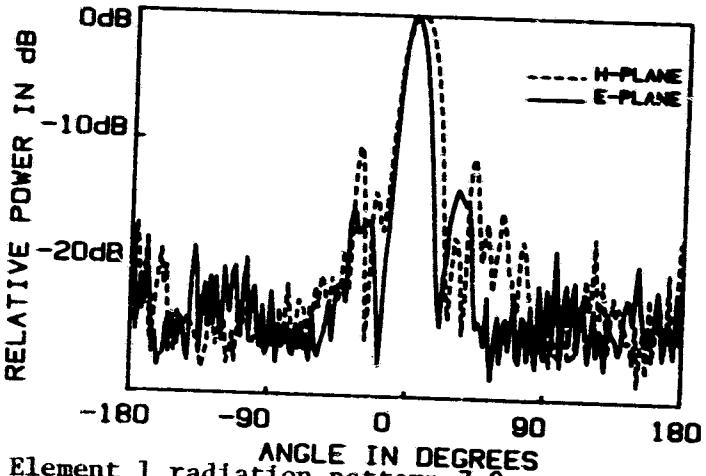

Element 1 radiation pattern 7.9 mm spacing

Figure 4.11b

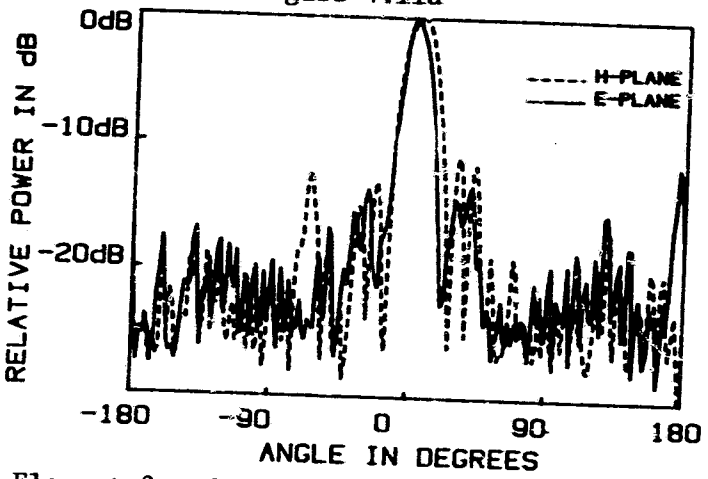

Element 2 radiation pattern 7.9 mm spacing

Figure 4.11c

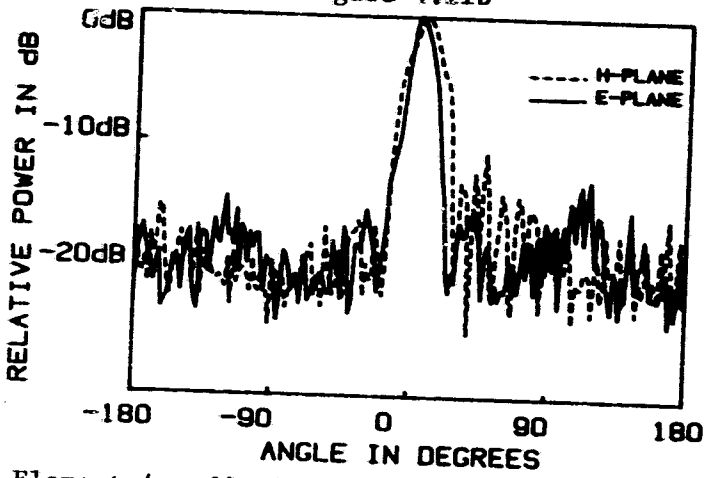

Element 4 radiation pattern 7.9 mm spacing

Figure 4.11d

ARRAY SYMMETRY	ELEMENT POSITION	H-PLANE 3dB	H-PLANE 10dB	E-PLANE 3dB	E-PLANE 10dB
Single Element		20.30	32.44	16.55	30.50
Hexagonal	1	19.95	31.64	13.02	22.99
Hexagonal	2	19.48	31.59	14.15	25.97
Hexagonal	3	19.61	38.30	13.93	27.05
Square	1	18.80	31.35	13.55	23.67
Square	2	17.32	30.40	14.20	25.87
Square	4	19.24	32.86	14.09	27.48

Beamwidths of LTSA elements in array with 7.9 mm spacing

Table 4.1

Another pair of arrays was constructed from these LTSA elements with a 5 mm next nearest neighbor spacing. Radiation patterns for these elements for the hexagonal and square symmetries are shown in Figures 4.12 and 4.13 respectively. It should be reiterated that these elements are by necessity shorter than the optimum length, only 2.54 cm long, thus the beamwidths are larger than what was seen for the 7.9 mm arrays. In this case elements 1 and 2 for both arrays are located on the central substrate and their radiation patterns have changed drastically from the single element; for example, they show a double peak in the H-plane. Table 4.2 includes the 3 and 10 dB beamwidths for these arrayed elements as well as for an identical single LTSA elements. In this case the 10dB beamwidths can be seen to have broadened. For the center substrate, most of the beam in the E-plane actually has narrowed, and the larger beamwidths recorded at the -10dB level are due to sidelobes, which have increased above -10dB. In general E-plane beamwidths have narrowed.

As a conclusion of these measurements, the 7.9 mm spacing (in the 94 GHz case) yields element patterns for all elements which are acceptably symmetric in the E- and H-planes. The 5 mm spacing array still yields useable element patterns, but would not illuminate the prototype f/D=1.9 Cassegrain system at the optimum taper, especially in the H-plane where the edge taper is close to -3dB. Larger sidelobes and increased spillover would be expected if one were to use the smaller spacing array in the prototype system.

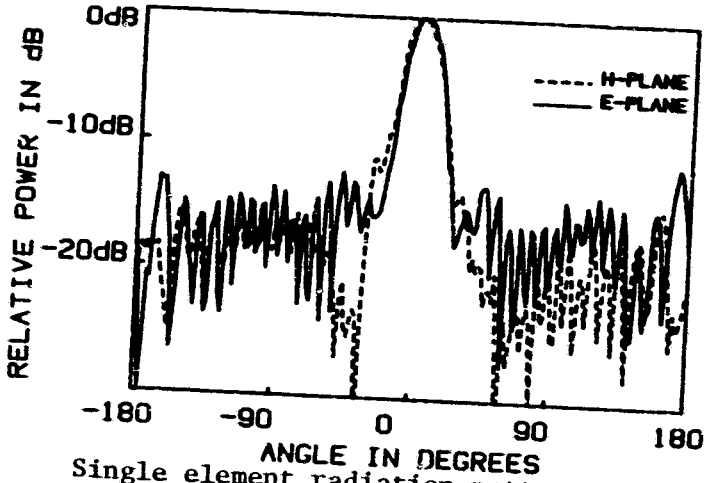

Single element radiation pattern

Figure 4.12a

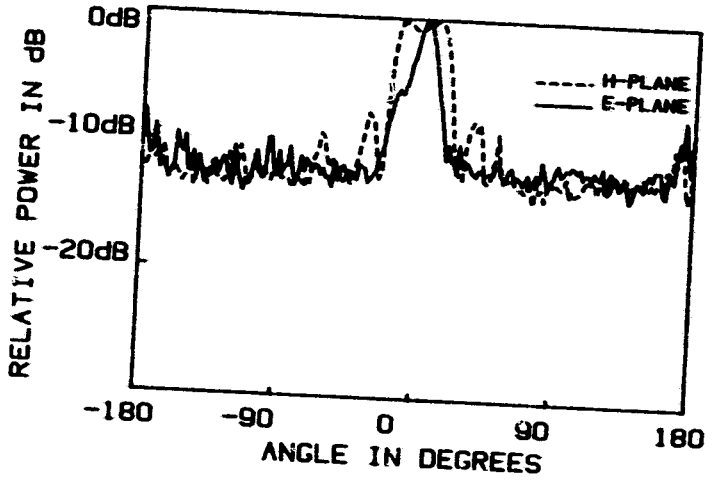

Element 2 radiation pattern 5.0 mm spacing

Figure 4.12c

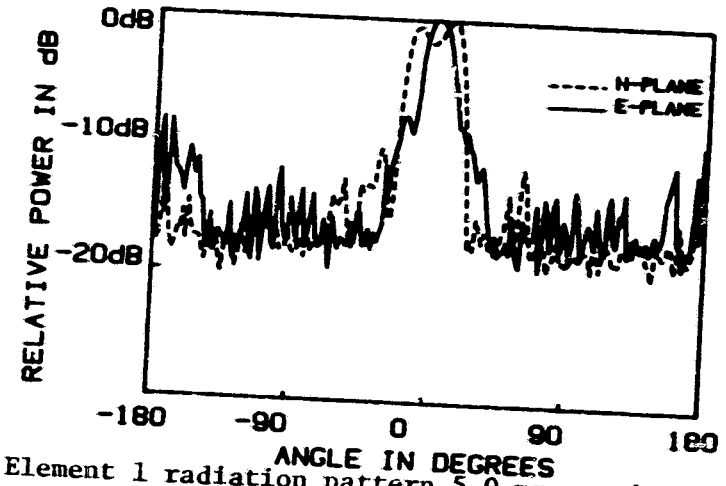

Element 1 radiation pattern 5.0 mm spacing

Figure 4.12b

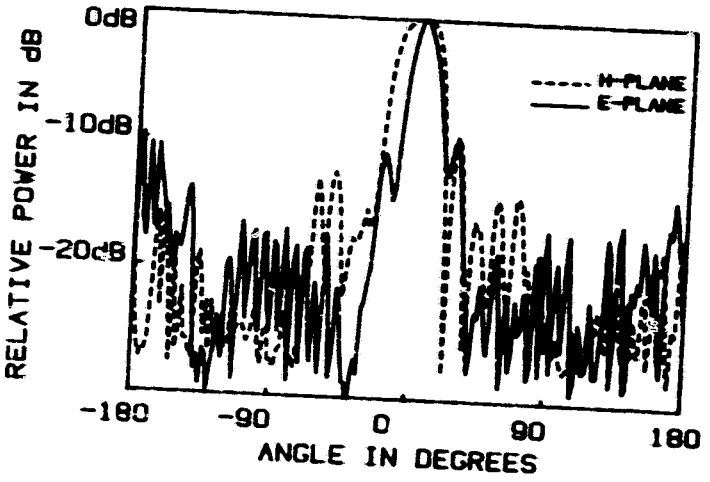

Element 3 radiation pattern 5.0 mm spacing

Figure 4.12d

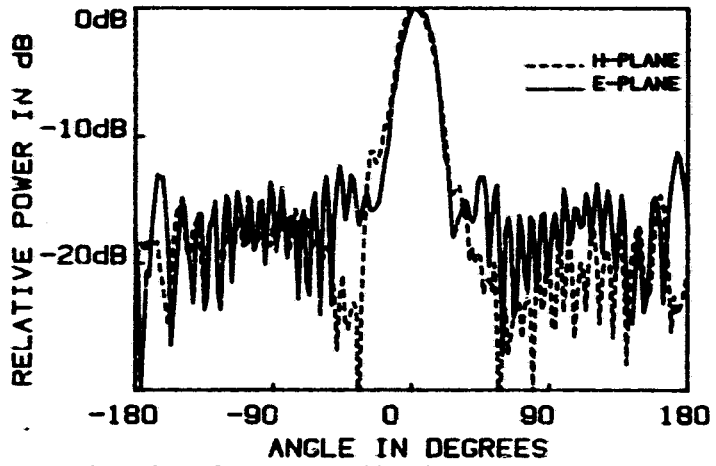

Single element radiation pattern

Figure 4.13a

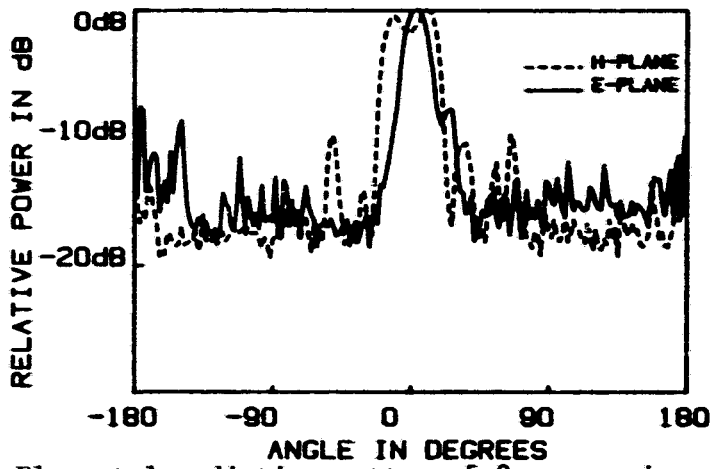

Element 1 radiation pattern 5.0 mm spacing

Figure 4.13b

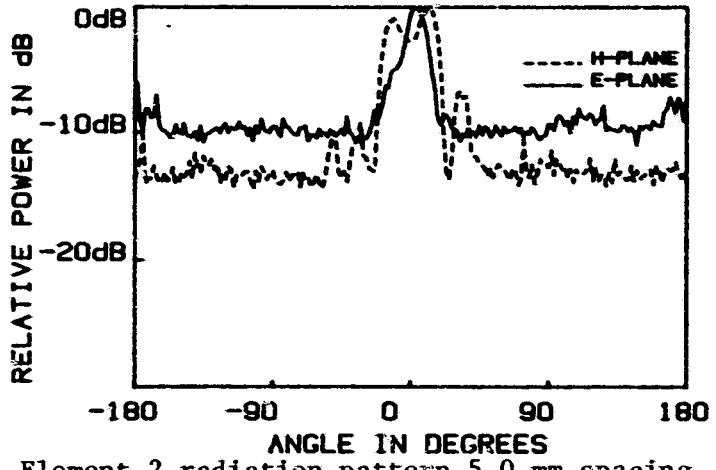

Element 2 radiation pattern 5.0 mm spacing

Figure 4.13c

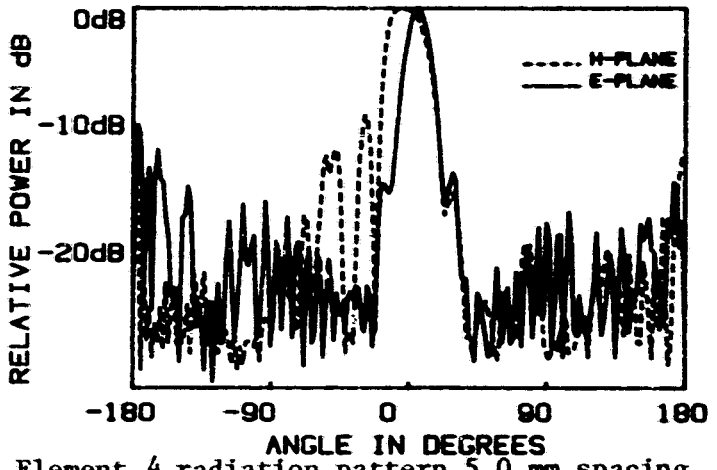

Element 4 radiation pattern 5.0 mm spacing

Figure 4.13d

ARRAY SYMMETRY	ELEMENT POSITION	H-PLANE 3dB	H-PLANE 10dB	E-PLANE 3dB	E-PLANE 10dB
Single Element		25.65	42.39	35.34	37.98
Hexagonal	1	36.41	45.25	18.87	48.54
Hexagonal	2	36.10	45.28	13.79	39.24
Hexagonal	3	30.27	41.01	15.83	28.81
Square	1	36.24	44.78	17.24	41.26
Square	2	36.16	43.83	15.60	57.31
Square	4	26.74	38.70	14.64	27.73

Beamwidths of LTSA elements in array with 5.0 mm spacing

Table 4.2

4.2 Mutual Impedance

Another property of interest, which can be affected by the arraying process, is the input impedance of the antennas. The simplified two port circuit shown in Figure 4.14 can be used to model the two antenna systems. This circuit has the current voltage relations:

$$V_1 = Z_{11} I_1 + Z_{12} I_2$$
$$V_2 = Z_{21} I_1 + Z_{22} I_2 \qquad (4.1)$$

These equations can be rewritten in form

$$Z_1 = \frac{V_1}{I_1} = Z_{11} + Z_{12} \frac{I_2}{I_1}$$
$$Z_2 = \frac{V_2}{I_2} = Z_{22} + Z_{21} \frac{I_1}{I_2} \qquad (4.2)$$

where Z_1 and Z_2 are the driving point impedances of the two antennas. When the elements are identical, the self impedances Z_{11} and Z_{22} are equal. Also, because of reciprocity, the mutual impedances Z_{12} and Z_{21} are equal. It can be seen from the above that the mutual impedance can be derived by measuring the input impedance of element 1 while element 2 is alternately open and then short circuited [16]. The first measurement reveals the self impedance of the element, while the second measurement is that of the driving point impedance. Under the above conditions it can be shown that the mutual impedance is

$$Z_{12} = (Z_{11} (Z_{11} - Z_1))^{1/2} \qquad (4.3)$$

Input impedance measurements were conducted on a one and a half element array (a previously described array on 0.15 mm Duroid, cut in

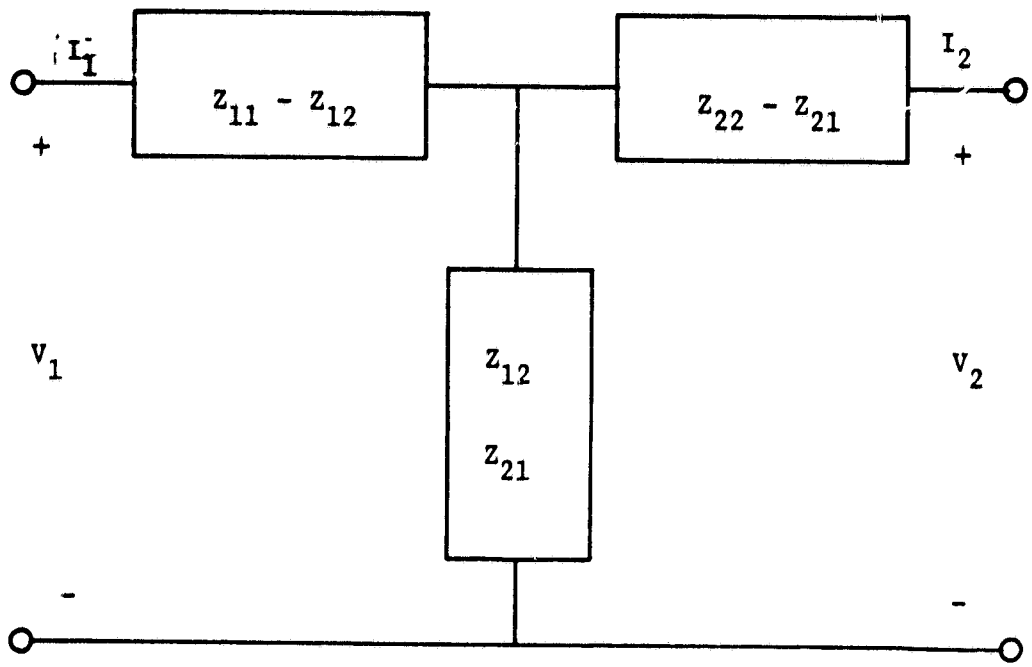

Two port circuit model

Figure 4.14

half) over a ground plane. The input of the half antenna was connected to a coaxial connector through the ground plane and a vector network analyzer used to make the impedance measurements directly. Impedance data taken using this method was obtained over the frequency band of 2.0 to 12.4 GHz.

H-plane arrays were made from LTSA antennas with 11.2 degree taper angle and 25.4 cm length on 0.153 mm thick OAK-605 substrates. Differences between the driving point and self impedance could only be seen for frequencies less than 4 GHz for the 7.62 cm spacing case and below 6 GHz for the 5.08 cm spacing case.

To conclude, measurable coupling in the H-plane occurs when the antennas have less than a wavelength spacing. Similar results were also obtained for an E-plane array with 7.62 cm spacing. Since the spacings used in the 94 GHz imaging arrays were scaled from these values (5 and 7.9 mm, respectively, for a wavelength of 3.19 mm), we do not expect the mutual impedance to give any observable effects on the array performance.

CHAPTER V

IMAGING ARRAY ANTENNA

5.1 Overview

Imaging systems may be described in terms of spatial frequency distribution. Thus, one deals in the Fourier domain when describing the properties of the optical transfer function of the system. A generalized imaging system is shown in Figure 5.1. In this system, the object is transformed by a function $H(f_x,f_y)$ onto an image plane [17]. This function $H(f_x,f_y)$ relates the spatial frequencies of the image to those of the object and the absolute magnitude of H is called the optical transfer function of the system. To detect this image an array of antennas with individual detectors was used. LTSA elements were chosen for this purpose because of their narrow beamwidths and minimal interelement coupling. The imaging element of this system was chosen to be a parabolic reflector antenna, specifically an Alpha/TRG 30.5 cm diameter Cassegrain dish. The subreflector is seen from the focus to require a full angle of 30 degrees, setting the f# of this system to be 1.9 (see Figure 3.2). The measured beamwidths for this dish with a conical feed horn, also supplied by Alpha, were 0.73 degrees in the E-plane and 0.70 degrees in the H-plane, with first sidelobe levels of -17.8 dB and -18.5 dB respectively. This conical feed, which was supplied with the dish, had 10 dB beamwidths of 23° in the E-plane and 30° in the H-plane. The subreflector of the Cassegrain dish has a

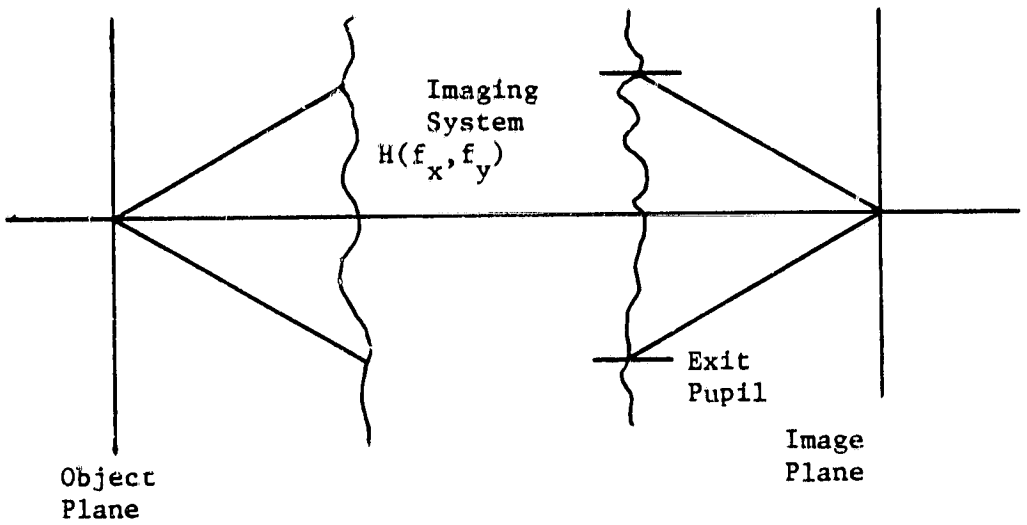

Generalized imaging system

Figure 5.1

diameter of only 3.17 cm and the expected total aperture efficiency is about 50%.

The desire to construct a maximally efficient imaging system therefore drove the development of an array of antenna elements which would satisfy the beamwidth requirements. In Chapter III it was found that LTSA antennas could be fabricated at 94 GHz which would have symmetric 10 dB beamwidths of, for this purpose, 30 degrees. In Chapter IV it was learned that these elements could be arrayed without exhibiting noticeable changes to the radiation patterns when the elements are spaced greater than 2.5 wavelengths apart. Therefore the array, described in Chapter IV, with the 7.9 mm interelement spacings, was expected to be maximally efficient when used as a focal plane imaging receiver. A second, less efficient, array was also constructed with an interelement spacing of 5 mm, described in Chapter IV, and was evaluated with the Cassegrain dish.

5.2 Review of Imaging Theory

Before delving into a description of the imaging system, some basic concepts should be reviewed. First, the difference between coherent and incoherent radiation should be explored. Illumination for which the phasor amplitude varies concurrently, but which may have a constant relative phase difference, is referred to as spatially coherent. Illumination for which the phasor amplitudes vary in unrelated fashions is called spatially incoherent. Imaging systems can have different

properties, depending upon which type of illumination is present. Generally, it is assumed that the radiation being dealt with is monochromatic. Since radiation in the microwave spectrum tends to be narrowband, it is near-monochromatic, and the assumption is valid.

Optical systems can be thought of as low pass filters, because diffraction only allows spatial frequency components less than some system cutoff-frequency, which we shall call f, to be passed through the system. From basic sampling theory, we know that a band-limited signal can be exactly reconstructed if one samples the signal at greater than twice the system cutoff-frequency. Thus, the complex E-field of the image can be reconstructed if it is sampled at twice the spatial cutoff-frequency. Since the intensity is the square of the complex E-field, and a multiplication in the spatial domain is a convolution in the frequency domain, the intensity distribution will contain frequencies up to twice the cutoff of the imaging system for coherent fields. Hence, if only the intensity is sampled, the sampling rate must be two times the coherent sampling rate, i.e. with a sampling interval, T_I , of one over four times the coherent cutoff-frequency, to reconstruct exactly the intensity distribution at the image plane.

A coherent imaging system with a circular exit pupil can be defined as

$$P(x,y) = \text{circ}\,[(x^2 + y^2)^{1/2} / d/2\,], \qquad (5.1)$$

where d is the diameter of the pupil (see Figure 5.2). The corresponding transfer function would also be a circular function with a definite cutoff-frequency of $d/(\lambda F)$, where F is the distance between

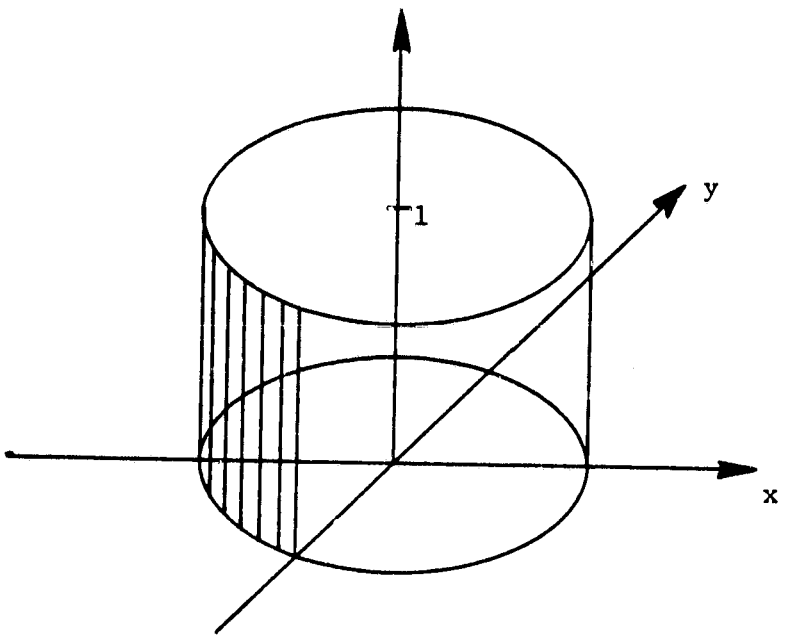

Circ function

Figure 5.2

the exit pupil and the image plane. So, the maximum spacing interval T for exact reconstruction of an intensity-sampled diffraction-limited imaging system is

$$T_I = 1/4f = \lambda F/2d \qquad \text{for intensity sampling ;} \tag{5.2}$$

$$T_E = 1/2f = \lambda F/d \qquad \text{for complex field sampling .}$$

For the case of a parabolic dish, d is the diameter and F is the focal length of the equivalent paraboloid. Thus, the smaller the f# of the dish, the closer the elements must be placed for exact reconstruction of the image. For the 30.5 cm Cassegrain dish at 94 GHz, the diffraction-limited spacing for an intensity-sampled image system is 3 millimeters. If the complex E-field is sampled with heterodyne detection, preserving the phase information, then the sampling interval can be doubled to 6 millimeters.

The half power beamwidth of a parabolic reflector antenna is approximately

$$\theta_{-3dB} = 1.2\ \lambda_o/D \tag{5.3}$$

The off-axis deviation of a receptor, Δx, is related to the number of 3 dB beamwidths scanned, n, by

$$\Delta x = 1.2\ n\ (f/D)\ (BDF)\ \lambda_o \tag{5.4}$$

The ratio of the actual beam scan to the scan predicted from geometrical optics is called the beam deviation factor (BDF). The BDF ranges from less than 1 for concave reflectors to values greater than 1 for convex reflectors. When dealing with a flat plate reflector, the the BDF equals 1. For the case of a $f^{\#}$=1.9 dish the beam deviation factor is 0.99 [14].

Thus for elements spaced 7.9 mm apart, one finds by using Equation 5.4, beam spacings of 0.74 degrees and 0.64 degrees for the respective E- and H-plane cuts (note that in the hexagonal array used, the H-plane interval is 6.8 mm). Measured values of beam spacing for the array are slightly less, roughly 0.63 and 0.50 degrees. This narrowing may be due to a misplacement of the array elements with respect to the focus of the dish, or may in general be seen as an indication that the actual physical optics properties of the array in the Cassegrain system deviated from what one predicts from geometrical optics. Note especially that the array is not much smaller than the subreflector.

Classical optics has its roots in the visual spectrum where incoherent imaging is more suited. In classical optics, the closest distance that two incoherent point-sources can be placed, and still be just barely resolved, is defined as the Rayleigh distance. This is where the Fraunhofer diffraction pattern of one aperture overlaps the first minimum of the second. In the case of circular apertures, it is where the Airy patterns satisfy the center/minimum condition. This is satisfied when the interelement spacing is

$$\Delta x_R = 1.22\, z\, (\lambda_o/d) = 1.22\, \lambda_o\, f\# \qquad (5.5)$$

where d is the aperture diameter and z is the distance between the image and aperture planes, equal to the focal distance in our case. For the Cassegrain system Δx_R is 7.4 mm. It is therefore reasonable to assume that the prototype system developed in this dissertation can resolve two incoherent point sources at the Rayleigh distance, since the array with 7.9 mm inter-element spacing gave very well behaved beam patterns.

It is useful to compare the ability of imaging systems to resolve two point source of either coherent or incoherent radiation. The intensity at the image plane for an incoherent imaging system under these circumstances is shown in Figure 5.3a. The image intensity of a coherent system illuminated by two point sources would be a function of the relative phase difference between the points and is plotted in Figure 5.3b. Compared with two coherent point sources in phase, two incoherent sources are better resolved; while for the case of phase opposition, the coherent sources are better resolved. For the case of two coherent sources in phase quadrature, the resolution is identical to that of two incoherent sources. Therefore, no definite statement can be made about the two-point resolution, since the type of illumination occurring in a particular application is very important in determining the resolution obtained. It is also clear that the nature of most objects encountered is different from the simple two-point source and that this will influence the actual resolution obtainable in a given application.

5.3 Experimental Data for the 94 GHz Imaging System

10 dB beamwidths and calculated 30 degree beam efficiencies for arrays of LTSA elements, with both the 5 mm and 7.9 mm spacings, are listed in Table 5.1 along with the given data for the conical feed horn. It can be seen that these performance parameters for the LTSA elements on the central substrate of the 7.9 mm spaced array are quite similar to

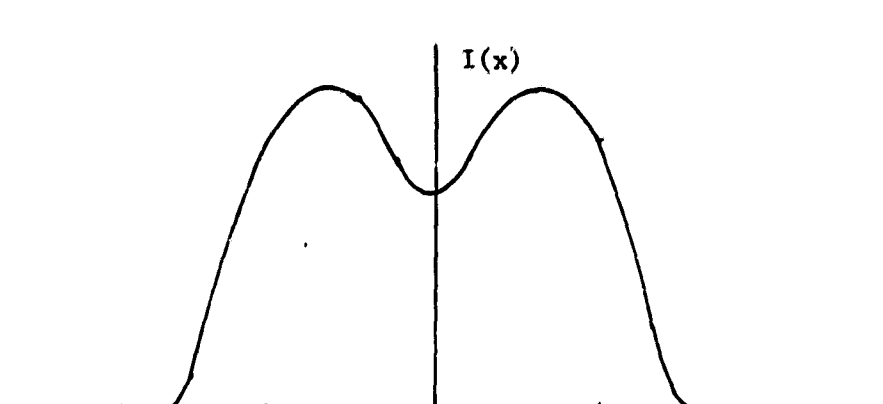

Two point source response of incoherent imaging system

Figure 5.3a

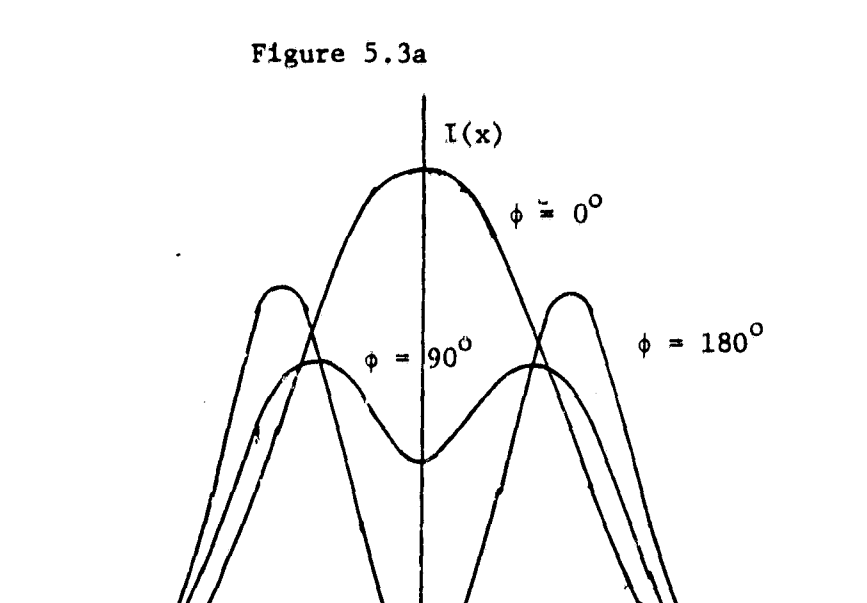

Two point response of coherent imaging system

Figure 5.3b

	CONICAL FEED	7.9 mm SPACING CENTRAL SUBSTRATE	7.9 mm SPACING EDGE SUBSTRATE	5.0 mm SPACING CENTRAL SUBSTRATE	5.0 mm SPACING EDGE SUBSTRATE
10dB E-plane Beamwidth	23°	24.5°	27°	40° (1	28°
10dB H-plane Beamwidth	30°	31°	38°	44°	40°
30° Eff.	55%	30-34%	26%	10-15%	30%
10dB Eff.	—	30-33%	27%	20-30%	31%
Direct.	—	14-15dB	13.5dB	10dB	13dB

1) Beamwidth actually narrowed (see Figures IV.12 and IV.13) the larger recorded beamwidth is due to sidelobe level increasing above -10dB.

Comparison between conical feed horn and arrayed LTSA elements

Table 5.1

what is available with the conical horn. The efficiency is somewhat less than for the horn and degrades even more for elements not on that substrate. As expected, the 30° beam efficiency for the 5 mm spaced array has degraded even more. This time, however, the edge elements possess the higher efficiency. Looking back to the radiation patterns for these elements shown in Figures 4.12 and 4.13, we see that part of the reason for the low efficiency is the high average sidelobe levels. Unfortunately, the detected signal in the sidelobe region can be partly hidden in the noise, due to a worse than average diode. This makes the calculation of the beam efficiency from the raw data susceptible to error. Yngvesson [18] has calculated the effect of an assumed average sidelobe level on the 10 dB efficiency of an antenna, and the results are reproduced in Figure 5.4. The measured sidelobe levels are between 13-16 dB and from Figure 5.4, we would expect the 10 dB efficiency for 40 degree 10 dB beamwidth to be between 15 and 30%. If the sidelobe level fell to -20 dB, we could expect the efficiency to improve to 50%. This would be strictly true for the 40 degree 10 dB beamwidth case only but does indicate that the value of 30 degree beam efficiency for the 5 mm spacing on the central substrate may be underestimated by perhaps a factor of 2 in this table, due to the above mentioned effect of an unusually noisy diode.

All these arrays were designed such that the elements radiated perpendicularly to the plane of the parabolic dish. Thus the elements not at the center of the array tend to have less of their energy impinging on the subreflector. Although this array, as it is, does obey

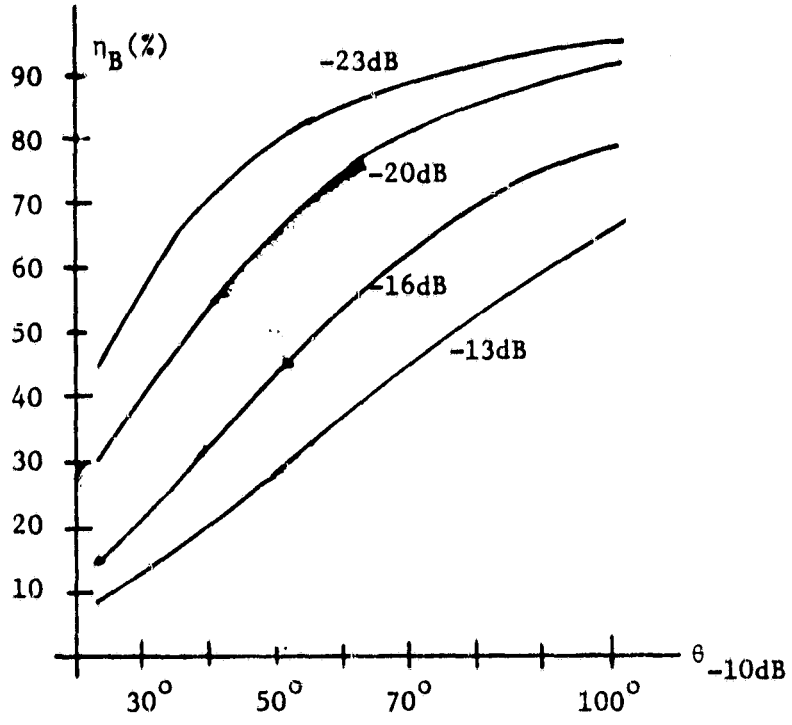

Antenna efficiency versus average sidelobe level

Figure 5.4

the telecentric condition [19] of optics, each non-central beam will have lower efficiency since there will be greater spill-over past the subreflector. One way to help alleviate the problem is to disregard the telecentric condition and tilt the elements toward the subreflector. This is a very simple task in the H-plane but requires special etching of the antennas to accomplish in the E-plane. A quick study was undertaken to see if it was possible to change the direction of radiation in the E-plane by angling the LTSA antenna on the substrate. Shown in Figure 5.5 is the radiation pattern at 10 GHz of an 11.2 degree LTSA on a 0.153 mm thick OAK-605 substrate angled at 15 degrees to the substrate's perpendicular axis. The length of this antenna was 31.75 cm along the center of the antenna. One sees that the antenna radiation pattern has been directed roughly 15 degrees off endfire in the E-plane, while the H-plane, which was recorded through the beam maximum, remained unaffected. Although it was found unnecessary to use an array with tilted elements, such an arrangement remains a possibility.

Hexagonally symmetric arrays with both 7.9 and 5.0 mm spacings were placed at the focus of the Cassegrain system and radiation patterns taken for 3 elements in the array at at time. E- and H-plane cuts through an array with an interelement spacing of 7.9 mm are shown in Figures 5.6 and 5.7, respectively. We can see that the central element, 1, of the hexagonal array, see Figure 4.1b, is very well behaved. The antenna has half power beamwidths of 0.73 degrees in the E-plane and 0.66 degrees in the H-plane, with sidelobe levels of about -22 dB and -16 dB in the respective planes. The H-plane beamwidth is narrowed when

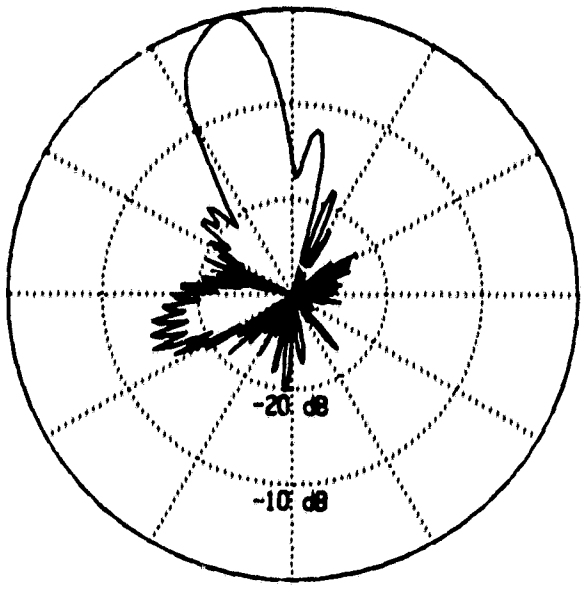

5.5a E-Plane 15 degree angled LTSA

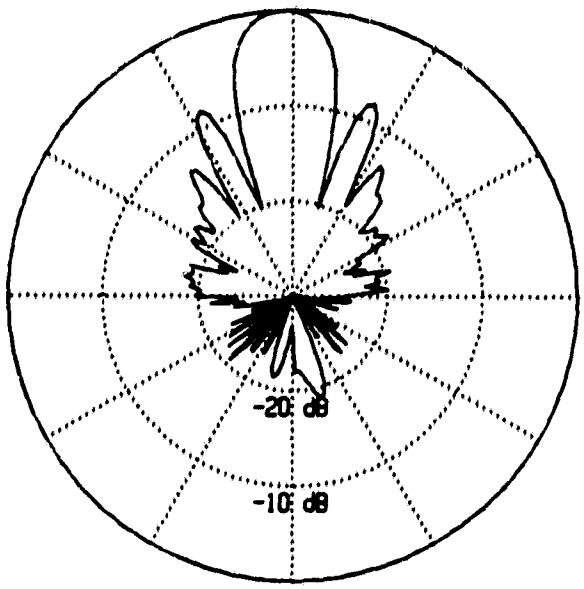

5.5b E-plane 15 degree angled LTSA

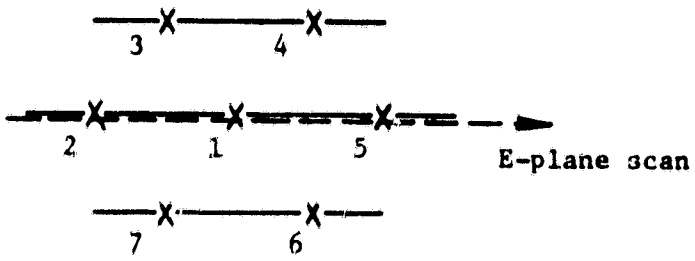

7.9 mm hexagonal array scan
Figure 5.6a

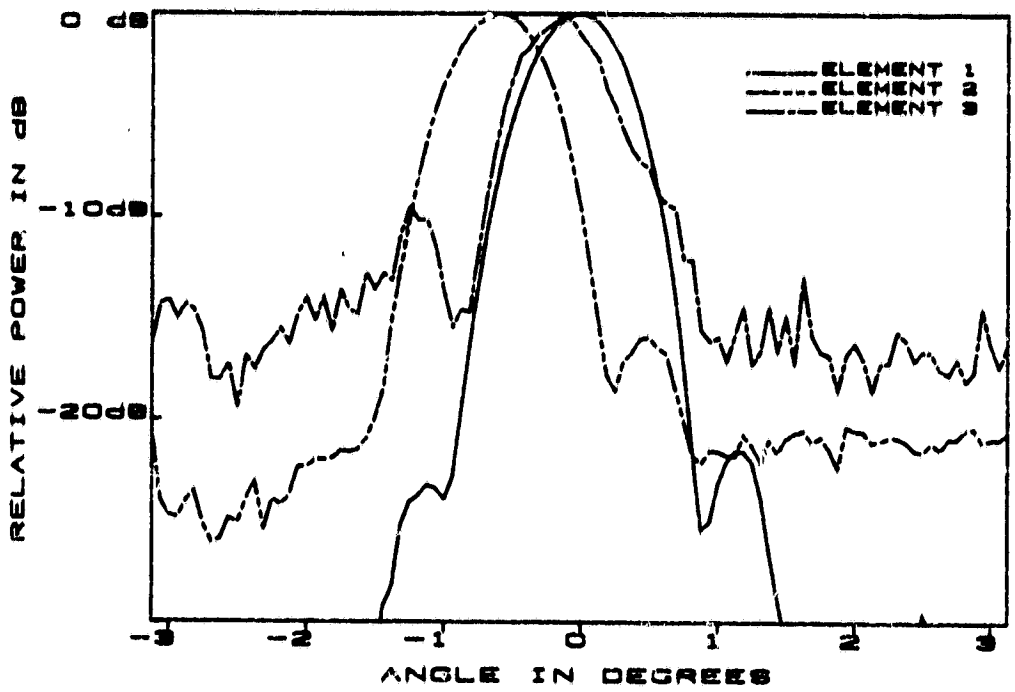

Element responses

Figure 5.6b

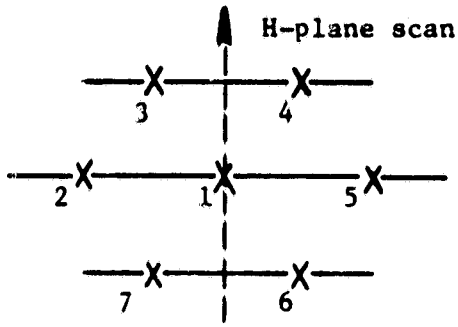

7.9 mm spaced array scan

Figure 5.7a

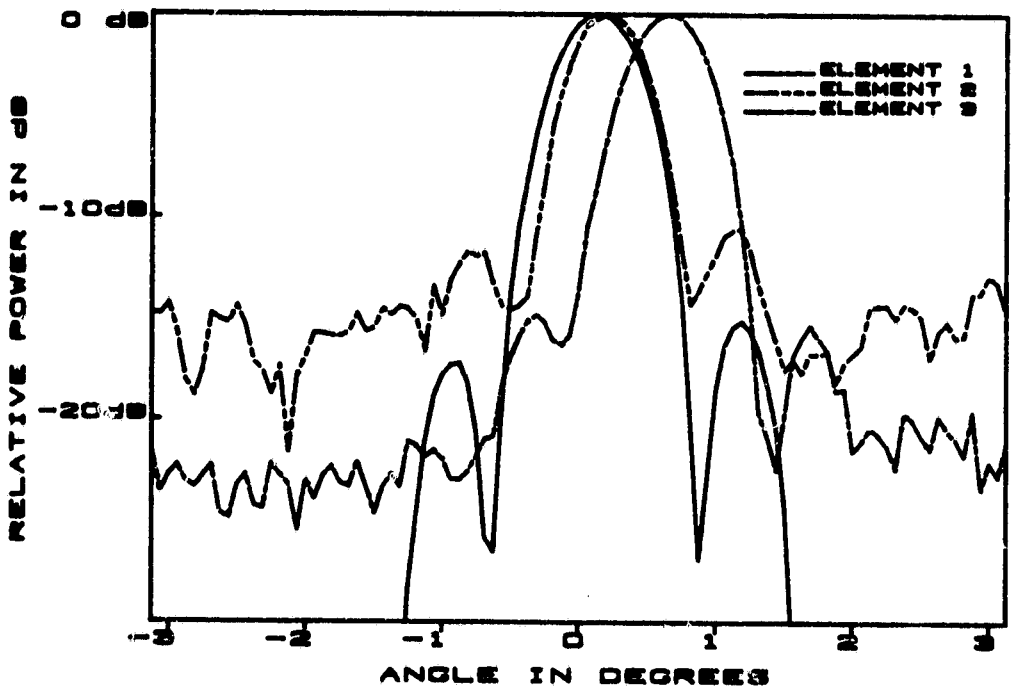

Element response

Figure 5.7b

C-2

compared to the conical feed horn with increased sidelobe levels in this plane. A calculation of beamwidth assuming a uniformly illuminated aperture, indicates that the minimum expected beamwidth is 0.61 degrees with sidelobe levels predicted to be -17.5 dB. The measured values for beamwidth and sidelobe level are well within the expected range. The other elements, which are offset from the focal point, tend to have higher sidelobe levels. Note that the scan through element 3 in Figure 5.6 does not cross its beam maximum, and does not yield actual sidelobe level correctly.

Radiation patterns for the hexagonal array of LTSA elements with 5 mm spacings were also measured in the Cassegrain dish, and are shown in Figures 5.8 and 5.9 for the respective E- and H-plane scans. The step-like features in the E-plane curves are due to the mechanical gear tolerances in the azimuth drive to which the antenna system was mounted for testing. In this case, beamwidths of 0.76 and 0.63 degrees with average spacings of 0.56 degrees in the E-plane and 0.50 degrees in the H-plane were obtained. The calculated beam shifts were 0.47 degrees for the E-plane and 0.40 degrees for the H-plane. The explanation for this discrepancy in beam shifts must in general be the same one as for the larger array. Looking back to Figure 4.12, we see that the H-plane 10 dB beamwidth for these 5 mm antennas has become very broad. The radiation pattern is only about 3 dB below its maximum value at the 15 degree points. Since the elements illuminate the subreflector almost uniformly, one expects the beamwidth to narrow to almost the uniform case of 0.61 degrees, as observed. In the E-plane, the 10 dB beamwidths were measured

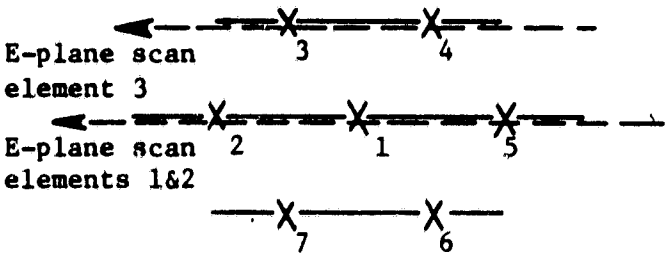

5.0 mm hexagonal array scan

Figure 5.8a

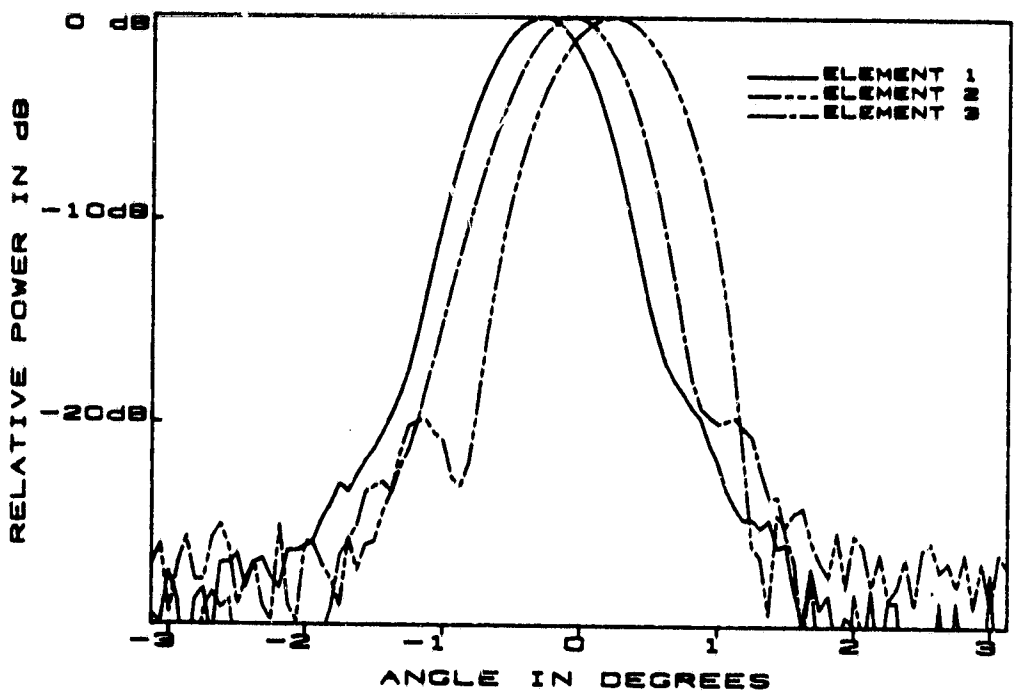

Element response

Figure 5.8b

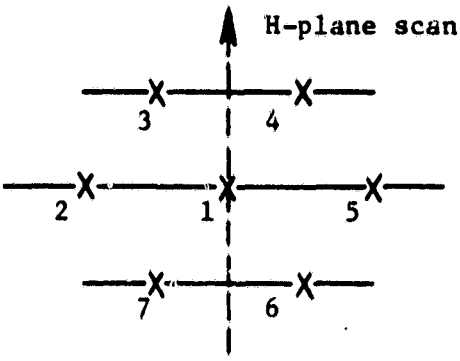

5.0mm spaced hexagonal array scan

Figure 5.9a

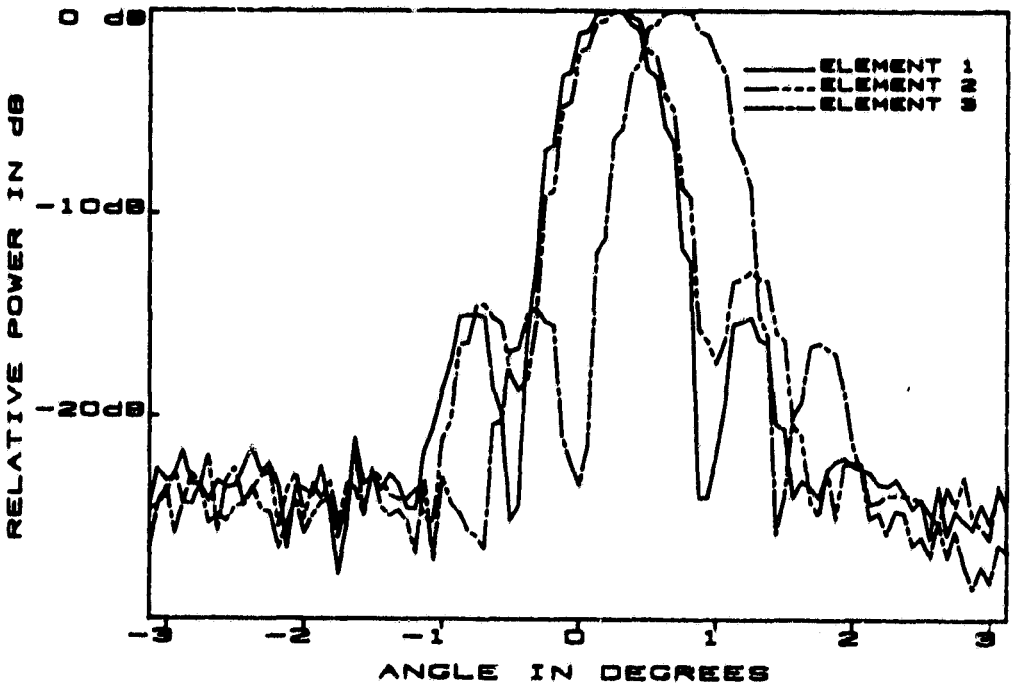

Element response

Figure 5.9b

to be 40 degrees. Also in the E-plane, one sees that the major part of the beam has actually narrowed slightly with respect to the single element case, hence the system beamwidth should broaden slightly.

Before expanding on an application of this array system, a discussion of its novelty is in order. Rahmat-Samii et.al. [20] have investigated the packing of various feed elements in the focus of a reflector antenna system. They found that the minimum element spacing could be related to either the directivity or the beamwidth of the element. Feed elements such as circular or rectangular waveguides are essentially limited by the size of their aperture. Cigar antennas can be spaced much closer together because the traveling wave nature of these elements narrow their beamwidths and increase their directivity. LTSA antennas also exploit the traveling wave mechanism to narrow their beamwidths, and can be spaced closer together than the aperture antennas. For example, the conical waveguide feed horn designed for use with this Cassegrain dish has an outer diameter of 14 mm, while measurements of arrays of LTSA elements with an interelement spacing of 7.9 mm reveal no appreciable change in radiation patterns. An array with interelement spacing of 5 mm with somewhat broader beamwidths was found to couple to the dish with somewhat lower beam efficiency. Thus, the LTSA elements can be spaced at least a factor of two closer than an array of waveguide horns. Waveguide feed horns could be spaced closer together, as in the 5 mm, case only with a large loss of efficiency due to spill-over.

Another way to consider the minimum spacing question utilizes the Equivalence Principle, which says that the radiation pattern of an antenna can also be calculated from its aperture fields. Because LTSA antennas do not have a well-defined geometrical extent, it is difficult to determine an aperture size. However, the previously presented data of mutual impedance and beamwidth modification of LTSA antennas in an array environment indicate that most of the fields remain within the spacing of the array elements. Thus, we can define an aperture size approximately as the period of the LTSA array, i.e. for 11.2 degree LTSA elements on 0.025 mm Kapton substrates the period would be 7.9 mm. If one assumes a uniform illumination of this circular aperture, then the half power beamwidth of these LTSA antennas can be calculated to be 23.1 degrees. In fact, the measured values are much less than that, or about 17.5 degrees. The smaller beamwidth could be explained if the illumination function were heavily weighted toward the perimeter of the active area of the antenna. Going to the extreme and assuming that the illumination function consists of a delta function at the perimeter, the half power beamwidth would be 18 degrees, which is measured value. It is thus possible to very roughly understand that aperture antenna elements cannot be spaced as closely as an LTSA antenna elements.

One application for this array is a monopulse radar [21]. Similar optical constraints govern the operation of the overall system, but tradeoffs of different system parameters are possible. The proposed system consists of a two-dimensional four element array of LTSA antennas spaced 7.9 mm apart at the focus of the same Cassegrain dish. Although

most monopulse systems are designed to sample the complex E-field, this was designed to sample only the intensity. Because the array is at the focus of the dish, where the phase is essentially constant across the array, the system can be considered to be amplitude monopulse and intensity sampling is justified.

Single element patterns of the array are shown in Figure 5.10 for the E-plane and in Figure 5.11 for the H-plane. Once again the step-like features seen in the E-plane were due to mechanical tolerances in the gears of the azimuth drive. It can be seen from these figures that the patterns are well behaved and the sidelobe levels are more than 13 dB down. The H-plane 3 dB beamwidths were about 0.7 degrees, while being slightly larger, or about 0.7½, degrees in the E-plane. Beam spacings for the E- and H-planes were approximately 0.62 degrees.

A computer program was written for a HP-85 microcomputer which controls the elevation and azimuth of the antenna pedestal to which the system was mounted. The HP-85 computer would sample the outputs from the four elements in the array and mathematically form the monopulse sum and E- and H-plane differences of the signals. Based upon the difference magnitude, the computer would make a decision as to which direction to step the array's pointing. When the array was aimed off target, the system could return the array such that the pointing was back on target to within the step increments of the pedestal.

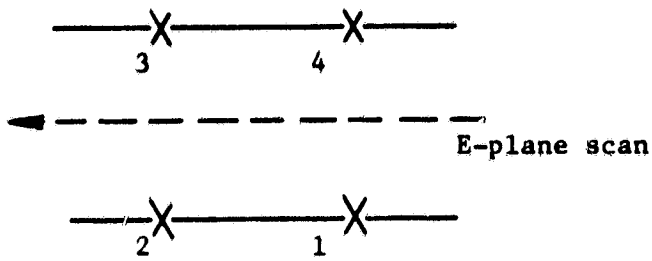

7.9 mm spaced square array scan

Figure 5.10a

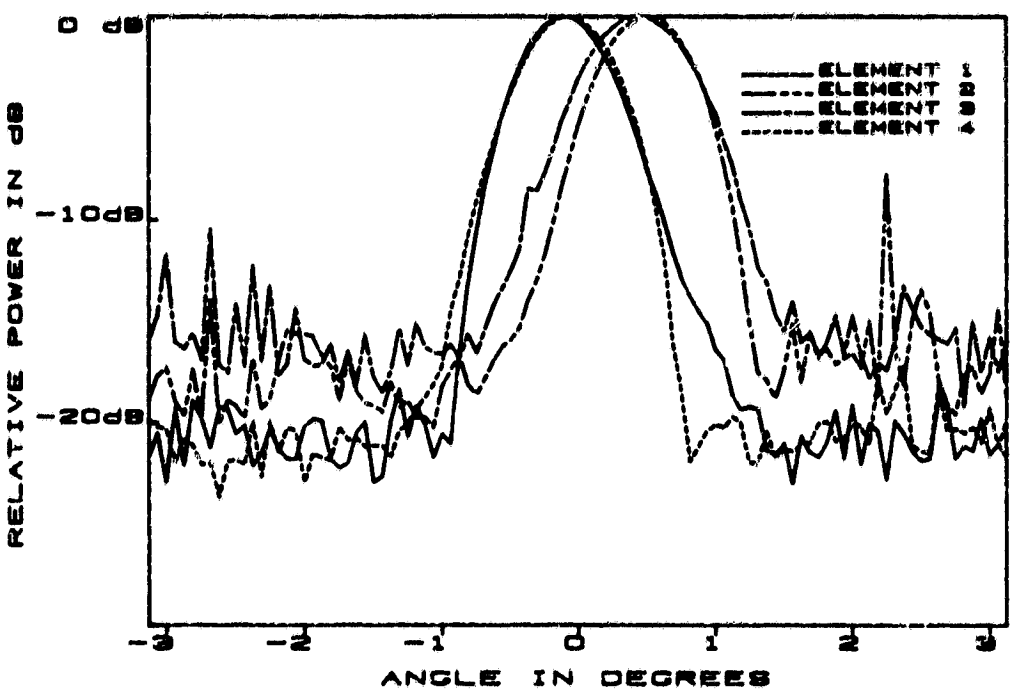

Element response

Figure 5.10b

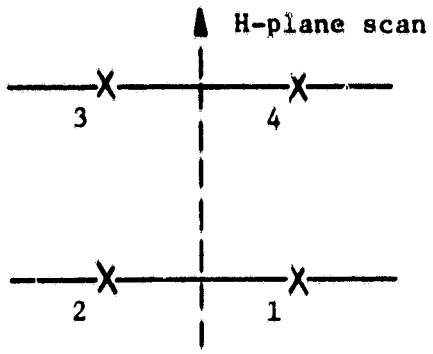

7.9 mm spaced array scan
Figure 5.11a

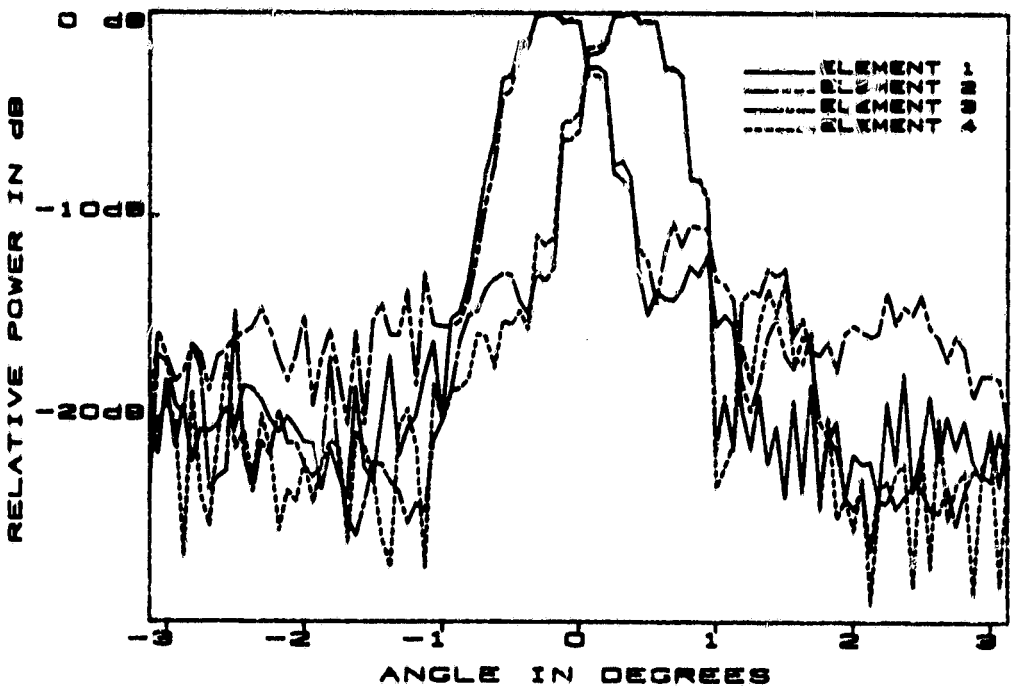

Element response

Figure 5.11b

C H A P T E R VI

CONCLUSIONS AND RECOMMENDATIONS FOR FUTURE WORK

During the course of this dissertation, an experimental investigation of the endfire slotted-line antennas was undertaken to elucidate the effects of different substrate and metalization parameters on antenna radiation properties. Although all the antenna's parameters effect both the E- and H-plane radiation characteristics, it was found that these antennas have H-plane beamwidths which are basically dependent upon the substrate properties, whereas the E-plane beamwidth is more strongly a function of the slot's size and shape. The LTSA antenna radiation beamwidths are not always within the standard curves given by Zucker, but usually follow those curves for some ranges of normalized length and effective thickness. This compliance with the standard data is evidence that the slotted-line radiators do indeed employ the traveling wave mechanism for radiation. In particular, the TWA data can be used as an empirical design guide, provided the effective thickness, defined in Chapter III, is within a certain range. For antennas defined by the design guide, E- and H-plane beamwidths are roughly equal. Finally, it was found that using the design guides, an LTSA antenna could be fabricated with a symmetrical E- and H-plane beamwidth of 30 degrees, as required for the prototype imaging system.

An indication of the extent of the fields in these antennas was provided when the elements were arrayed. Mutual impedance measurements,

using the vector network analyzer, show that the itennas couple significantly when spaced less than a wavelength apart. Radiation pattern measurements of these arrays reveal that the elements couple even out to a relative spacing of 2.5 wavelengths. Thus an array which met the 2.5 wavelength condition was explored indepth.

Arrays with first nearest neighbor spacings of 2.5 and 1.5 wavelengths were evaluated in free space and then as focal plane arrays with integrated detectors. Free space measurements of the radiation patterns for both an X-band array with 7.62 cm spacing and a 94 GHz array with 7.9 mm spacing were found to be essentially unaffected by the arraying process. A 94 GHz array with 5 mm interelement spacing was found to have single element patterns which were altered noticebly. In this case, the H-plane beamwidths were broadened while the E-plane beamwidths were narrowed.

Both of these arrays were subsequently placed in the focal plane of the Cassegrain reflector antenna with radiation pattern measurements performed on the system. The 94 GHz array with 7.9 mm spacing was found to produce well behaved single element patterns with sidelobe levels of -22 dB in the E-plane and - 5 dB in the H-plane. The beam separation was less than a 3 dB beamwidth and also was found to be less than predicted by simple geometrical optics for an f#=1.9 dish. The latter discrepancy is due in part to the fact that the size of the subreflector is only about twice the size of the array and therefore geometrical optic predictions are not expected to be valid. Also, there was the

possibility that the phase centers of the LTSA antennas were not at the focal plane of the dish. The 94 GHz array antenna with a 5 mm interelement spacing was also tested in the Cassegrain dish even though it did not satisfy the criterion for optimum illumination of the dish. It was also found to have single element patterns which were well behaved and with beamwidths as predicted from aperture theory for a circular aperture with different illumination functions. The beam spacings, however, were again smaller than expected from geometrical optics. Once again, it is believed that the reason for this is that geometrical optics does not hold for this array.

It was shown in Chapter V that there is a minimum spacing necessary for exact reconstruction of a sampled image in a diffraction limited system. The LTSA antenna element can comply with the minimum separation without element interactions, if complex E-field sampling were to be performed. If one is prepared to accept some minor interactions between elements, the elements can be spaced even closer together, although some loss of efficiency is incurred. Rahmat-Samii et. al. have shown that there is a minimum size of aperture necessary if a typical horn antenna is to be used as a feed element of a reflector system. It was shown that the LTSA antennas can be spaced two times closer than the feed horn antennas with comparable beamwidth, and that the estimated resolution of two incoherent point sources should be about one Rayleigh distance.

REFERENCES

[1] Clarricoats, P. and Poulton G., "High-Efficiency Microwave Reflector Antennas-A Review", Proceeding of the IEEE, vol. 65, no. 10, Oct. 1977.

[2] Neikirk, D., Rutledge, D., Muha, M., Park, H., and Yu, C., "Far-Infrared Imaging Antenna Arrays", Appl. Phys. Lett., vol. 40, no. 3, Feb. 1982.

[3] Lewis, L., Fassett, M., and Hunt, J., "A Broadband Stripline Array Element", AP-S Symp., June 1974.

[4] Reuss, M., "A Cursory Investigation of a Slot Line Radiator", NRL Memorandum Report 2796, Naval Research Laboratory, May 1974.

[5] Prasad, S., and Mahapatra, S., "A New MIC Slot-Line Aerial", IEEE Trans. Antennas and Propagat., vol. AP-31, no. 3, May 1983.

[6] Blass, J., in Jasik, H. (Editor), "Antenna Engineering Handbook", chap. 8, McGraw-Hill, New York, (1961).

[7] Gibson, P.J., "The Vivaldi Aerial", 9th Eur. Microw. Conf., Brighton, U.K., 1979, pp. 101-105.

[8] Yngvesson, K.S., Schaubert D.H., Korzeniowski, T.L., Kollberg, E.L., Thungren, T., and Johansson J., "Endfire Tapered Slot Antennas an Dielectric Substrates", to be Published in IEEE Trans. Antennas Propagat.

[9] Kollberg, E.L., Johansson, J., Thungren, T., Korzeniowski, T.L., and Yngvesson, K.S., "New Results on Tapered Slot Endfire Antennas on Dielectric Substrates", 8th Inter. Conf. Infr. Millimeter Waves (1983).

[10] Zucker, F.J., in Jasik, H. (Editor), "Antenna Engineering Handbook", chap. 15, McGraw-Hill, New York, (1961).

[11] Hansen, W.W., and Woodyard, J.R., "A New Principle in Antenna Design", Proc. IRE, vol. 26, no. 3, March 1938, PP. 333-345.

[12] Ehrenspeck, H.W., and Poehler, H., "A New Method for Obtaining Maximum Gain from Yagi Antennas", IRE Trans. Antennas Propagat., vol AP-7, 1959, p. 379.

[13] Milligan, T., "Modern Antenna Design", McGraw-Hill, New York, (1985).

[14] Carrel, R., "The Characteristic Impedance of Two Infinite Cones of Arbitrary Cross Section", IRE Trans Antennas Propagat., pp. 197-201, 1958.

[15] Rutledge, D.B., Neikirk, D.P., and Kasilingam, D.P., in Button, K. (Editor), "Infrared and Millimeter Waves", vol. 10, pp. 1-90, Academic Press, New York, (1983).

[16] Jasik, H., "Antenna Engineering Handbook", pp. 34-11, McGraw-Hill, New York, (1961).

[17] Goodman, J.W., "Introduction to Fourier Optics", McGraw-Hill, New York, (1968).

[18] Yngvesson K.S., in Button, K. (Editor), "Infrared and Millimeter Waves", vol. 10, pp. 91-110, Academic Press, New York, (1983).

[19] Clark, J.A., and Dewey, R.J., "Millimeter Wave Imaging Lens Antenna", Inter. Jour. Infr. Millimeter Waves, vol. 5, no. 1, 1984.

[20] Rahmat-Samii, Y., Cramer, P., Woo, K., and Lee, S.W., "Realizable Feed-Element Patterns for Multibeam Reflector Antenna Analysis", IEEE Trans. Antennas Propagat., vol. AP-29, no. 6, pp. 961-963, Nov. 1981.

[21] Korzeniowski, T.L., Pozar, D.M., Schaubert, D.H., and Yngvesson, K.S., "Imaging System at 94 GHz Using Tapered Slot Endfire Antenna Elements", 8th Inter. Conf. Infr. Millimeter Waves (1983).

A P P E N D I X

Vivaldi Antennas

A graph of the half power beamwidth of Gibson's Vivaldi antenna is shown as a function of normalized length, L/λ_o, in Figure A.1. One sees from this graph that Gibson's antennas do not follow the optimum curves for traveling wave antennas. This is due to the fact that Gibson's Vivaldi antennas are designed for wide bandwidths and thus trade off the optimum gain condition. Because the topology of this antenna structure is slot line, the waves will be coupled to the structure in such a mode. Thus, not only will metalization shape affect the radiation properties of the structure, but the dielectric constant and thickness should also do so. In an effort to separate the effects on the radiation properties of the dielectric constant of the substrate and the ground plane's exponential tapers, Vivaldi style antennas were constructed on low dielectric constant ($\varepsilon_r \leq 3$) materials of different thicknesses.

Two Vivaldi antennas were constructed on 0.79 and 1.54 mm Rexolite ($\varepsilon_r = 2.54$) substrates using the taper equation:

$$y = \pm 0.55 \exp(0.015\, x) \qquad (A.1)$$

where x and y are in millimeters. Shown in Figure A.2 is a graph of the 3 dB beamwidth versus normalized length for these two antennas. It can be seen that both E- and H-planes agree well with the Zucker's standard TWA curves. Further, the thicker substrate antenna tends to have slightly broader than standard beamwidths at long antenna lengths. One possible interpretation is that the substrate creates a situation where

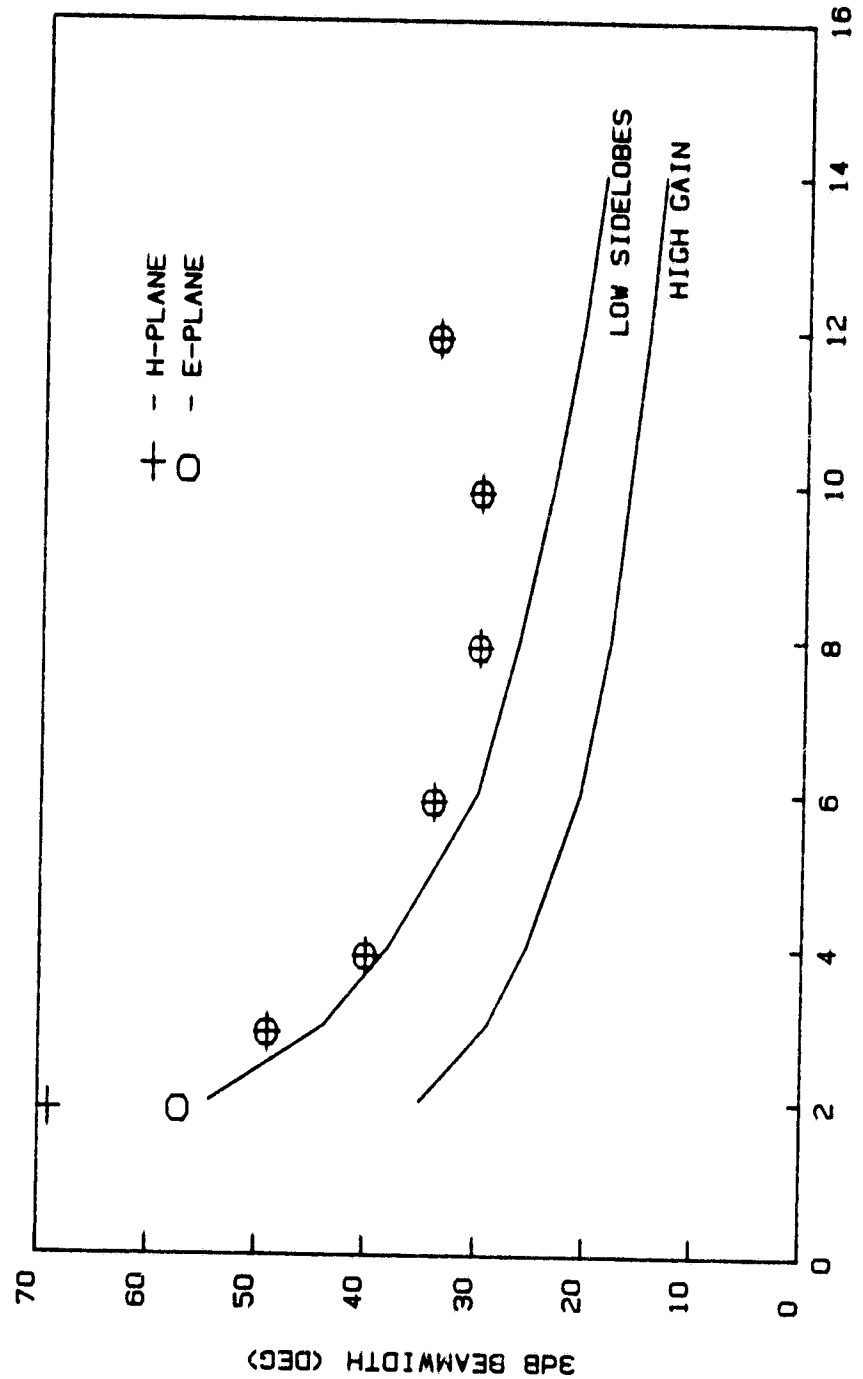

A.1 3dB beamwidth of Gibson's Vivaldi antenna

Figure A.1

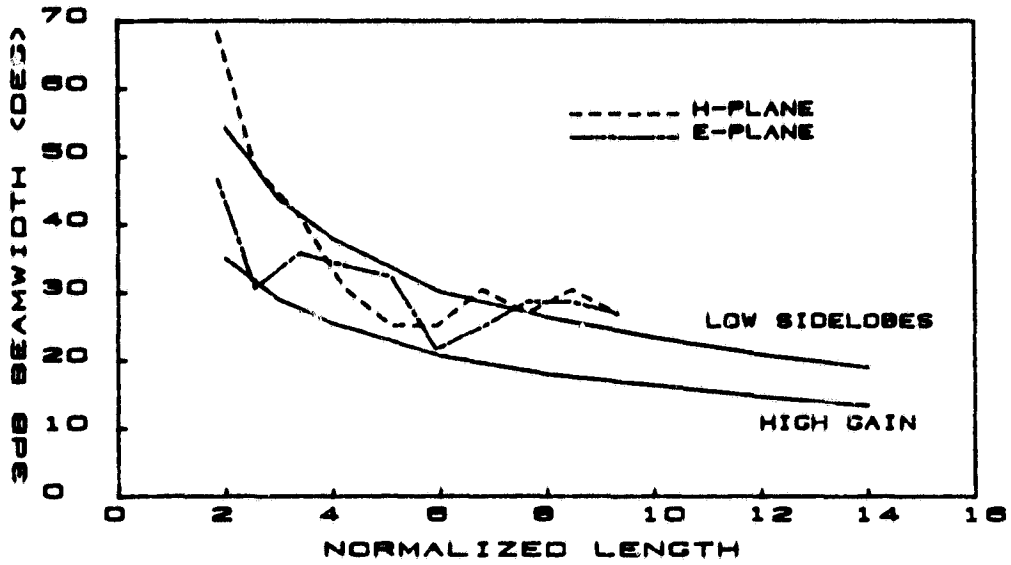

A.2a 3dB beamwidth of Vivadli on 1.58 mm thick OAK-605 substrate

Figure A.2a

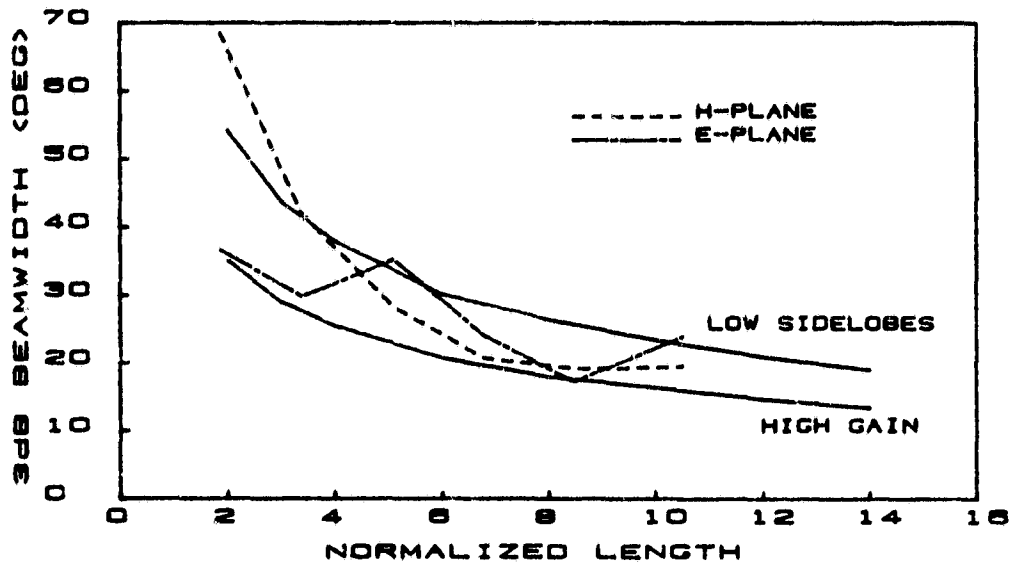

A.2b 3dB beamwidth of Vivaldi on 0.79 mm thick Rexolite substrate

Figure A.2b

the effective thickness of the structure is increased, additionally slowing the waves beyond the value which gives maximum gain and hence minimum beamwidth according to the traveling-wave antenna theory.

Subsequently, a Vivaldi antenna was constructed on a 2.54 cm thick styrofoam (ε_r = 1.05) substrate. Shown in Figure A.3 are the E- and H-plane 3 dB beamwidths as a function of normalized length. The beamwidths can be seen to have separated from one another, and the H-plane has broadened with respect to the Rexolite antennas, shown previously, which were of the same length and shape. At very long lengths, the beamwidths become more similar in the E- and H-planes, and approach those of the standard traveling-wave antennas, indicating that the styrofoam substrate can produce the optimum slowing of the phase velocity for these longer antenna.

Linearly Tapered Slotted Line Antennas (LTSA Antennas)

We first discuss LTSA antennas without a dielectric substrate, an "air" LTSA antenna.

One "air" LTSA antenna with full taper angle of 11.2 degrees was constructed and measured as a function of length at 8, 10, and 12.4 GHz. Shown in Figure A.4 is a graph of beamwidth as a function of the antenna's normalized length. The H-plane beamwidths are symmetrical and roughly track each other for all three frequencies especially for the longer antennas. The E-plane beamwidths tend to diverge as the length increases neither, however, follow the optimum TWA antenna curves. As

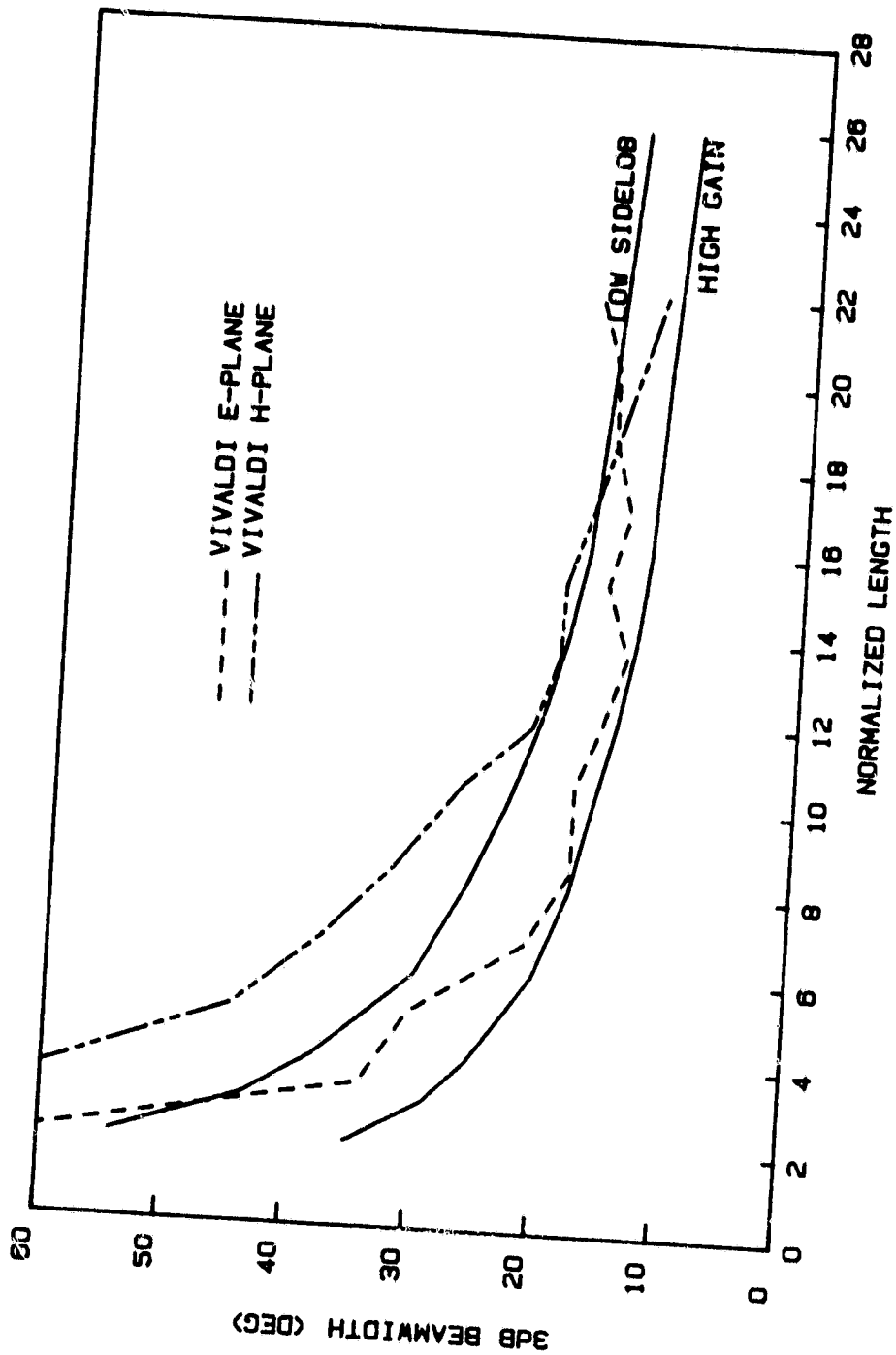

A.3 3dB beamwidth of Vivaldi on 25.4 mm thick styrofoam substrate

Figure A.3

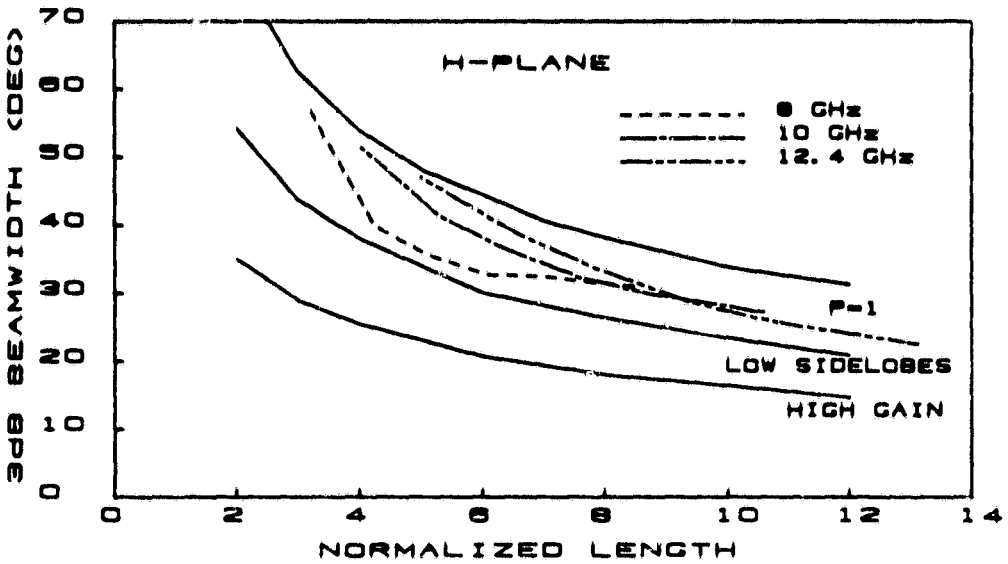

A.4a H-plane 3dB beamwidth of "air" LTSA antenna

Figure A.4a

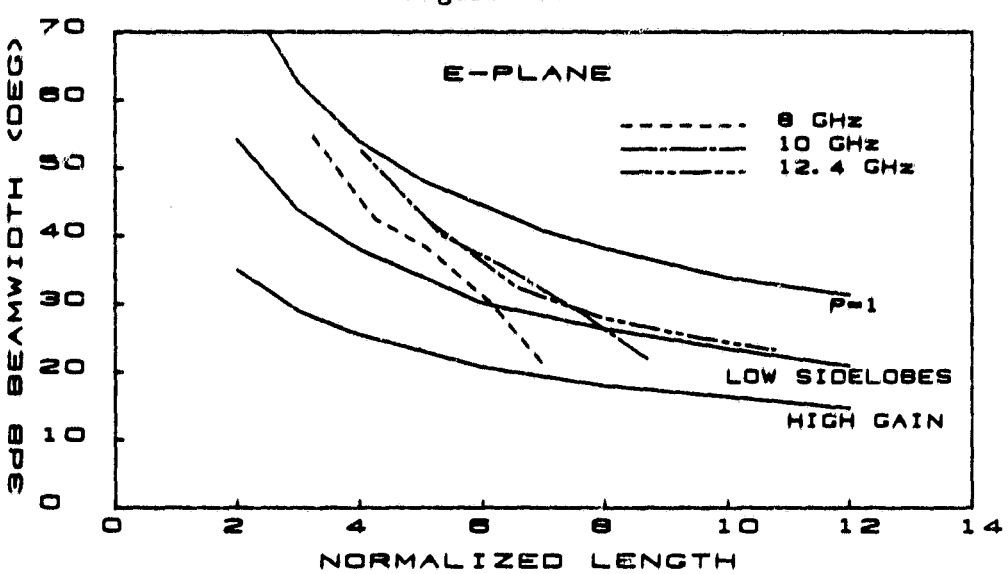

A.4b E-plane 3dB beamwidth of "air" LTSA antenna

Figure A.4b

was discussed in Chapter III, traveling wave antennas with $v_{ph} \rightarrow c$ do not satisfy the optimum gain conditions and as can be seen from Figure III.3, the gain is falling off as the wave velocity increases. Milligan's P=1 half power beamwidth curve has also been included in Figure A.4 for comparison purposes. We see that these "air" LTSA's have beamwidths which lie between the optimum curves and $v_{ph} = c$ curve, indicating that there still exists some small amount of phase velocity slowing even though there is no dielectric substrate present.

We next discuss the effect on beamwidth of changing the effective length of LTSA antennas on a dielectric substrate, while keeping the opening angle constant. The effective length was changed in two different ways, i.e. 1) the length of the antennas was varied while the frequency was held constant and 2) the length of the antenna was held constant while the frequency was varied. One would not expect the two techniques to yield identical results as the substrate thickness remained constant in both methods. Beamwidths for a 16.4 degree full taper angle LTSA antenna on a 2.54 cm thick styrofoam substrate at 8, 10 and 12.4 GHz, taken by cutting the length down gradually, are shown in Figure A.5. The E- and H-planes are no longer symmetrical with the E-plane having been narrowed significantly. Further, the H-plane data for different frequencies no longer track each other when plotted versus normalized length, and attain different minimum values with a breakpoint in the curves occuring at different normalized lengths. When a 25.4 cm long styrofoam LTSA with the same full-angle was measured by changing the frequency, different results were obtained as expected from the

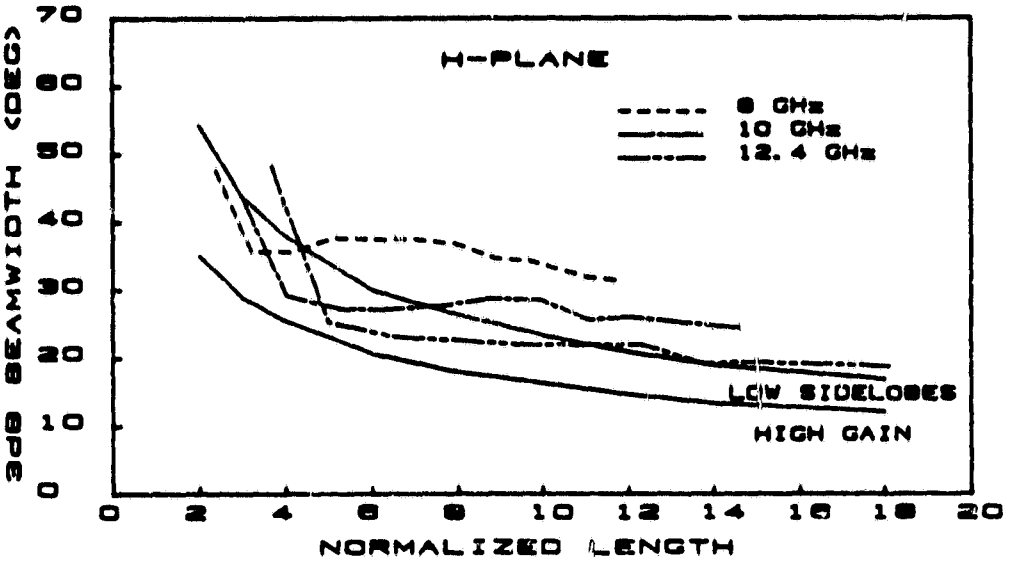

A.5a 3dB beanwidth of LTSA on 25.4 mm thick styrofoam substrate

Figure A.5a

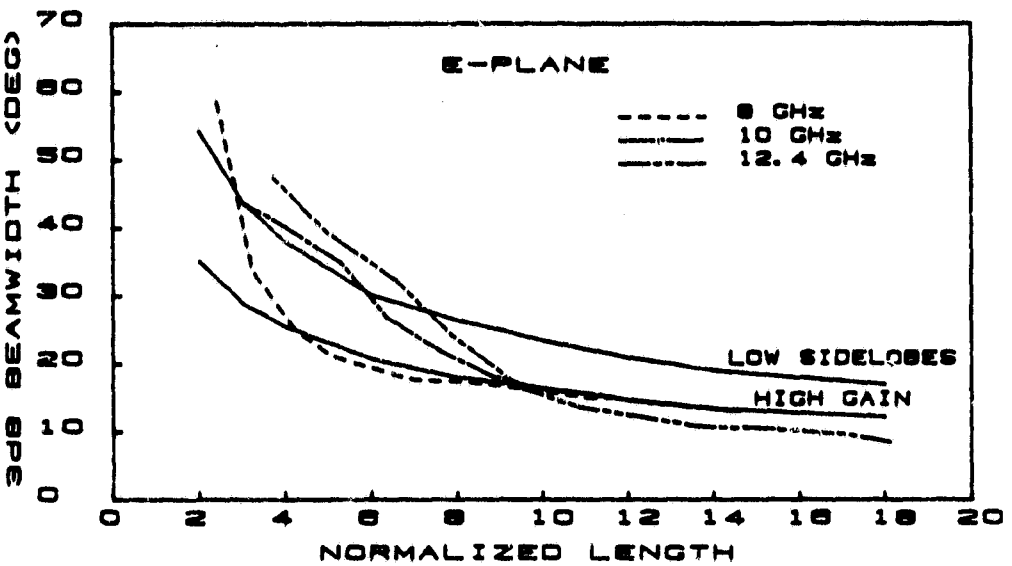

A.5b 3dB beamwidth of LTSA on 25.4 mm thick styrofoam substrate

Figure A.5b

previous discussion. As can be seen in Figure A.6, the behavior of the E-plane beamwidth is similar to the changing length case but the H-plane beamwidth, which is initially much wider, continues to narrow to the point where it joins the E-plane curve between the optimum TWA curves.

Substrate Thickness

A series of measurements taken versus frequency was made on three identical LTSA antennas with 16.4 degree full taper angles and 25.4 cm length on OAK-605 laminated substrates with dielectric constant 2.33, and thickness of 0.15, 0.79 and 1.54 mm respectively, see Figure A.7. These data indicate that the beams tend to become symmetrical as substrate thickness is increased, as a result of the H-plane width steadily narrowing, while the E-plane curve is essentially un-affected. The H-plane beamwidth for the 1.54 mm thick substrate also shows the unique property of broadening beyond a normalized length of 8 λ_o. Similar behavior was also seen in data taken at Chalmer's University for antennas on thick, low dielectric constant substrates [9].

A second series of measurements taken as a function of length were performed on a similar LTSA antenna with full taper angle of 11.2 degrees on a 0.15 mm thick OAK-605 laminated substrate at 8, 10, and 12.4 GHz. The half power beamwidths of this antenna are shown plotted versus normalized length in Figure A.8. In this case the H-plane beamwidth curves are following the low sidelobe TWA curves while in the E-plane the beamwidths begin in the same place and end up between the

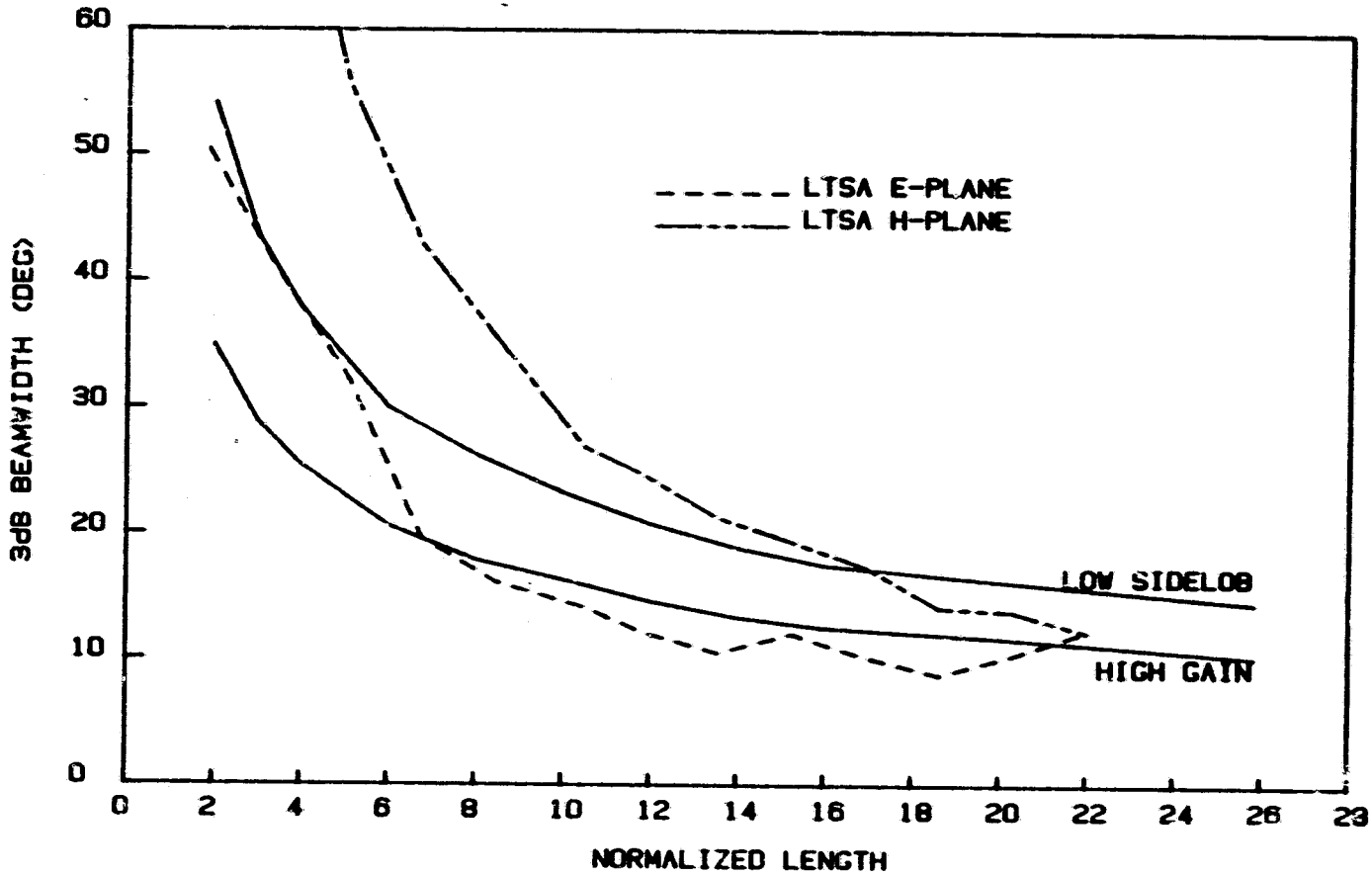

A.6 3dB beamwidth of LTSA on 25.4 mm thick styrofoam substrate by changing frequency

Figure A.6

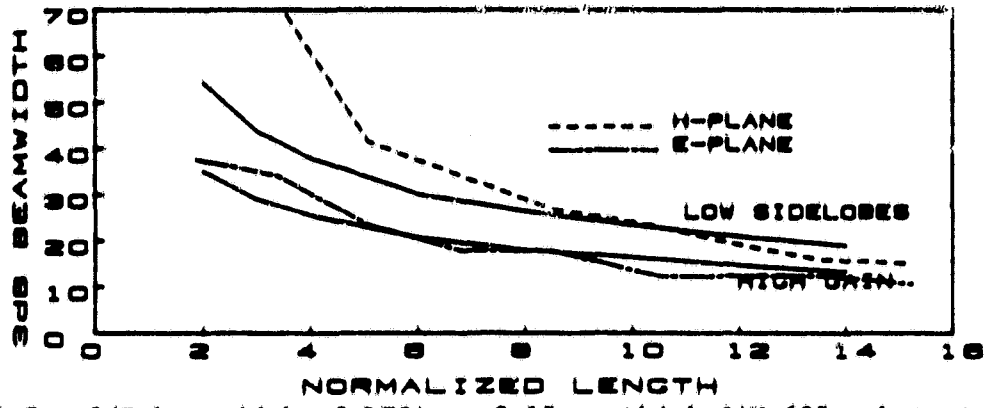

A.7a 3dB beamwidth of LTSA on 0.15 mm thick OAK-605 substrate

Figure A.7a

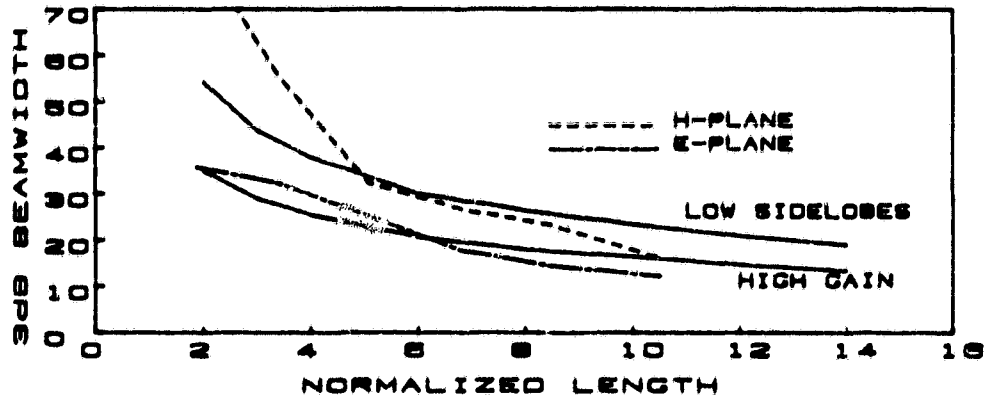

A.7b 3dB beamwidth of LTSA on 0.79 mm thick OAK-605 substrate

Figure A.7b

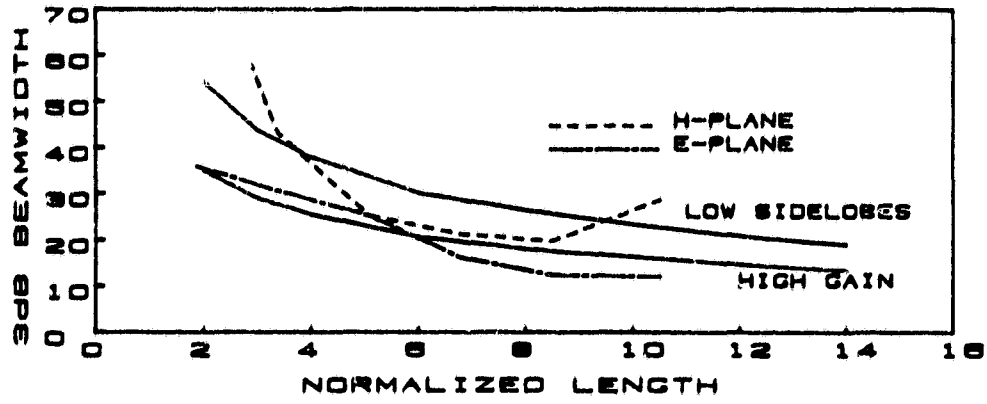

A.7c 3dB beamwidth of LTSA on 1.59 mm thick OAK-605 substrate

Figure A.7c

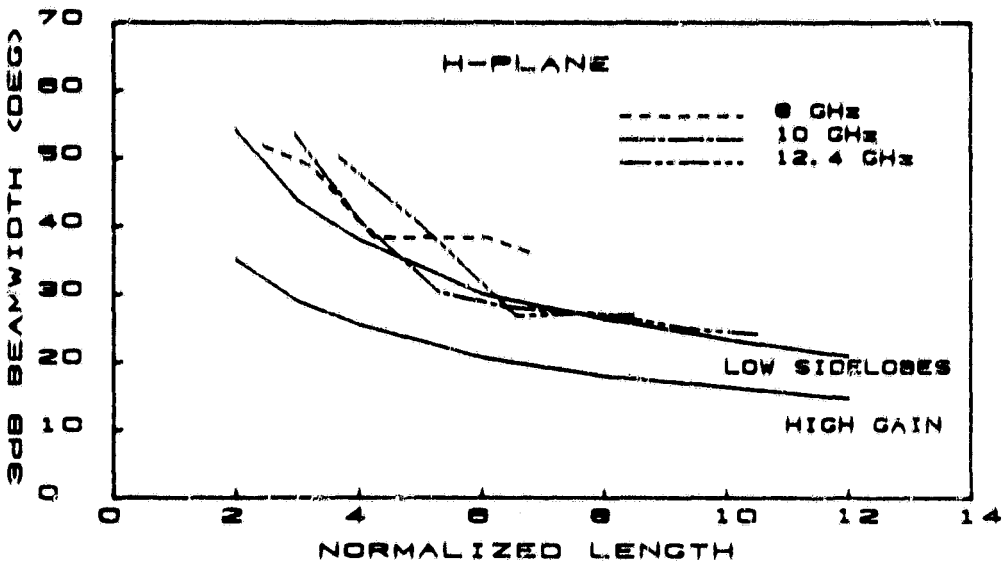

A.8a 3dB beamwidth of LTSA on 0.15 mm thick OAK-605 substrate

Figure A.8a

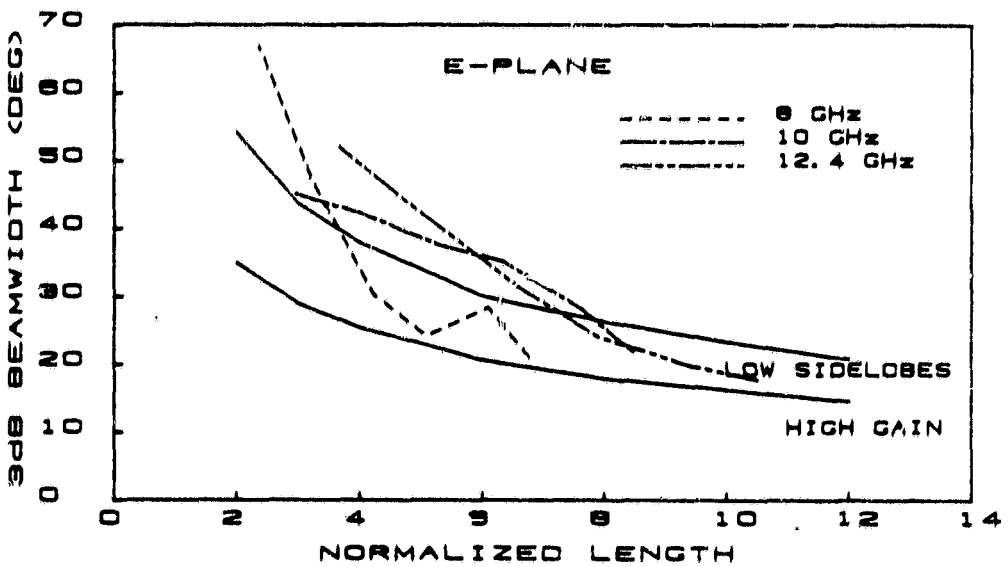

A.8b 3dB beamwidth of LTSA on 0.15 mm thick OAK-605 substrate

Figure A.8b

two TWA curves for long lengths. This indicates that we are approaching the optimum directivity for these antennas with a rather thin dielectric substrate.

Another set of measurements were made at 94 GHz on three LTSA antennas with 11.2 degree full taper angle for various substrate thicknesses as a function of length. The substrate material was Kapton (ε_r = 3.5) of thicknesses 0.025 mm, 0.051 mm, and 0.076 mm respectively (see Figure A.9). This series shows a radical progression from the low sidelobe curve, to high gain, to asymmetrical E- and H-plane beamwidths. Note the rough similarity of Figure A.7b with Figure A.9a, and Figure A.7c with Figure A.9b, respectively.

An identical 11.2 degree taper angle LTSA antenna was fabricated on a .127 mm thick Duroid (ε_r = 2.33) substrate and beamwidth measured as a function of length, see Figure A.10. As with the 0.051 mm Kapton substrate (Figure A.9b), the beamwidths tend to follow the high gain curve. X-band models on thick low dielectric constant substrates have not duplicated the symmetrical high gain beams seen in these higher dielectric constant materials. For instance, Figure A.11 is a graph of half power beamwidth of an 11.2 degree taper angle LTSA on a 25.4 cm long, 1.54 mm thick OAK-605 laminated substrate. For this case the H-plane beamwidth tends to be wider than the E-plane and widens more as the length of the antenna is increased. This behavior is different from that seen in Figure A.9c for 0.076 mm Kapton, where the E-plane beamwidth has become broader than the H-plane beamwidth. It should be pointed out that most measurements of the 1.54 mm thick substrate

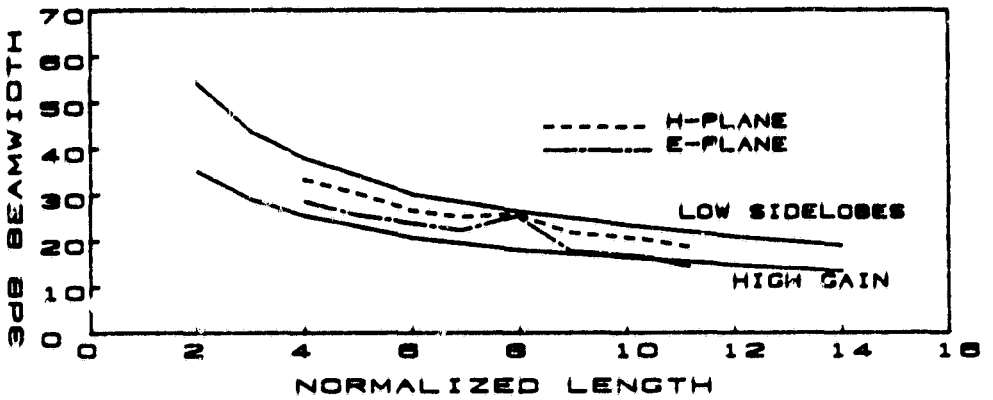

A.9a 3dB beamwidth of LTSA on 0.025 mm thick Kapton substrate

Figure A.9a

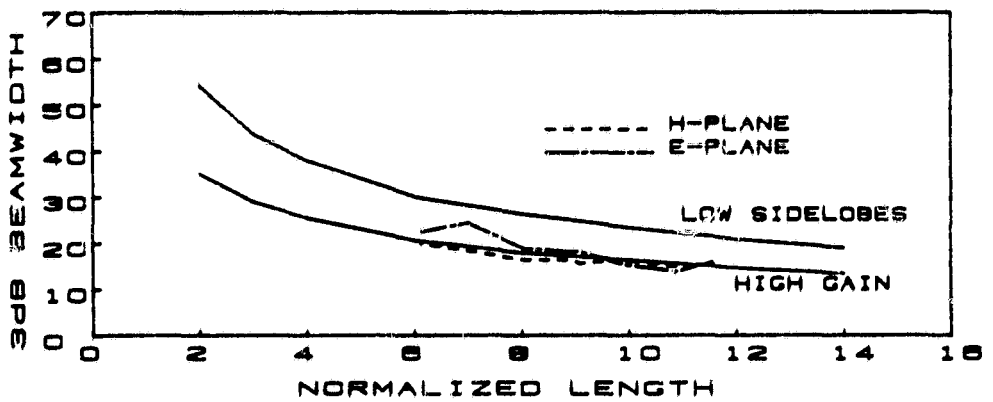

A.9b 3dB beamwidth of LTSA on 0.051 mm thick Kapton substrate

Figure A.9b

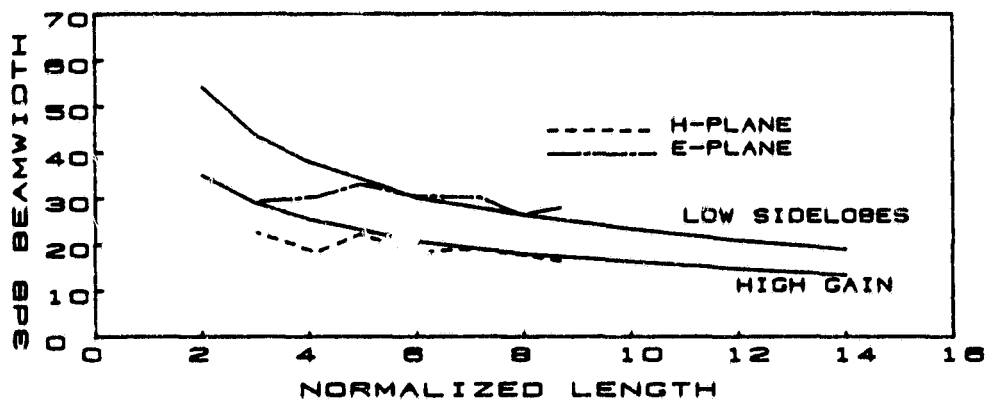

A.9c 3dB beamwidth of LTSA on 0.076 mm thick Kapton substrate

Figure A.9c

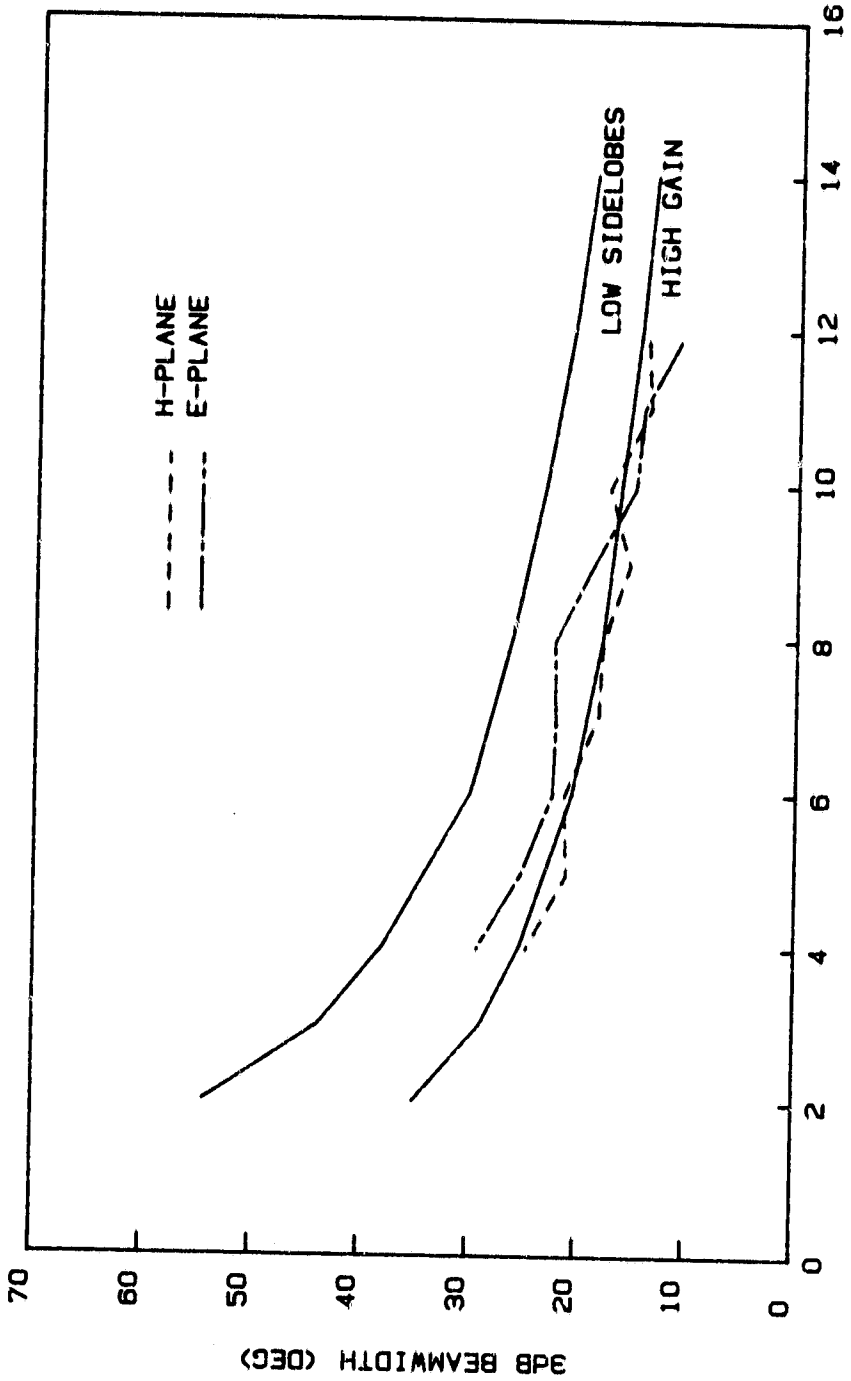

A.10 3dB beamwidth of LTSA on 1.54 mm thick OAK-605 substrate

Figure A.10

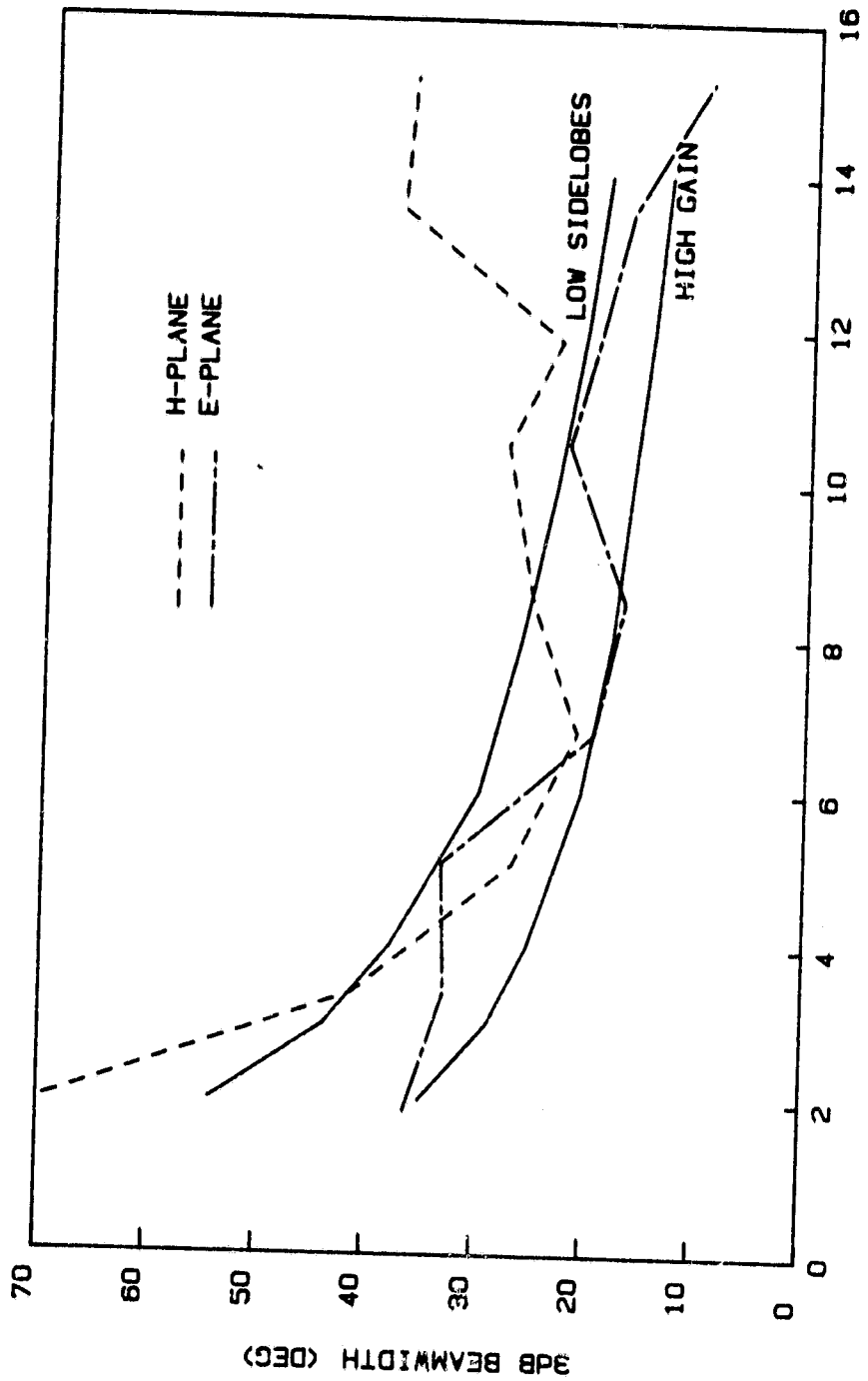

A.11 3dB beamwidth of LTSA on 1.54 mm thick OAK-605 substrate

Figure A.11

antennas have been made as a function of frequency, whereas all the 94 GHz measurements have been made as a function of length. However, it remains clear that the substrate can be used to modify the effective dielectric constant of the structure, thereby changing the radiated beamwidths. It is also clear that a different behavior is seen for very long antennas on thick substrates.

The traveling wave antenna theory reviewed in Chapter III leads to conditions which can be looked on as implying that optimum radiation occurs when there is a specific relative phase difference between a wave in free space and a wave in the radiating structure with an effective dielectric constant. Assume that there exists a structure 6λ long, which radiates optimally. This requires that the phase difference between the wave in the structure and that of free space be 120 degrees or

$$6\lambda_0 - 6\lambda_{eff} = 1/3\lambda_0 \qquad (A.2)$$

Because the wavelength is inversely proportional to the square root of the dielectric constant, it can be shown that for optimum radiation to occur the antenna should have an effective dielectric constant of 1.029.

Now consider the case of a small taper angle LTSA antenna on a styrofoam substrate. It has been shown previously that antennas of this type can satisfy the optimum beamwidth curves for TWA antennas over some range of frequencies. This antenna can be crudely modeled as a slotline. To first order, the effective impedance of a slotline on a semi-infinite substrate can be calculated as the average of the dielectric constants of the materials on the two sides of the antenna

metalization. The styrofoam substrates used for these antennas were one-inch thick and can be considered for this example to be infinitely thick. The dielectric constant of the styrofoam was measured to be 1.05, and thus, to first order, the antenna can be said to have an effective dielectric constant of 1.025. Thus, to first order styrofoam antennas would be expected to radiate optimally at the frequency where the antenna is $6\lambda_o$ long.

This analysis assumes that the propagation of the electro-magnetic fields are in the slotline mode. The slot width of these antennas are actually larger and the substrate's dielectric constant is much lower than normally used for slotted lines, and the fields would not be expected to couple tightly to it. Also, the slot is of changing width and would further complicate the radiation mechanism. However, for LTSA antennas with slots that remain much narrower than a wavelength, the analysis will help indicate when the radiator can be expected to show optimum traveling-wave behavior.

High Dielectric Constant Substrates

Measurements were also conducted on LTSA antennas on a high (ε_r = 10.2) dielectric constant material, 3M Epsilam-10. In this case, 11.2 degree full angle LTSA antennas were fabricated on 0.25 mm thick Epsilam-10 substrates and half power beamwidths measured versus both frequency, Figure A.12, and length, Figure A.13. Included for comparison are graphs of half power beamwidths of similar LTSA's on 1.54

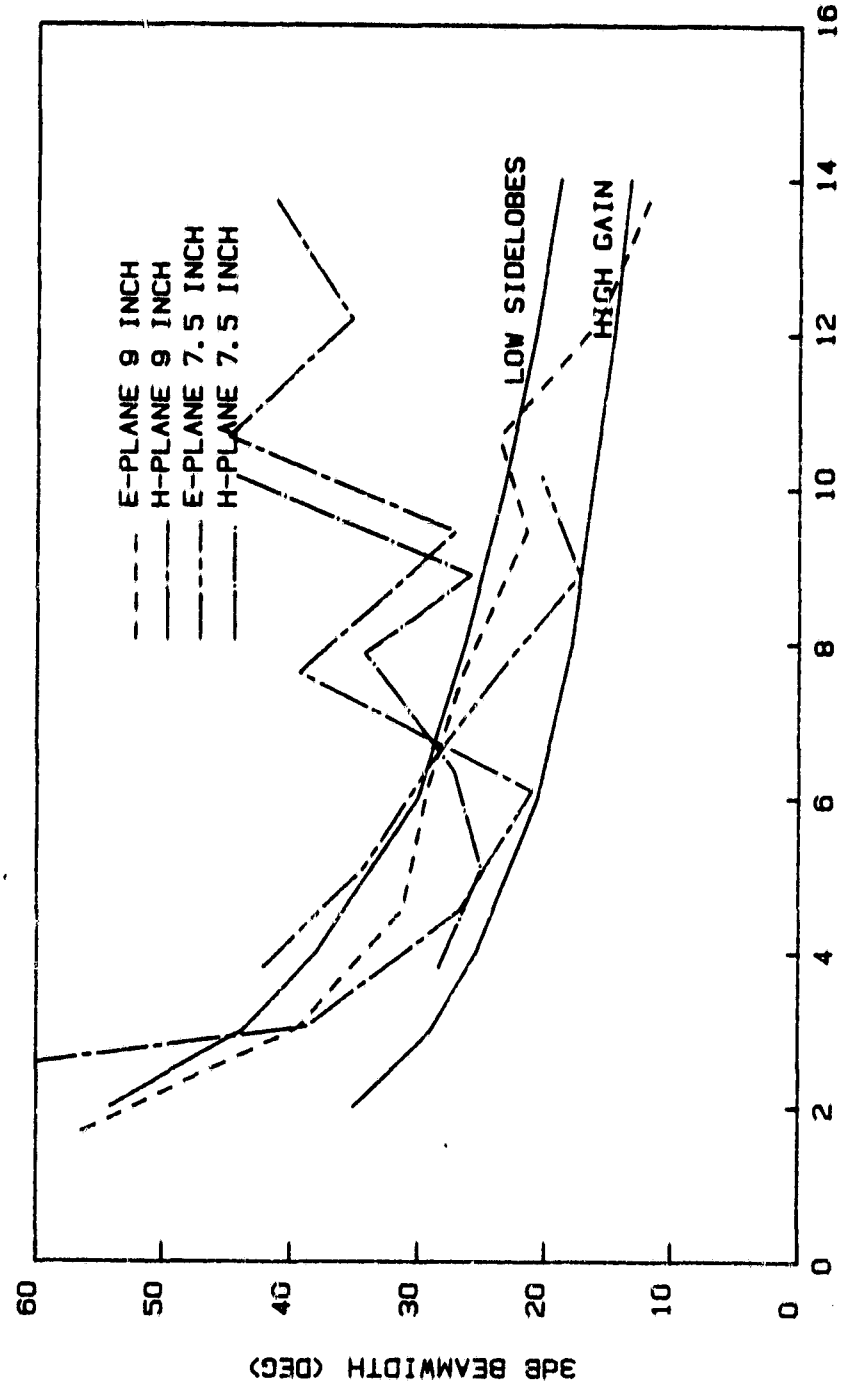

A.12 LTSA on 0.25 mm thick Epsilam-10 by changing frequency

Figure A.12

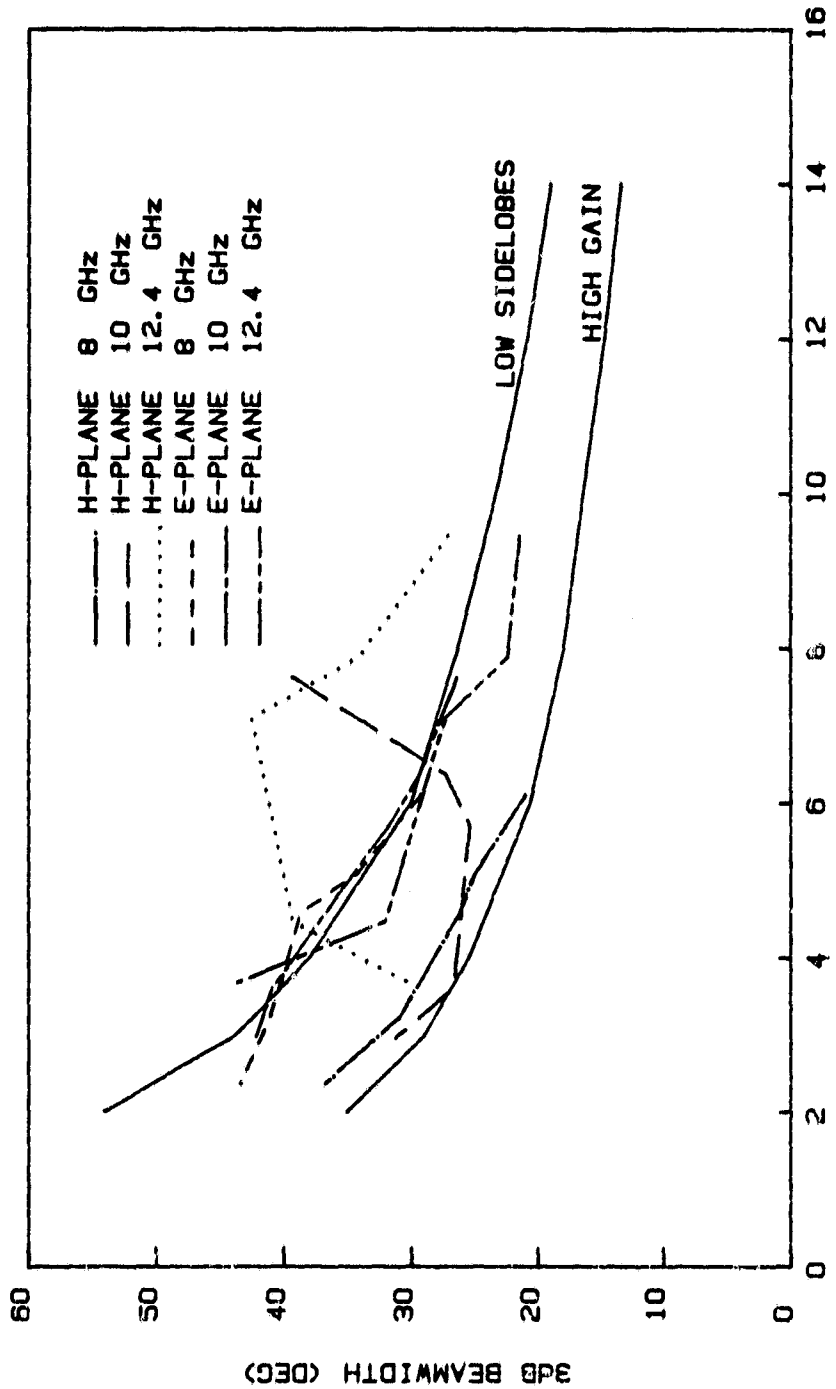

A.13 LTSA on 0.25 mm thick Epsilam-10 by cutting length

Figure A.13

mm thick OAK-605 substrates also measured as a function of length and frequency in Figures A.14 and A.15, respectively. For both sets of data taken versus frequency, the H-plane beamwidths broaden and the E-plane beamwidth narrow as the antenna is effectively lengthened beyond about 6 λ_o. For relatively short antenna lengths, $L<6\ \lambda_o$, the antennas do follow the standard TWA curves. Similarly, the LTSA antennas on 1.54 mm thick OAK-605 substrates do also follow the standard data for short normalized lengths, while for longer antennas the H-plane beamwidth tends to become much broader than the E-plane beamwidth for the 12.4 GHz case. The simple TWA curves presented earlier cannot explain this behavior.

Metalization Angle

It is expected that the shape of the metalization will effect the radiation properties of the LTSA antenna. Two 25.4 cm long LTSA antennas were constructed on 2.54 cm thick styrofoam with full angles of 11.2 and 16.4 degrees. Patterns taken as a function of frequency and plotted in Figure A.16 show that the H-plane beamwidths are very similar, but that a small shift of the E-plane curve to narrower beamwidths occurs for the wider taper angle. Data taken on a 16.4 degree LTSA on a 0.15 mm thick OAK-605 laminated substrate and an 11.2 degree LTSA on a 0.127 mm thick Duroid substrate also show similar results, Figure A.17. The fact that the E-plane beamwidth narrows for a wider final aperture can be looked at from either of 2 points of view:

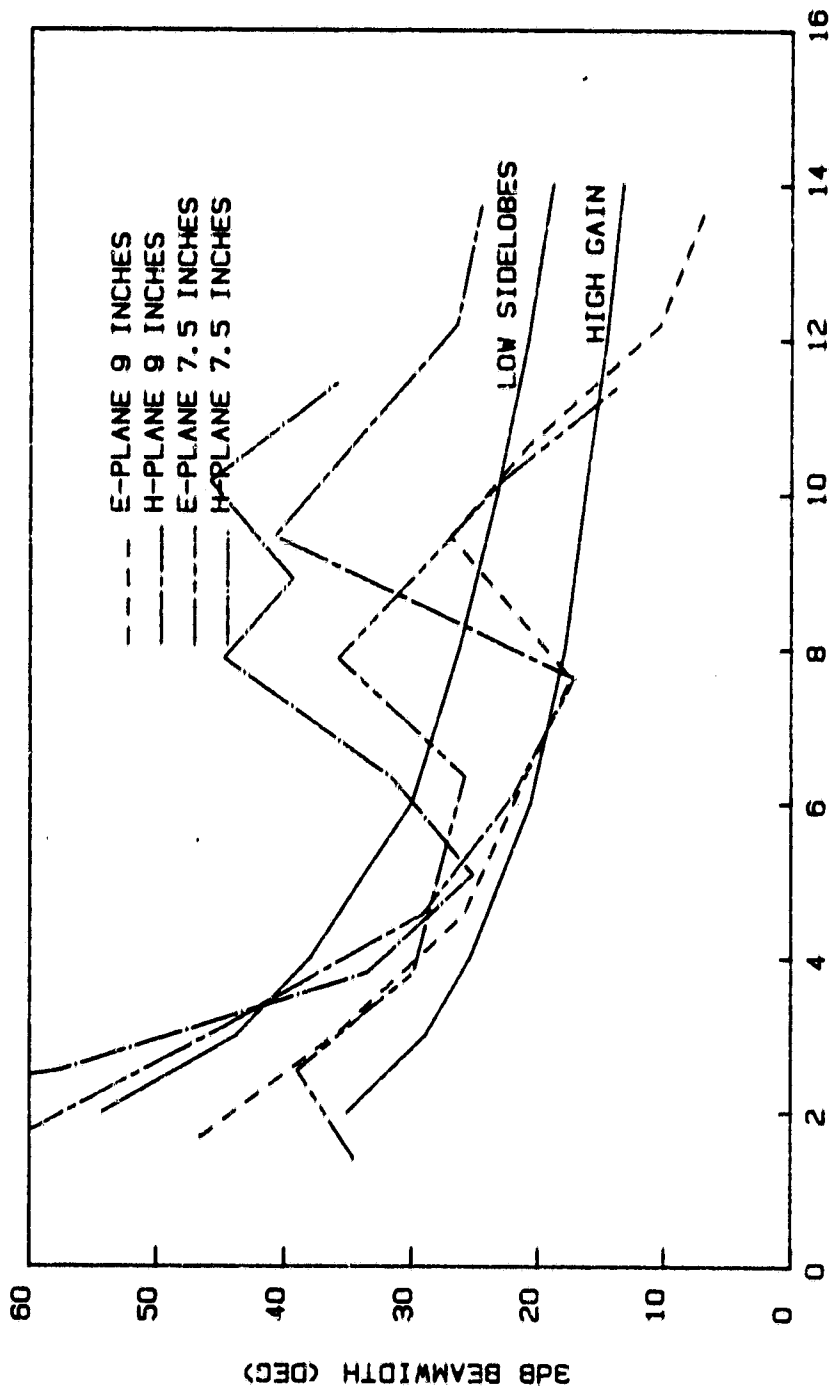

A.14 LTSA on 1.54 mm thick OAK-605 by changing frequency

Figure A.14

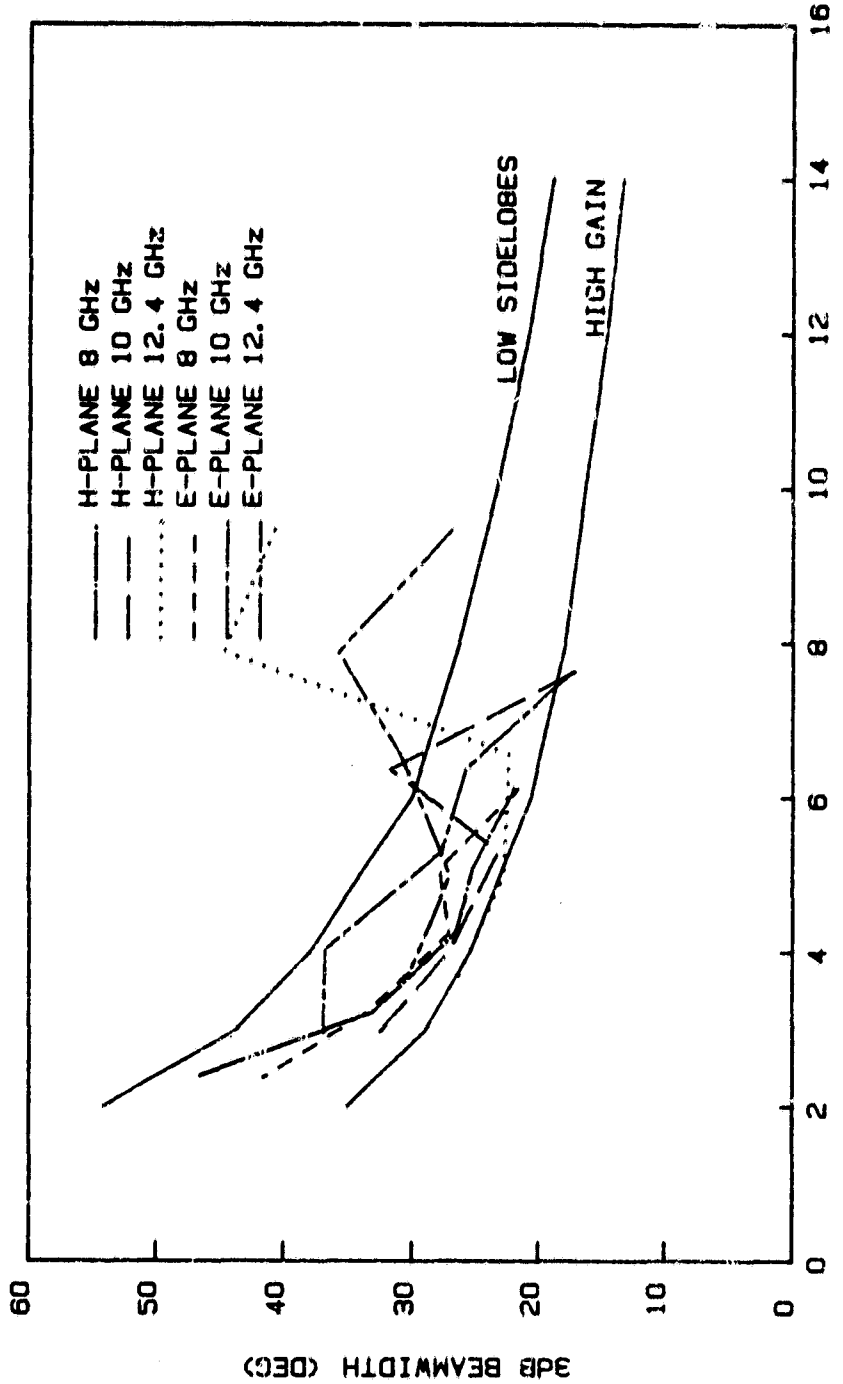

A.15 LTSA on 1.54 mm thick OAK-605 by cutting length

Figure A.15

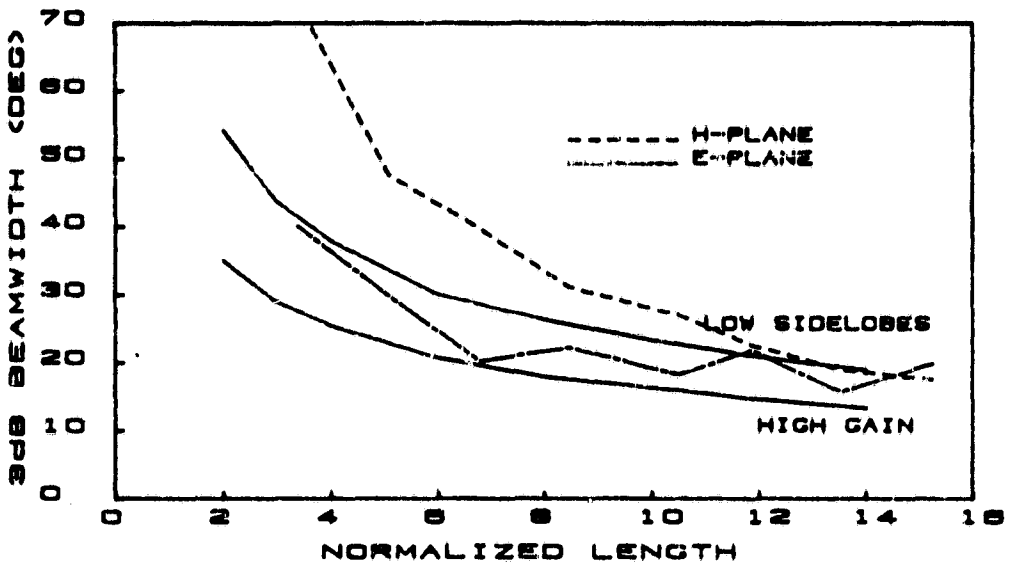

A.16a 11.2 degree LTSA on 25.4 mm thick styrofoam substrate

Figure A.16a

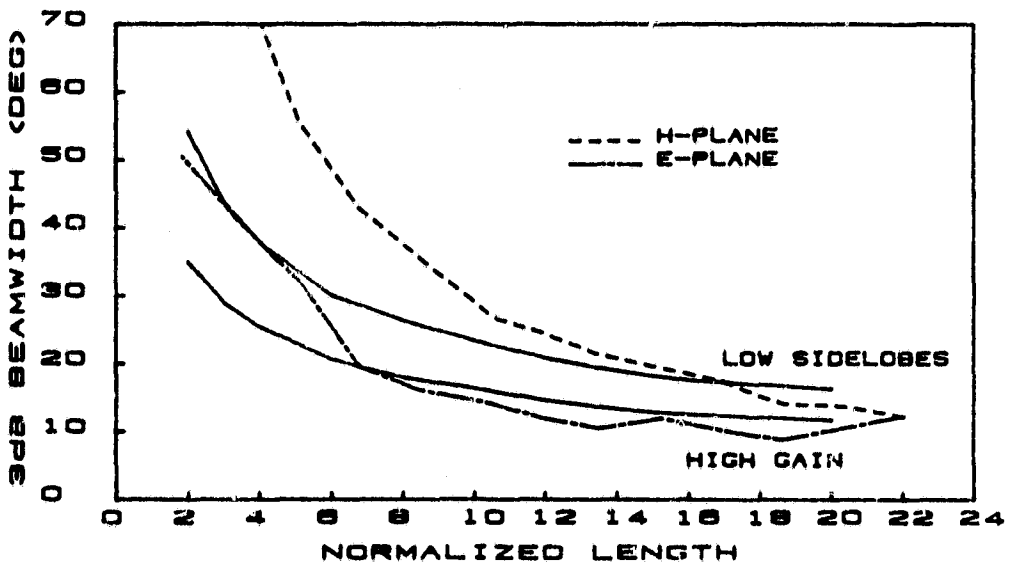

A.16b 16.4 degree LTSA on 25.4 mm thick styrofoam substrate

Figure A.16b

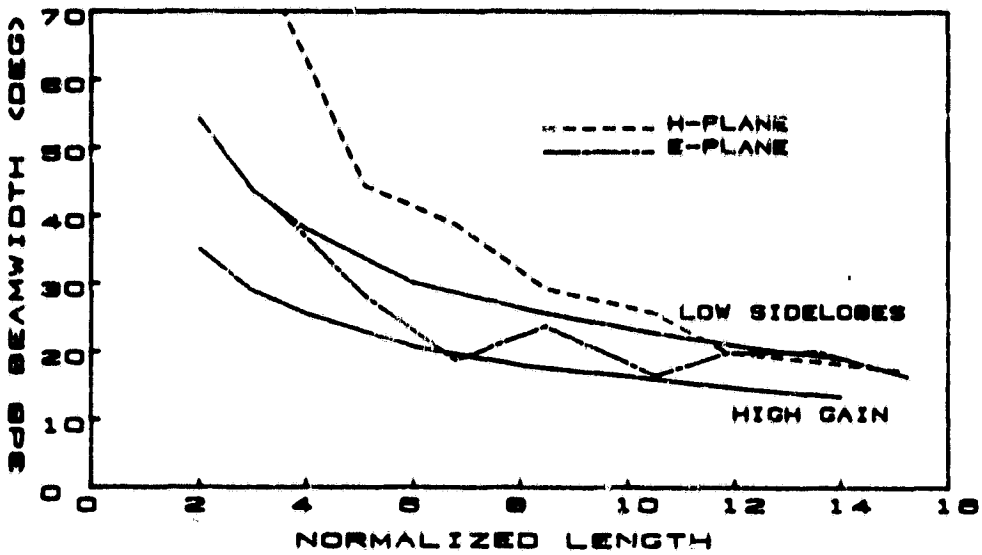

A.17a 11.2 degree LTSA on 0.154 mm thick OAK-605 substrate

Figure A.17a

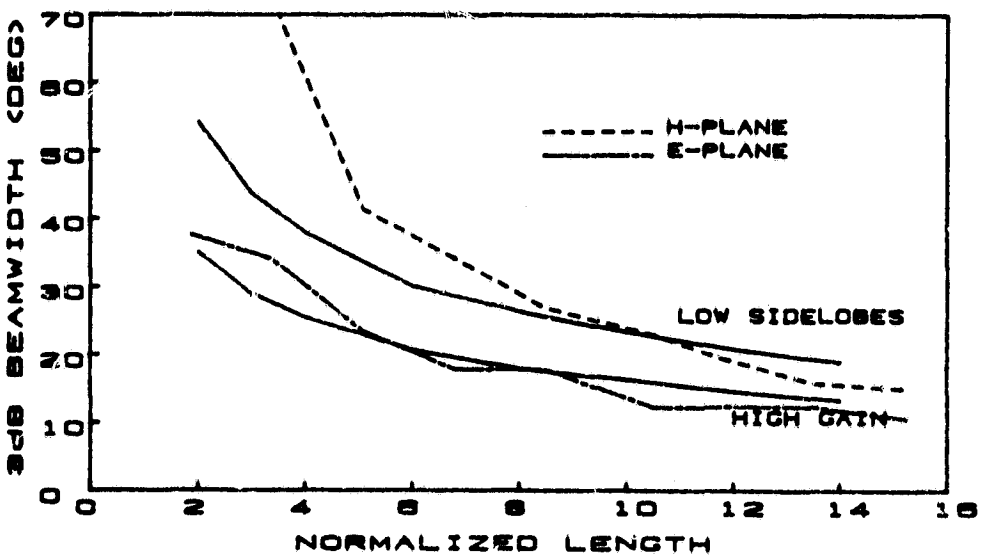

A.17b 16.4 degree LTSA on 0.154 mm thick OAK-605 substrate

Figure A.17b

1.) the greater opening angle has changed the phase velocity of the waves in the antenna bringing them closer to the optimum gain condition in the case of the 16.4 degree taper angle, or 2.) the final aperture of the 16.4 degree LTSA is larger than for the 11.2 degree antenna of same length, thus from aperture theory, the beamwidth must decrease.

The Wire Vee Model

A simple and most natural model to propose for the LTSA antenna is the wire Vee antenna. This model would consist of two wires diverging at the same angle as the LTSA's slot edges. A plot of measured E- and H-plane radiation patterns of a Vee antenna with full taper angle of 11.2 degrees on a 2.54 cm thick styrofoam substrate are shown in Figure A.18. Radiation patterns for Vee antenna of same taper computed using the moment method [courtesy of W. Farshori] are shown in Figure A.19. These patterns are seen to be remarkably similar, except the measured H-plane beamwidths are narrower by about 7 degrees, which could be attributed to the styrofoam substrate. Also, a series of radiation patterns were measured for a 16.4 degree Vee antenna on a 2.54 cm styrofoam substrate as a function of length. The measured half power beamwidths are shown plotted in Figure A.20. Shown in Figure A.21 is a plot of calculated 3dB beamwidth [courtesy of W. Farshori] versus normalized length for a 16.4-degree styrofoam LTSA, we see the LTSA has a much broader H-plane beamwidth. In this case, the measured data follow the optimum curves while the calculated values remain far wider.

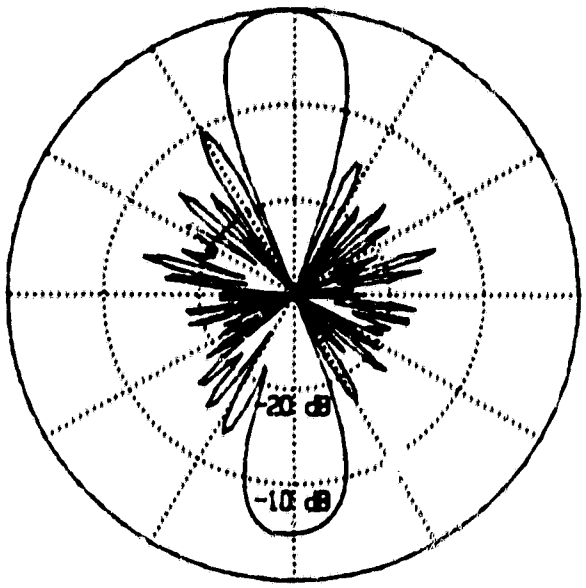

A.18a Measured H-plane of 11.2 degree wire-Vee on a styrofoam substrate

Figure A.18a

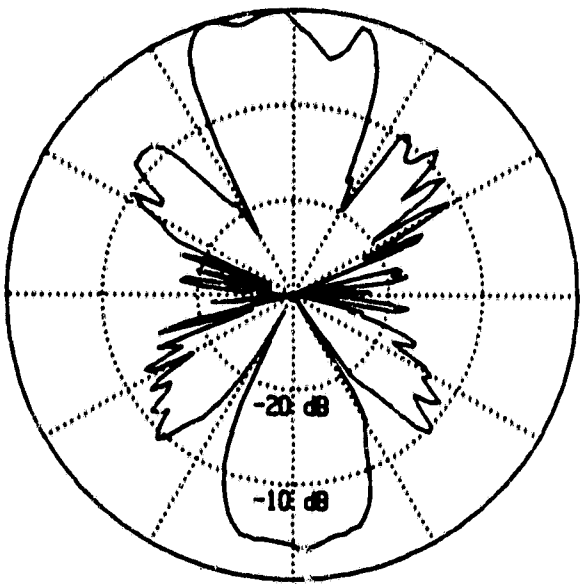

A.18b Measured E-plane of 11.2 degree wire-Vee on a styrofoam substrate

Figure A.18b

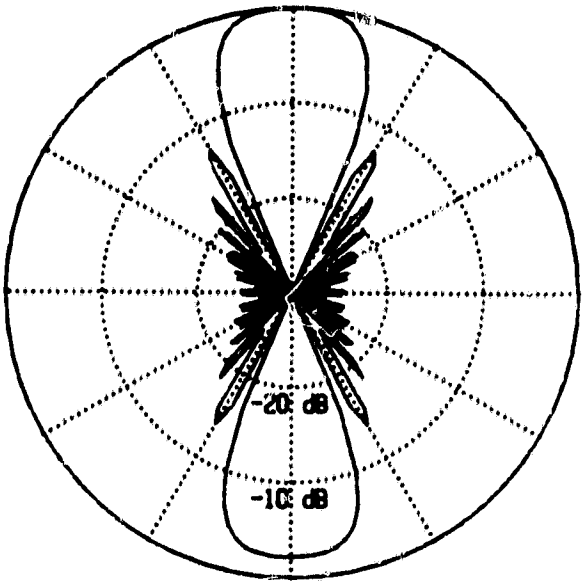

A.19a Calculated H-plane of 11.2 degree wire-Vee on a styrofoam substrate

Figure A.19a

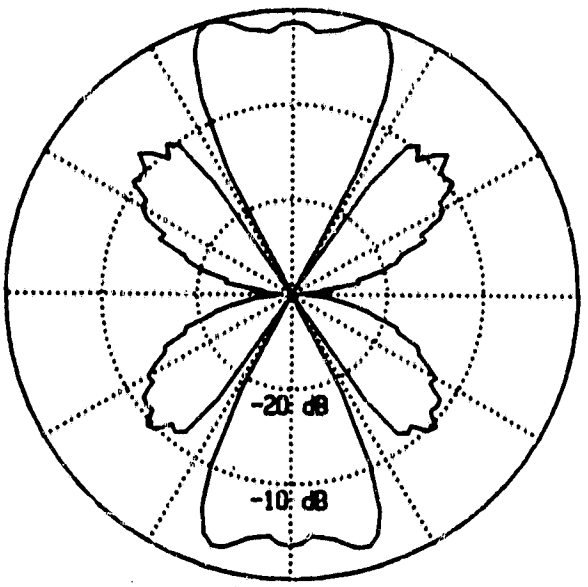

A.19b Calculated E-plane of 11.2 degree wire-Vee on a styrofoam substrate

Figure A.19b

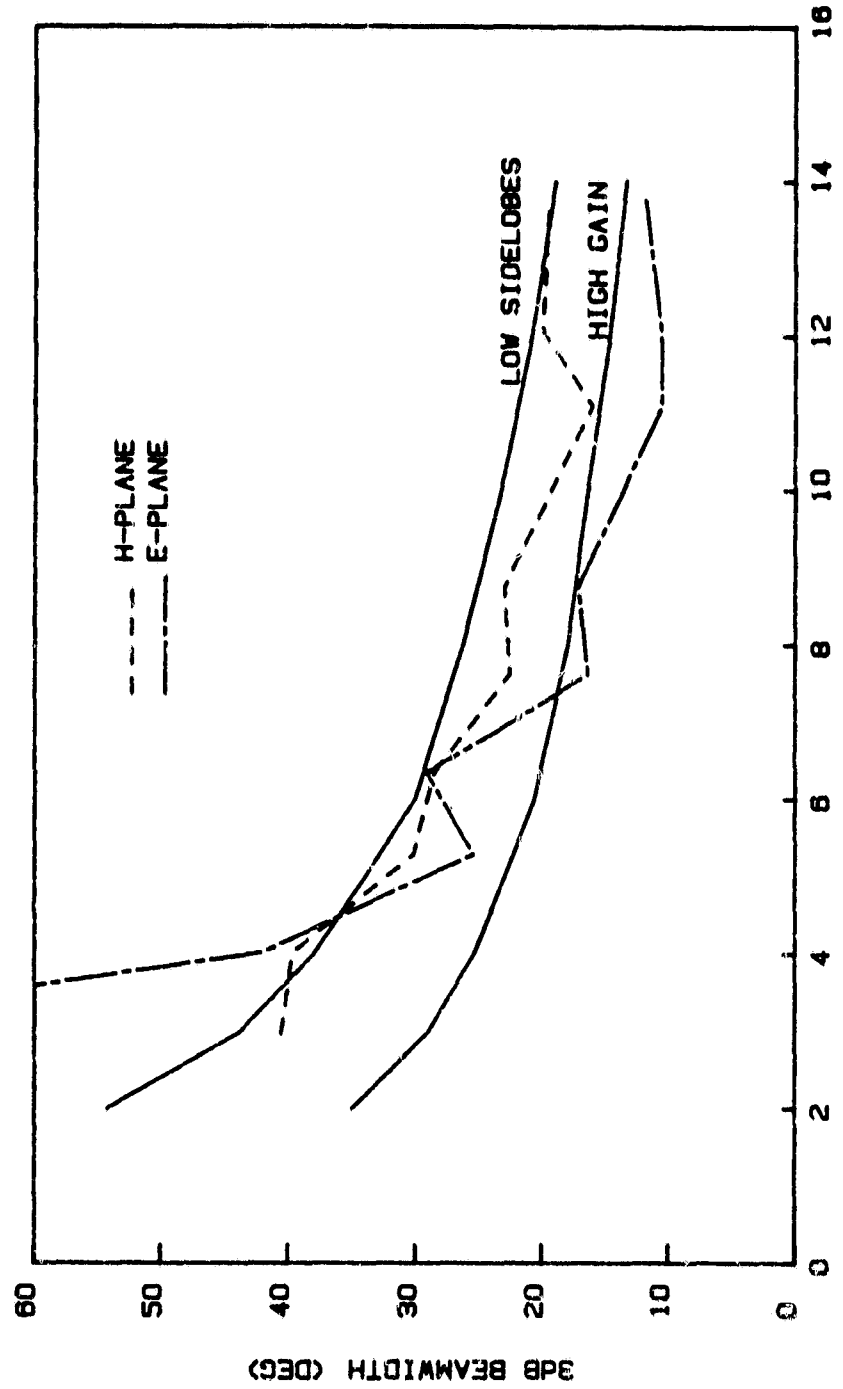

A.20 Measured 3dB beamwidth of 16.4 degree wire-Vee on a styrofoam substrate

Figure A.20

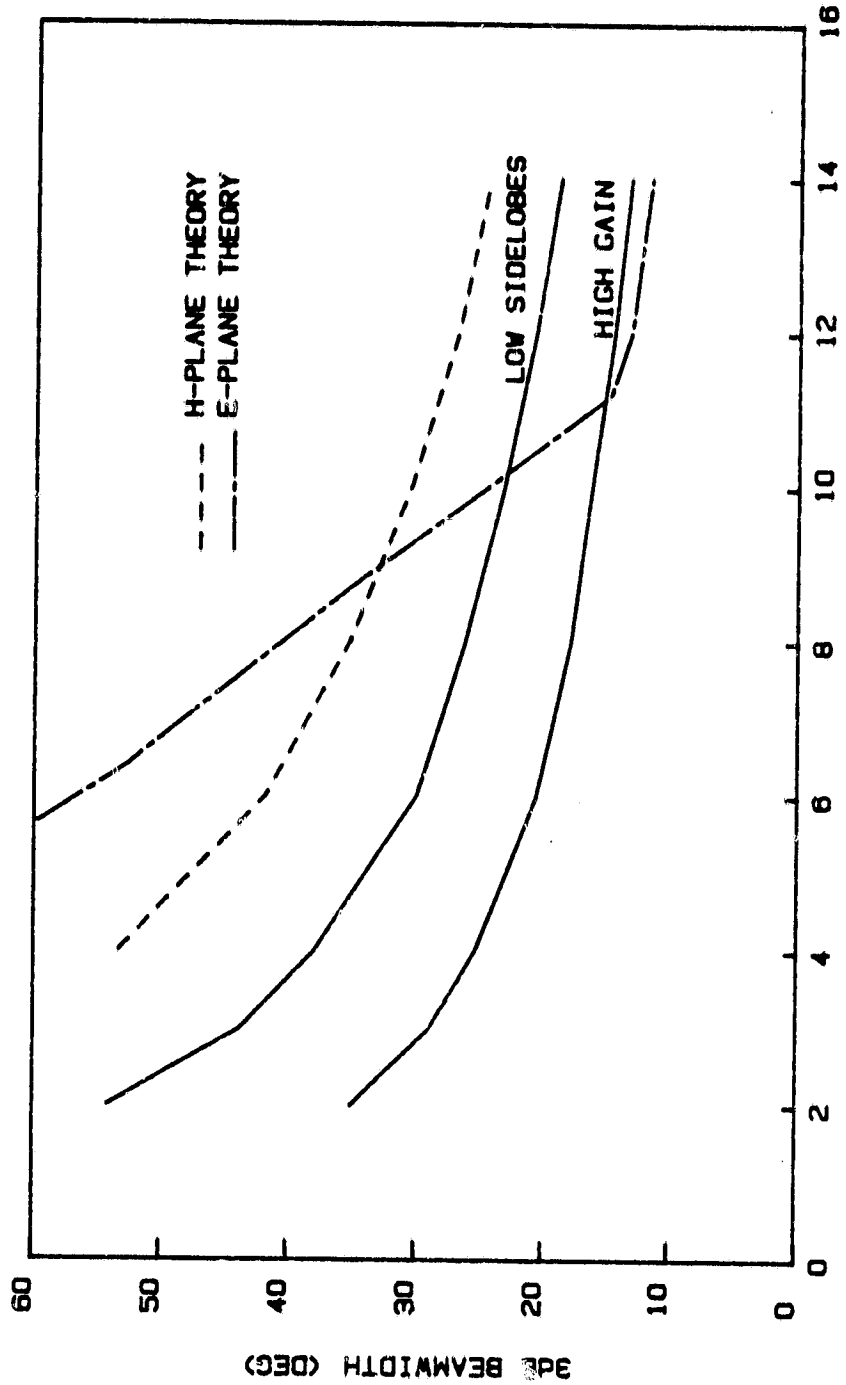

A.21 Calculated 3dB beamwidth of 16.4 degree wire-Vee on a styrofoam substrate

Figure A.21

The difference between the 3 dB beamwidth of the calculated values to those of the measured values cannot be easily explained. The biggest disparity between the way the measurements were made and the calculations performed stems from the use of a styrofoam substrate. Measurements of an "air" LTSA antenna also differed from the moment method calculated values. This indicates that the wire Vee is not an appropriate model for the LTSA antenna. A theory that takes into consideration the dielectric substrate and ground plane must be formulated for useful beamwidth predictions.